Thesis submitted to obtain the title of Doctor of Philosophy of the University of Lille 1

Modeling and synchronization of biological rhythms: from cells to oyster behavior

Prepared at **Inria** by

HAFIZ AHMED

Thesis defended on **September 22nd 2016**

Jury members:

Advisors:	Denis Efimov	Chargé de recherche, Inria
	Rosane Ushirobira	Chargé de recherche, Inria
Co-advisor:	Damien Tran	Chargé de recherche, CNRS
Reviewers:	Jean-Luc Gouzé	Directeur de recherche, Inria
	David Angeli	Reader, Imperial College London
Examiners:	Jean-Charles Massabuau	Directeur de recherche, CNRS
	Pierre-Alexandre Bliman	Directeur de recherche, Inria and Assoc. Professor, FGV, Rio de Janeiro

Acknowledgements

The PhD work presented in this thesis has been conducted at Non-A team of Inria Lille Nord Europe, from October 2013 to September 2016, under the supervision of Dr. Denis Efimov (CR Inria), Dr. Rosane Ushirobira (CR Inria) and Dr. Damien Tran (CR CNRS). It was supported by Inria and the "Conseil Régional de la Région Hauts-de-France".

I would like to express my sincere gratitude to my advisers Denis Efimov, Rosane Ushirobira and Damien Tran for everything they did for me in the last three years. First of all, I would like to thank my supervisors from Inria (Denis and Rosane) for giving me the opportunity to work with them. I would also like to thank all my supervisors for their trust on me and my work during these years, for their patience, and for their availability. I have learned a lot about control theory and mathematics from Denis and Rosane. Similarly, I have learned a lot about oysters from Damien. All these will help me immensely in my future endeavor. I am forever grateful to them.

I would also like to express my sincere gratitude to each and every member of my PhD committee, for having accepted to read and examine the present work, namely Dr. Jean-Luc Gouzé (Research Director, Inria Sophia Antipolis Mediterranean), Dr. David Angeli (Reader, Imperial College London), Dr. Pierre-Alexandre Bliman (Research Director, Inria Paris and Associate Professor, FGV, Rio de Janeiro) and Dr. Jean-Charles Massabuau (Research Director, CNRS).

I would like to thank all the members of the Non-A team of Inria for the discussions we have had and for the great atmosphere. I would specially like to thank all my current and former colleagues and friends specially Maxime, Francesco, Hector, Yue, Manuel, Ivan, Zohra, Lucian, Yacine, Stas, Nadhynee, Konstantine, Roudy, Matteo, Diego, Anja, Antonio, Qi, Zilong, Zhaopeng, Xinxin, George and others. I am also grateful to the help and supports I have received from the premanent members of our team - Prof. Richard, Prof. Perruquetti, Prof. Belkoura, Dr. Polyakov, Dr. Zheng, Dr. Quadrat and Dr. Floquet. Special thanks also to secretary of Non-A team Corinne Jamroz and everyone from the HR department of Inria, Lille. Finally, I would like to thank my family for their continuous help and support.

Abstract

This PhD thesis is dedicated to modeling, analysis and control of oscillations, notably biological rhythms. The thesis is divided into two parts. Part I deals with a real-life application while part II studies more theoretical problems, with potential practical applications.

In the first part, motivated by a practical problem of environmental monitoring of coastal environment, this thesis considers the biological rhythms of oysters. It is well-known that oysters valve movement activity is heavily influenced by biological rhythms like circadian and circatidal rhythms. Moreover, pollution in the surrounding marine environment can perturb these rhythms, and influence the valve movement activity. Using this information, we propose an indirect environmental monitoring solution using oysters as bio-sensor. The proposed solution works on estimating the perturbation by modeling the biological rhythm of oysters through Van der Pol oscillator model. An inherent limit of this approach is that it works through detecting abnormal behavior only. However abnormal behaviors are not all related to pollution. So, we consider the detection of a particular type of abnormal oscillatory behavior *i.e.* spawning (behavior during reproduction) which is a natural phenomenon and not related to pollution. The spawning detection algorithm is inspired by the engineering literature of oscillatory fault detection.

In the second part, oscillations are studied from a theoretical point of view. Having better understanding of the modeling, analysis and control of oscillations may give rise in the future improved environmental monitoring solutions. The first problem of this part is the robustness of oscillations under cell division. Oscillations persist in genetic oscillators (circadian clocks, synthetic oscillators) after cell division. However, in the literature through stochastic simulation it was found that the phase of the oscillation diverges under high variability of extrinsic noise (variability in the cell division time and in the partition of the molecules into daughter cells, cell–cell variability in kinetic parameters, *etc*). So, in this thesis, we provide analytical conditions that guarantee phase synchronization after cell division using Phase Response Curve (PRC) formalism. Our results corresponds to the existing stochastic simulation results. Finally we consider the

problem of synchronization of multi-stable systems using Input-to-State (ISS) stability tool. Many oscillatory systems are multi-stable. Using a recent generalization of ISS theory for multi-stable systems, we propose sufficient conditions for the synchronization of multi-stable systems. As a side result, this work has been applied for the global synchronization of a recently proposed oscillator model called the Brockett oscillator.

Contents

List of Figures

Chapter 1

General introduction

1.1 Background and motivation

Since the last century, the quality of our world's environment has changed swiftly causing significant changes in the marine water quality. For this reason, nowadays, local, regional and international legislation has strict laws and recommendations on the protection of aquatic environment against the disposal of harmful and dangerous substances[1]. In order to abide by these laws and recommendations for the protection of the aquatic environment, a large scale monitoring of water quality is essential [110]. However, the realization of such an extensive network of aquatic monitoring is very costly and technically challenging from an engineering point of view. Researchers and engineers are then working on an indirect monitoring of the aquatic environment from behavioral and physiological responses of representatives of the marine fauna [31, 32, 89, 90, 121, 130]. For instance, bio-indicators demonstrate high efficiency through bio-accumulation of contaminants/pollutants in their tissues[2]. Nevertheless, until now large scale extensive aquatic monitoring does not seem viable and realistic as it involves intensive exploitation of human resources for the collection of samples, complex chemical analysis and so on [141].

A solution for the aforementioned problem is to develop unmanned autonomous systems using biosensors, able to work round the clock, at high frequency by remote control. As of today, networks of such online sensors, operating on a large scale do not exist and are still a matter of research. To fulfill the objective just mentioned before, an installation of numerous online remote sensors is required, working at high frequency for instant

[1] http://europa.eu/legislationsummaries/environment/waterprotectionmanagement/l28017aen.htm
[2] For example, see the US Mussel Watch, http://ccma.nos.noaa.gov/about/coast/nsandt/musselwatch.aspx.

collection of information on a daily basis in a marine environment [97]. Behavioral and physiological responses of wildlife to contamination are very sensitive and these responses can be used for an indirect monitoring of the aquatic environment [142]. However, a limiting factor today is that it requires high volumes of data, whose analysis sufficiently accurate models of animal behavior in natural conditions [67]. Other difficulties lie in the fact that animals may be heavily influenced by the surrounding environment, group interactions and internal rhythms (*e.g.* feeding, breathing, spawning) [6].

The observation of the opening and closing activities of bivalves is a possible way to evaluate their physiological behavior in reaction to nearby water. It is well-known from the literature that behavior of bivalves (like oysters) follows very strict biological rhythms (like circadian and circatidal) according to the relative moon and sun positions [145]. Moreover, it was also reported in [82] that the presence of toxic substances changes significantly the behavior of the oysters. From these informations, it can be inferred that bivalves have the potential to be used for indirect monitoring of the nearby environment through behavioral analysis of their valve movement. This inspired the ecotoxicology[3] community to explore the opportunity of using oysters as bio-indicators through valvometry (*i.e.* recording of valve movement of bivalves). The basic idea of valvometry is to use the bivalve's ability to close its shell when exposed to a contaminant as an alarm signal [25, 28, 29, 48, 92, 96, 133]. Using this natural idea, various studies have been done for the purpose of environmental monitoring [1, 105, 106, 137]. However, a major challenge in implementing the existing literature for real-world environmental monitoring is that most of the works rely on laboratory experiments and chemical analysis. Bivalves behave quite differently in laboratory and in open water (river, sea *etc.*). Again in open water, the behavior depends on the habitat condition [62]. Moreover, the existing literature is not very suitable for online large scale monitoring since most of them consider local monitoring solutions. As a result, there exist the scope to provide a monitoring solution that works for any natural condition (river, sea, Arctic/Mediterranean environment *etc.*), free from chemical analysis and that it can be deployed for large scale online monitoring.

If environmental pollution can be considered as something that causes oysters to have a faulty behavior (*i.e.* deviation from normal behavior), then model-based approach [27, 47, 154] can be very useful for the development of a monitoring solution which has the properties mentioned before. Since pollution perturbs the oysters rhythms, then modeling the rhythm can provide information on this perturbation. Using model

[3]Ecotoxicology is the study of the effects of toxic chemicals on biological organisms, especially at the population, community, ecosystem level.

information, a residual signal can be generated. With the aid of the residual signal, a monitoring system can be developed which will give an alarm of pollution when the residual exceeds a predefined threshold. This idea of a model based fault detection will be developed in this thesis for the purpose of environmental monitoring.

The model based environmental monitoring solution relies on the fact that deviation from the oyster's normal behavior can be considered as a pollution, which is often the case. However, not all abnormal behaviors of the oysters are related to water pollution. They can behave abnormally for a multitude of reasons, for example sound pollution. When a heavy boat/ship passes through an area nearby to the oysters habitat, it may impact the behavior of oysters. Although no formal scientific study has yet been published on this topic, this point cannot be ignored. A particularly abnormal behavior of oysters is spawning (*i.e.* behavior during reproduction) [68]. During spawning, oysters behave in an oscillatory manner to expulse eggs in the water. The behavior lasts for only 10-40 minutes and can be seen once or twice in a year in female oysters. The reaction of male oysters is sometimes similar to the female oysters, but the characteristics are very mild in comparison to their female counterparts. Genetically modified oysters like triploids do not exhibit this behavior. The detection of this abnormal behavior is necessary to avoid any false alarm from the monitoring system. This detection will also be considered in this thesis. The idea of this detection comes from the engineering literature. Oscillatory faults are quite common in various kinds of systems like aircraft, rotating machinery *etc.* The detection techniques that will be developed later in this thesis could be very interesting for engineering systems as well.

One of the important phenomenon that heavily influence the behavior of an oyster is its internal biological rhythms or oscillations. Oscillations play an important role in many dynamic cellular processes in the molecular level also. This fact was mentioned by A. Goldbeter in the introduction of his famous book [74] "*Rhythms are among the most conspicuous properties of living systems. They occur at all levels of biological organization, from unicellular to multicellular organisms, with periods ranging from fractions of a second to years*". Because of its omnipresence in biological systems, the study of oscillations in biology has attracted a lot of attentions since the beginning of the last century. Substantial progresses have been made in the past 100 years in this field. However, constructing viable models of complex rhythmic phenomena can often be quite a challenge.

Oscillations in biochemical systems originate from the existence of feedback loops in genetic and metabolic networks as a result of various modes of cellular regulation. Feedback regulations are arguably the most common control mechanisms employed by

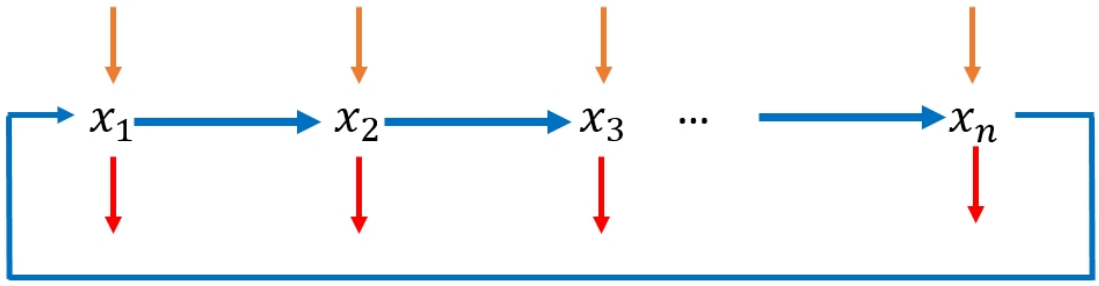

Figure 1.1: A feedback loop. Each arrow directed into x_i (and out of x_i) represents processes contributing to the synthesis (and degradation) of x_i, while each of the arrow directed from x_i to x_{i+1} represents either a negative or positive effect to the next variable in the chain [42].

cellular systems [115]. Biological systems contain many types of regulatory circuits, both positive and negative. Feedback is very important in the context of cell dynamics. The feedback interactions can impart precision, robustness and versatility to intercellular signals, while feedback failure can cause disease [66]. A negative feedback loop is one that tends to slow down a process, whereas the positive feedback loop tends to accelerate it. In biochemical systems, negative feedback loop is responsible for oscillation while the existence of positive feedback loop promotes oscillation in negative feedback loops [11]. A graphical representation of feedback loop can be seen in Fig. 1.1.

As mentioned before, the behavior of oysters are heavily influenced by biological rhythms. Biological rhythm resulted from negative feedback loop induces natural oscillation. Having better insight on oscillations may be useful in future to develop improved monitoring systems. Keeping this in mind, analysis and control of oscillation can be considered as an important theoretical problem. Oscillations (in the form of rhythm) are not only present in oysters but also in any kind of living organisms. One such oscillation is called circadian rhythm. It drives the circadian clock in living organisms. The period of circadian rhythm is approximately 24 hours. Circadian rhythm can be generated by synthetic genetic oscillators also [60]. In molecular biology, an oscillating gene is a gene that is expressed in a rhythmic pattern or in periodic cycles. Oscillating genes are usually circadian and can be identified by periodic changes in the state of an organism. Genetic oscillators play an important role in the area of synthetic biology and can be useful to generate artificial circadian clocks.

Recently, [77] has studied the impact of cell division on the phase of genetic oscillators through stochastic simulation. For this purpose [77] has used two oscillator models

namely the *repressilator* [60] and the Goodwin model [78]. Both of them can be used to model circadian clocks. Circadian clocks continue to oscillate across the cell division cycle. Since cell divisions create discontinuities in the dynamics of genetic oscillators, the question about the resilience of oscillations and the factors that contribute to the robustness of the oscillations may be raised. From the result of the stochastic simulations, it was found that for both models, extrinsic noise (variability in the cell division time and in the partition of the molecules into daughter cells, cell-cell variability in kinetic parameters, *etc.*) can destroy the synchronization among the mother daughter cells after the cell division. The result presented in [77] is numerical in nature and opens up the possibility to provide analytical results which correspond to the stochastic simulation results. In this thesis, we consider this problem with main focus on the cell division time which is one of the sources of extrinsic noise as well. Our work will be to provide sufficient conditions of phase synchronization after cell division which depends on the variability of cell division time. Our work is based on Phase Response Curve (PRC) approach [53]. PRC illustrates the transient change in the cycle period of an oscillation induced by a perturbation as a function of the phase at which it is received. Since cell division introduces discontinuities in the concentration of molecules which in turn reset the phase of oscillation, PRC could be very useful to analyze the impact of cell division on the phase of oscillations.

Many oscillatory systems are of multi-stable nature. For example, Van der Pol oscillator, FitzHugh–Nagumo model *etc.* Multistability accounts for the possible coexistence of various oscillatory regimes or equilibria in the phase space of the system for the same set of parameters. For a system exhibiting such behavior, it is frequently very difficult to predict the asymptotic regime which this system will attain for the given initial conditions. In this regard, an important theoretical problem is how to guarantee robust synchronization for this kind of systems. In this thesis, we will consider the synchronization problem for multistable systems based on the framework of Input-to-State Stability (ISS). ISS is a well established tool to study the stability and robustness of nonlinear systems. The classical definition potentially allows to formulate and characterize stability properties with respect to arbitrary compact invariant sets (and not simply equilibria). The implicit requirement is that these sets should be simultaneously Lyapunov stable and globally attractive. These requirements restrict the classes of system where ISS tool can be applied. Various attempts have already been taken to overcome the limitations or relax the restrictions [13, 16, 17, 37, 50]. A recent attempt was made in [14, 15]. They have extended ISS theory for multistable systems with decomposable invariant sets. In this thesis, this result will be applied to provide sufficient conditions that guarantees

robust synchronization for multistable systems.

Recently, [30] has proposed an oscillator model in the context of synchronization. This model will be called Brockett oscillator for further use. The specialty of this model lies in the fact that depending on a model parameter, the conventional averaging theory does not predict the existence of a periodic (almost periodic) solution. However, qualitative synchronization together with small amplitude irregular motion can be seen through numerical studies. Brockett oscillator exhibits multi-stability. As an application of our result on synchronization of multistable systems, this model will be considered and can be found in the appendix.

1.2 Outline of the thesis

This thesis is divided into two parts. In the first one, we discuss the use of oysters for the purpose of environmental monitoring. In the second part, the problem of synchronization of oscillatory systems is considered. Each part consists of two chapters for which side results are given in Appendix. Outline of the two parts can be consulted below:

Part I

Chapter 2

In this chapter the foundation of this thesis is presented. First, a detail review on the use of oysters as bio-indicators for environmental monitoring is given. Then we give an outline of our proposed model-based environmental monitoring approach. The proposed approach depends on EPOC High Frequency Non-Invasive (HFNI) valvometry dataset. Details of the HFNI based data collection can be found after the bibliography on existing bivalve based monitoring system. Then we present detailed description on the identification of the Grey-box model of valve movements activity considering biological rhythms. Next, we discuss the utility of this model for indirect environmental monitoring through abnormal behavior detection. Finally, an experimental validation of the proposed approach is given [8].

Chapter 3

In this chapter, we present the detection of a particular abnormal behavior (*i.e.* spawning) which is not related to pollution. First, we give the context of this work and present the existing literature on the detection of spawning. Next, we discuss in details

the spawning behavior and the behaviors we are particularly interested in. After that we present the detection algorithm. The algorithm depends on the energy signal which can be obtained by differentiation of valvometry signal (*i.e.* distance). The summary of various numerical differentiation techniques as well as associated signal processing methods (two types of filtering, decision logic *etc.*) are presented. Finally, this chapter ends with experimental validation of our algorithm on three different datasets collected in 2007, 2014 and 2015 [9].

Part II

Chapter 4

This chapter discusses the problem of phase resetting during cell division in the context of genetic oscillators. First, we present a motivating example through a simple model of circadian oscillations in *Neurospora.* We show that if cell division period varies widely, the phase among the mother daughter cell diverges after cell division. However, it is possible to overcome this problem through common entrainement. Next, we present Phase Response Curve (PRC) based phase model for an oscillator with cell division followed by main result of this chapter. Our result gives an analytical condition which can provide phase synchronization in the presence of cell division. Details about PRC can be found in Appendix A. We provide numerical simulation results on two different oscillator models to show the effectiveness of our theoretical results to conclude the chapter [2].

Chapter 5

This chapter discusses the problem of robust synchronization for multistable systems based on ISS framework. First, we give a brief literature survey on the classical definition of ISS and possible relaxations. Next, we provide the problem formulation and our contribution. Finally, this chapter ends with numeral simulation results. The results obtained in this chapter are global. Preliminaries on ISS of multistable systems with respect to decomposable invariant sets can be found in Appendix C [5].

Appendix B

This chapter applies the result of Chapter 5 to Brockett oscillator. First, we provide the stability analysis of autonomous and non-autonomous Brockett oscillator which helps to

prove the existence of decomposable invariant set. Next, we give global synchronization result for a family of non-identical Brockett oscillators with respect to decomposable invariant sets. Two synchronization protocols have been considered. Finally, we provide numerical simulation and experimental results to verify the theoretical results [3].

1.3 List of publications

1.3.1 Peer-reviewed international journals

1.3.1.1 Published

1. H. Ahmed; R. Ushirobira; D. Efimov; W. Perruquetti, "**Robust Synchronization for Multistable Systems**," in *IEEE Transactions on Automatic Control* , vol. 61, no. 6, pp. 1625-1630, June 2016.

2. H. Ahmed; R. Ushirobira; D. Efimov; D. Tran; M. Sow; L. Payton; J. C. Massabuau, "**A Fault Detection Method for Automatic Detection of Spawning in Oysters**," in *IEEE Transactions on Control Systems Technology* , vol. 24, no. 3, pp. 1140-1147, May 2016.

3. H. Ahmed; R. Ushirobira; D. Efimov; D. Tran; M. Sow; P. Ciret; J. C. Massabuau, "**Monitoring Biological Rhythms Through the Dynamic Model Identification of an Oyster Population**," in *IEEE Transactions on Systems, Man, and Cybernetics: Systems (early access)*

4. H. Ahmed; R. Ushirobira; D. Efimov, "**On robustness of phase resetting to cell division under entrainment**", Journal of Theoretical Biology 387 (2015): 206-213

1.3.1.2 Submitted

5. H. Ahmed; R. Ushirobira; D. Efimov; W. Perruquetti, "**Identification of a dynamical model for phytoplankton bloom based on high frequency measurements**"[4], *International Journal of Environment and Pollution* (2016) (Major Revision submitted).

6. H. Ahmed; R. Ushirobira; D. Efimov, " **Global robust synchronization of the Brockett oscillators**", *IEEE Transactions on Automatic Control* (2016) (Submitted)

7. L. Payton; H. Ahmed; R. Ushirobira; D. Efimov; D. Tran; M. Sow; J. C. Massabuau, " **Automatic harmful algal bloom detection using features based on laboratory experiment data**"[4] (2016) Under preaparation

[4]Not part of this thesis

1.3.2 Peer-reviewed international conferences

8. H. Ahmed; R. Ushirobira; D. Efimov, "**Robust synchronization of genetic oscillators subjected to cell division and common entrainment**", European Control Conference (ECC-2016), Aalborg, Denmark.

9. H. Ahmed; R. Ushirobira; D. Efimov, "**On the robust synchronization of the Brockett oscillators**", IFAC-PapersOnLine 49.14 (2016): 142-147.

10. H. Ahmed et al., "**On conditions of robust synchronization for multistable systems**", European Control Conference (ECC-2015), Linz, Austria.

11. H. Ahmed et al., "**Automatic spawning detection in oysters: a fault detection approach**", European Control Conference (ECC-2015), Linz, Austria.

12. H. Ahmed; R. Ushirobira; D. Efimov; D. Tran; J-C Massabuau, "**Velocity estimation of valve movement in oysters for water quality surveillance**", IFAC-PapersOnLine 48.11 (2015): 333-338.

13. H. Ahmed; R. Ushirobira; D. Efimov; D. Tran; M. Sow; J-C Massabuau, "**Dynamical model identification of a population of oysters for water quality monitoring**.", European Control Conference (ECC-2014), Strasbourg, France.

1.3.3 Local conference

14. H. Ahmed; R. Ushirobira; D. Efimov; W. Perruquetti, "**Identification d'un modèle dynamique du bloom phytoplanctonique basé sur des mesures à haute fréquence**"[4], Schmitt, F.G. et Lefebvre A. (Eds.) /Mesures haute résolution dans l'environnement marin côtier/, Presses du CNRS, ISBN - 978-2-271-08592-4. (2016)

Part I

Environmental monitoring using oysters as bio-sensors

Chapter 2

Identification of dynamical model of oysters population for water quality monitoring

2.1 Introduction

One of the most critical challenges that the global society currently faces is the risk of water pollution and scarcity. To circumvent this alarming problem, water resource management has been advocated all over the world and has become a cross-cutting issue. However, the management of aquatic ecosystems requires a well-designed and validated tool that is simple and inexpensive for the assessment and monitoring of these ecosystems to diagnose the causes of their degradation. This necessitates the development of an indirect environmental monitoring solution that can work 24/7 without any human intervention. In this context, bivalves can be very useful. The observation of the opening and closing activities of bivalves is a possible way to evaluate their physiological behavior in reaction to nearby water. The deviations from a considered normal behavior can be used for detecting a contaminant in surrounding water. Thus, our aim is to gain more insights into these reference natural conditions by focusing on the biological rhythms of the bivalve *in situ*.

The pioneer work that analyzes the bivalve's activities through the recording of their valve movements (e.g., valvometry) was realized by Marceau with smoked glazed paper [107]. Today, valvometers are commercially available[1] and are mainly based on the principle of electromagnetic induction, like the Mossel Monitor [96] or the Dreissena

[1] http://www.mosselmonitor.nl/

Monitor [28, 29]. In recent years, the interest for modeling and estimation of behavior of marine animals directly in real marine conditions has intensively increased [25, 69, 129].

A distinctive and remarkable monitoring solution has been realized in the EPOC CNRS UMR laboratory in Arcachon, France [131, 137, 144], where a new framework for noninvasive valvometry has been developed and implemented successfully since 2006. The system can work under field condition for a long period of time without *in situ* human intervention (> 1-2 years). No other system according to the best knowledge of the authors has operated for many years like this one, even in the laboratory environment. The monitoring solution was tested in the laboratory environment several years before being deployed into the sea. The designed method is strongly based on bivalve's respiratory physiology and ethology. The developed platform for valvometry was built using lightweight electrodes (approximately 100 mg each) linked by thin flexible wires to high-performance electronic units. The electrodes are capable to estimate the distance of the opening of the shell (see Fig. 2.2) for a mollusc with an accuracy of a few μm. Moreover, in the field, the energy consumption is very low, only 1 watt. One data point is generated every 0.1 sec (24 hours per day), for a bivalve, the electronic unit supports connection with 16 animals. Next, the results of measurements are transmitted by a wireless connection to the laboratory and the obtained data is publicly available online on the site of the project[2]. This system allows the bivalves to be studied in their natural environment with minimal experimental constraints. The obtained arrays of data of opening and closing activities of bivalves were used for analysis from different points of view using statistical approaches (estimation of probability density functions for time and amplitude of opening) [131, 137, 144].

Many researchers have studied the behavior of bivalves using valvometry and through chemical analysis of the tissues of oysters. In [106], authors have studied the impact of persistent organic pollutants on juvenile oysters through chemical analysis. They have shown that active biomonitoring is indeed possible on juvenile oysters. In [120], authors have studied the tissues of oysters collected from various locations of southern Texas. They have concluded through chemical analysis that the toxicity in the tissue could be used as an indicator of disturbed environments. Similar approach of using oysters as a biomonitoring tool through chemical examination can also be found in [1]. However, a chemical analysis is essential in all these cases.

In [61], authors have studied the valve activity behavior of two unionid mussel species in a eutrophic lake in southern Finland. Long term fluctuations in valve movements were observed and authors suggested that these fluctuations may be the reflection of the

[2]http://molluscan-eye.epoc.u-bordeaux1.fr/

enrichment of pollutants in the mussels. In [83], Asiatic clams were exposed to waters receiving chlorine containing industrial discharges. It was shown that the valves of the clams exposed to pollutants opened more often and for longer periods than clams not exposed to pollutants. A comparison of valve movement activity of fresh water mussel between lake and river was done in [62]. It was shown that the variability in valve opening is much higher in a river than in a lake. So, it can be concluded from this whole dataset that valve opening activities may have a relation to the habitat of the bivalves.

Recently, the effect of a specific pollutant (*i.e.* Arsenic) on the valve opening activity in freshwater clam in laboratory environment was done in [38, 91]. In these two papers, authors have used a statistical modeling approach (Hill [41] based dose response model) to see the effect of Arsenic on the valve opening activity by exposing the freshwater clams *Corbicula fluminea* to Arsenic contaminated water. In [61], it was shown that valve opening behavior is significantly different in their natural habitat than in a laboratory environment. This limits the scope of the results obtained in [38]. We propose here to develop an indirect monitoring system which is pollutant independent and also deals with natural habitat (*i.e.* the sea) through the rhythmicity identification of an oyster population.

For that purpose, the goal of this chapter is the identification of a physiological *dynamical* model of nonlinear autoregressive exogenous (NARX) type for bivalves using a high volume of data (~12.63 Gigabytes). The data came from a population of 16 oysters living in the Bay of Arcachon, France. The model takes into account the influence of external forces (like the sunlight and the moonlight, the tide level, precipitation, water salinity level). Since the behavior of oysters is also guided by internal circadian/circatidal rhythms, their influence is also incorporated in the developed NARX model. The type and the origin of the internal circadian/circatidal rhythms of bivalves is rather uncertain, that is why a side result of this chapter consists in verifying different hypotheses for modeling of circadian/circatidal rhythms for oysters. The proposed model is Grey-box type.

The outline of this chapter is as follows. A brief description of the measurement scheme and experiments is given in Section 2.2 (a more detailed information can be found in [131, 137, 144]). The model identification procedure is presented in Section 2.3. The verification of the model and its utility for an ecological monitoring of water quality are discussed in Section 2.4.

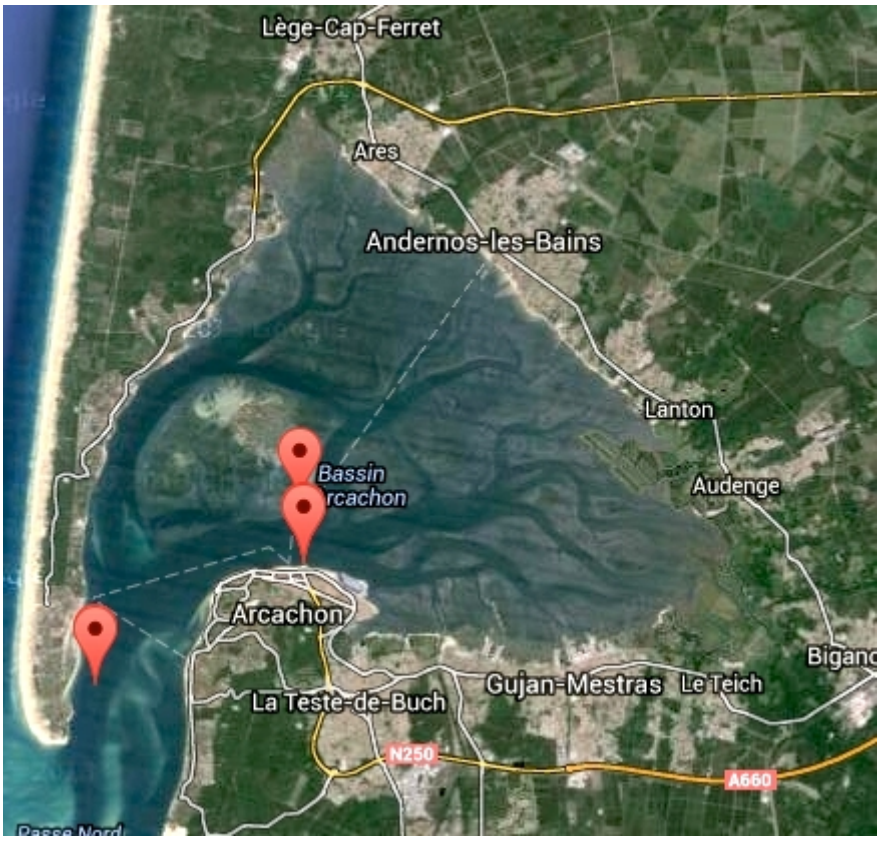

Figure 2.1: Location map (Courtesy of Google Maps), see also http://molluscan-eye.epoc.u-bordeaux1.fr/

2.2 Measurement System Description

The monitoring site is situated in the Bay of Arcachon, France, at the Eyrac pier (Latitude: 44°40 N, Longitude: 1°10 W). The map of the location can be seen in Fig. 2.1. Sixteen Pacific oysters, *Crassostrea gigas*, measuring from 8 cm to 10 cm in length were permanently installed on this site. These oysters were all from the same age group (1.5 years old) and came from the same local supplier. They also all grew in the Bay of Arcachon. They were submerged on the sea bottom (at 3 m to 7 m deep in the water, depending on the tide activity).

The principle of the total measurement process including the electronic equipment has been first described in [144]. The measurement system was further modified (adjusted to severe open ocean conditions and mainly mechanical not electronic) later on in [35, 145]. A significant advantage of the developed monitoring system (slave unit in the field) is that it is completely autonomous without *in situ* human interference for one full year. Each animal is equipped with two lightweight coils (sensors), $\approx$ 100 mg

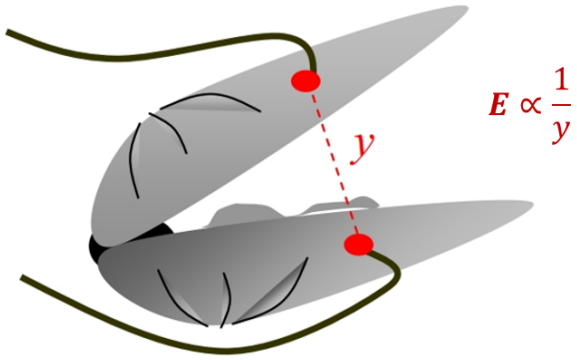

Figure 2.2: Graphical representation of the distance being estimated by the electrodes

each, attached to the edge of each valve. These coils measure $2.5 \times 2.5 \times 2$ mm and were coated with a resin sealing before attaching them on the valves. One of the coils sends a high-frequency sinusoidal signal, that is received by another coil. Measurements are performed every 0.1 sec successively (with the frequency 10 Hz) for each of the sixteen animals. This means that the behavior of a particular oyster is measured every 1.6 sec. Every day, 54000 triplets (1 distance, 1 stamped time value, 1 animal number) are collected for each oyster. The strength of the electric field produced between the two coils can be written as [137]:

$$E \propto \frac{1}{y} \tag{2.1}$$

where E is the strength of the electric field and y is distance between the point of measurement and the center of the transmitting coil. The equation (2.1) leads to an estimation of the distance between coils. The measured signal (y_{mv} in millivolts) is converted into distance in millimeters (y_{mm}) using the following calibration model [137]

$$\hat{y}_{mv} = \frac{151}{(\hat{y}_{mm})^{0.35}} - 1.48 \tag{2.2}$$

The distance being estimated can be seen in Fig. 2.2.

On the shore, a second electronic unit takes care of the data acquisition and transmission. This unit is equipped with a GSM/GPRS modem and uses a Linux operating system for driving the first control unit submerged in the water, managing the data storage with a time stamp, accessing the Internet, and transferring the data. An original self-developed software module runs on mobile phone technology. At the end of a working day, the collected data is transmitted to a central workstation server (the master unit) located in the Marine Station in Arcachon, France. The valve activity data is

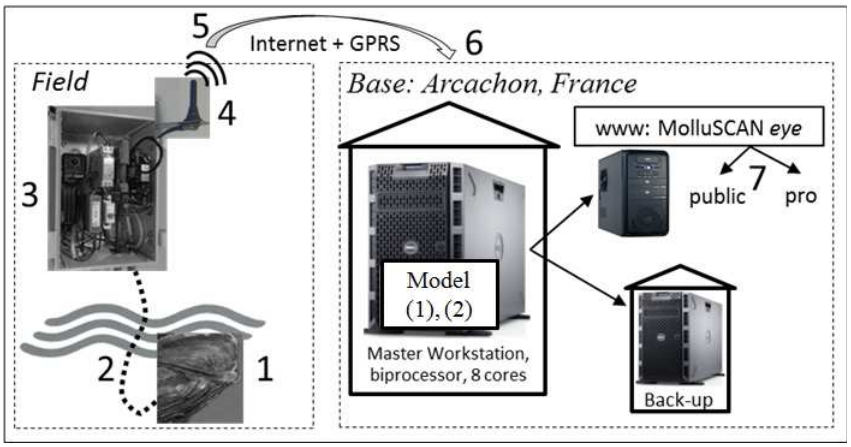

Figure 2.3: [131] Synoptic representation of the system, from field to laboratory: (1) Oyster equipped with two electrodes and 1st level electronic card in a waterproof case (immersed); (2) electrical connection between the first and the second electronic cards (umbilical); (3) 2nd level electronic card out of water; (4) GPRS antennae (5) GPRS and Internet connection; (6) Marine Station of Arcachon (Master unit) ready for daily update and for feeding internet (Google: molluscan eye); (7) daily update on internet for the general public (restricted access) and professionals (full access).

stored in a central database and the access to this database is provided via an Internet connection (under some restrictions on the amount of data). A schematic description of the monitoring system is presented in Fig. 2.3.

The collected tidal data includes a measurement of the height of the water column every hour, while the times and levels of low and high tides are provided by the hydrographic and oceanographic service of the marine[3]. To take into account the nycthemeral rhythm of the bivalve, the sun and the moon positions at the sampling site have been used.

It is worth to note that data losses in transmission were sometimes observed due to impairment of data transfer.

2.3 Model Identification

Summarizing the description given in the previous section, after a specified duration of the experiment, the electronic system provides a matrix of values of opening of valves for each oyster $P_{i,j}$ for $1 \leq i \leq N, \quad 1 \leq j \leq n, \quad$ where $n = 16$ is the number of oysters in the experiment and N is the number of measured points, $N = 54000 \times N_{days}$ with $N_{days} > 0$ is the number of days used for the identification of the model. The actual

[3]http://www.shom.fr/

valve distance is given in millimeters (mm) and the range is between 0 to 12 mm. In this chapter, the data of 2007 collected at the Eyrac pier in Arcachon has been used. So, $N_{days} = 365$. For the population *i.e.* for 16 oysters, the measurement system gave us total 315.36 million data points. In addition to the valve distance, the values S_i, M_i, W_i are also provided for $1 \leq i \leq N$. They characterize the sun and moon positions with respect to the horizon in degrees and the tide levels in meters respectively. The signals S_i and M_i take negative values for the corresponding positions below the horizon line. Besides the three periodic signals (*i.e.* S_i, M_i, W_i), some information regarding the rain profile (*i.e.* precipitation) and the water salinity level were also provided on a hourly basis and denoted as r_i and ℓ_i respectively for $1 \leq i \leq 24 \times N_{days}$.

The first problem that arises while dealing with the valve distance data is that its length is not uniform all through the year. Like almost every other animal, the size of oysters also changes as time passes by. We need to normalize the data between certain bound so that the effect of change of length of distance can be compensated. The normalization was done considering a 6 days window and with a bound $[0, 1]$, where 0 represents the complete closing of the valve while 1 represents the complete opening of the valve. The formula to calculate the normalized value is:

$$p_{i,j} = \frac{P_{i,j} - \min_{a=i-N_t,\cdots,i}(P_{a,j})}{\max_{a=i-N_t,\cdots,i}(P_{a,j}) - \min_{a=i-N_t,\cdots,i}(P_{a,j})} \tag{2.3}$$

where N_t is the total number of data points in last 6 days, $P_{i,j}$ is the actual valve distance and $p_{i,j}$ is the normalized valve distance. The next question that arises is how to use the data of 16 different oysters for the model identification of the population. The normalized valve distance of three different oysters can be seen in Fig.2.4. From this figure, it can be observed that although the behavior of all these oysters is not exactly the same, the correlation between the behaviors is also not that weak[4]. So, averaging the behavior of all oysters can be a good way to capture the dynamics of the population. Since $N \approx 2 \times 10^7$, to simplify the computation and the presentation of this study, the measurements have been averaged on an hourly basis *i.e.* define $\delta N = \frac{3600[sec]}{1.6[sec]} = 2250$ and $L = \frac{N}{\delta N}$, then for

[4]The correlation coefficient of oyster 1 with respect to oyster 2,3,...,16 are 0.4474, 0.5651, 0.4811, 0.5335, 0.3739, 0.4824, 0.3504, 0.4654, 0.2446, 0.1083, 0.4606, 0.2378, −0.181 and 0.3871 respectively.

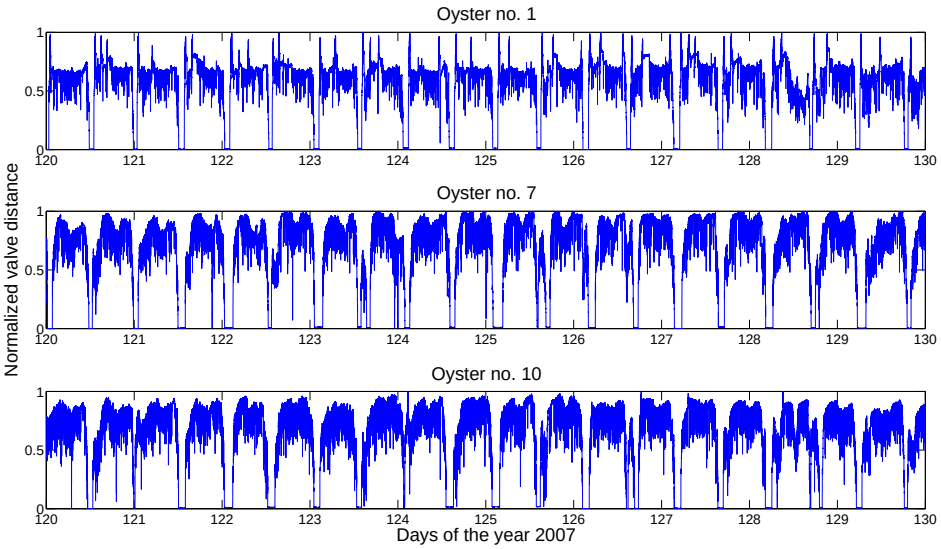

Figure 2.4: Examples of normalized valve distance of three oysters during 10 days (sampling period, $T_s = 1.6$ sec.)

all $1 \leq k \leq N_{days} \times 24$ and $1 \leq j \leq n$:

$$\begin{aligned} p_{k,j} &= \delta N^{-1} \sum_{q=(k-1)\delta N+1}^{k\delta N} P_{q,j}, \\ s_k &= \delta N^{-1} \sum_{q=(k-1)\delta N+1}^{k\delta N} S_q, \\ m_k &= \delta N^{-1} \sum_{q=(k-1)\delta N+1}^{k\delta N} M_q, \\ w_k &= \delta N^{-1} \sum_{q=(k-1)\delta N+1}^{k\delta N} W_q, \end{aligned} \tag{2.4}$$

corresponds to the hourly averaged opening of the valves, the sun and moon positions, the water level respectively. The examples of obtained signal s_k, m_k and w_k are shown in Fig.2.5 (top). In Fig. 2.5 (bottom), the frequency spectrum of these periodic/quasi periodic signals can be seen. Finally, precipitation and water salinity level information are shown in Fig. 2.6.

The averaged opening position of valves, on an hourly basis, for the investigated

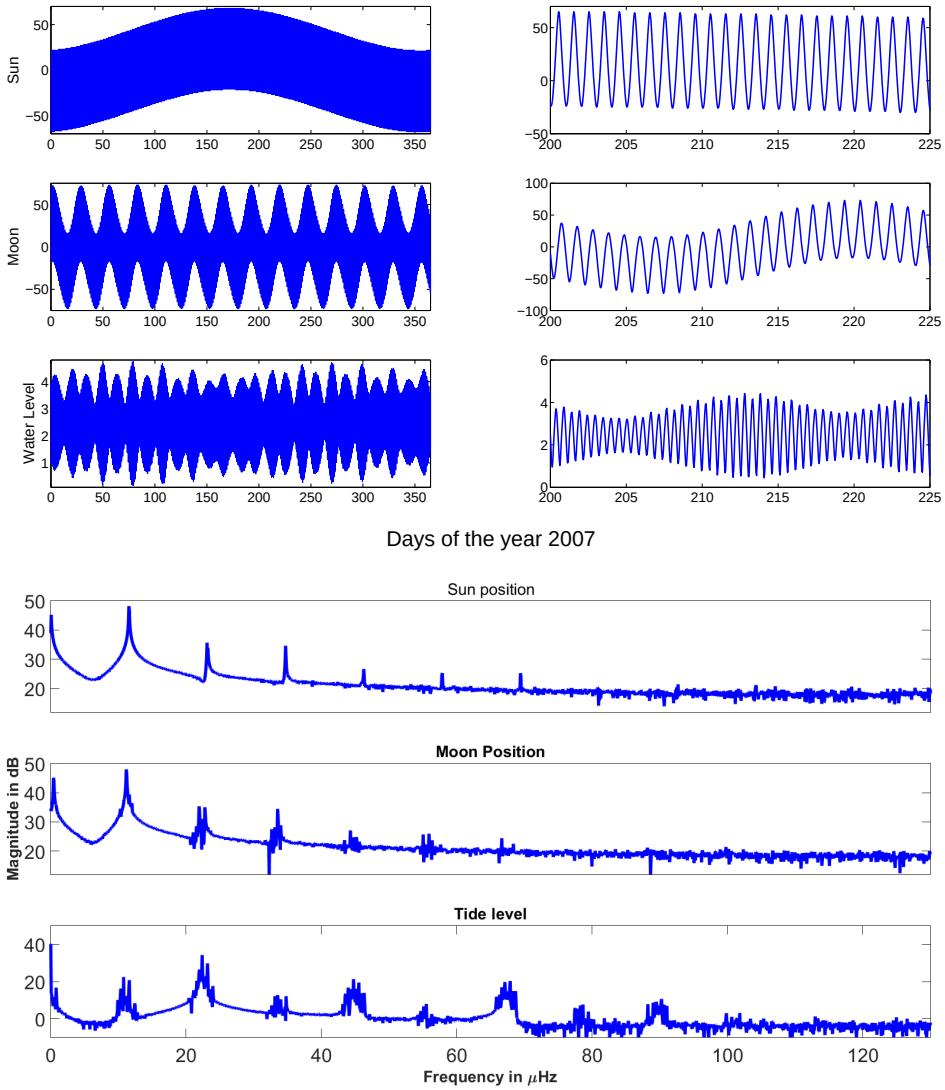

Figure 2.5: Top) Sun and moon position, tide level (left column-original signal, right column-zoomed version) during a whole year (2007) bottom) Frequency spectrum of the signals.

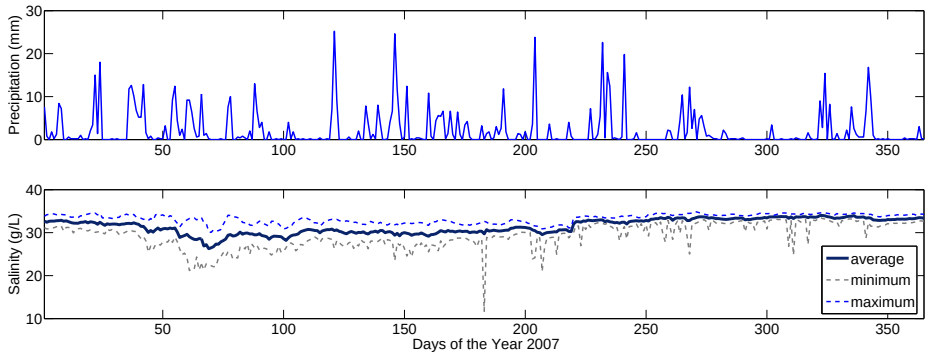

Figure 2.6: Precipitation (top) and water salinity level (bottom) during the year 2007 (one data point each day)

population of oysters can be defined as for all $1 \leq k \leq N_{days} \times 24$:

$$h_k = n^{-1} \sum_{j=1}^{n} p_{k,j} \tag{2.5}$$

The averaged valve opening of the population h_k can be seen in Fig. 2.7.

From Fig. 2.7, it can be easily inferred that the opening average of valves on an hourly basis for the population h_k has a more regular and smoother behavior than individual ones. This behavior leads us to consider the signal h_k as a suitable choice for forthcoming analysis and model identification. Thus an averaged physiological population dynamics has to be modeled and identified for oysters. An additional motivation for this choice is standard in modeling biological systems: each individual exhibits a proper variability according to stochastic exogenous and endogenous forces, which are hard to predict or measure, while an averaged signal h_k is less sensitive to these perturbations and represents mainly the regular physiological behavior of the animals. Naturally, this is especially true if the population size n is big (this is not the case in the considered application due to various experimental complexities forcing us to limit the population size to 16). Another alternative to averaging can be using population models similar to what is developed to characterize the effect of drug treatments in [152, 153]. However, those models require a larger population size and heterogeneity among the animals. In our case, the population size is very small. Moreover, the oysters are not very heterogeneous. They all are of the same age group (1.5 years), collected from the same local supplier and were raised in the same place (bay of Arcachon). The correlation among the oysters is not weak as well. All the inputs of our model (water salinity, water level, etc.) were also available on an hourly basis. Thus, an hourly averaging is natural in our

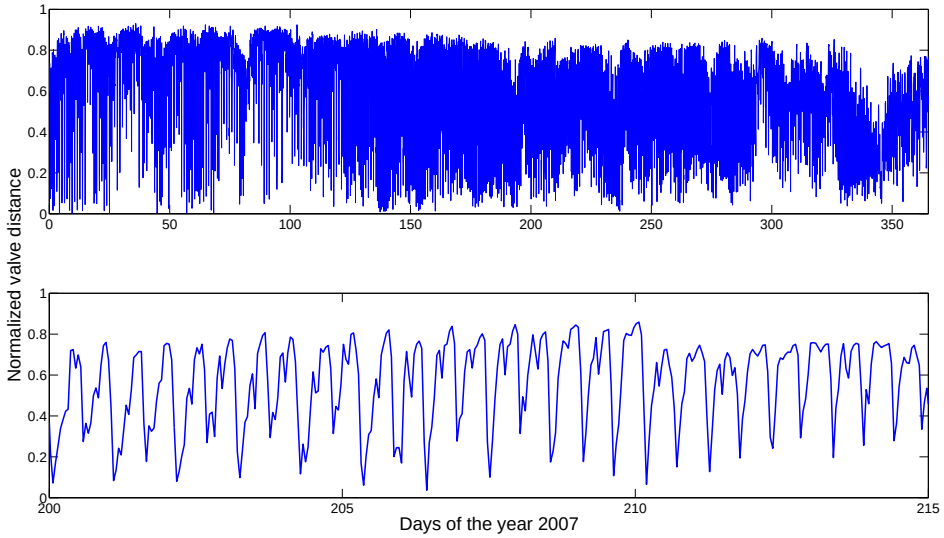

Figure 2.7: Hourly averaged valve opening of the population (top-original signal, bottom-zoomed version) (one data point each hour)

case.

It is known [145] that the opening activity of oysters h_k is externally governed by the sunlight, moon oscillations and the tidal activity, denoted here by s_k, m_k and w_k respectively. Moreover, the precipitation (r_k) and the salinity level in the water (ℓ_k) may also have an external impact on the opening activity of oysters. Other sources of rhythmicity are internal (feeding, breathing *etc.*) and supervised by internal clocks. The reference signal generated by circadian rhythm genetics, which is directly influencing h_k, will be denoted by c_k. The generic structure of a dynamical physiological model for a population of oysters can be presented as follows :

$$h_k = F(h_{k-1}, \dots, h_{k-\nu}, s_k, \dots s_{k-\mu}, m_k, \dots m_{k-\mu}, w_k, \dots w_{k-\mu}, r_k, \dots r_{k-\mu}, \ell_k, \dots \ell_{k-\mu}, c_k, \dots c_{k-\mu}, \theta) + \epsilon_k, \tag{2.6}$$

$$c_k = D(\xi_k), \tag{2.7}$$

$$\xi_k = G(\xi_{k-1}, s_k, \dots s_{k-\mu}, m_k, \dots m_{k-\mu}, w_k, \dots w_{k-\mu}),$$

where $\nu \geq 0$ represents the number of past events taken into account by the animals in order to determine the opening distance at the next time instant k (*i.e.* in this model $k-1$ is the current time instant and h_{k-1} is the current valve state); $\mu \geq 0$ is the number of previous values for the positions of sun/moon, tide levels, precipitation and water salinity levels that are used in the decision on the value of h_k (the model (2.6)

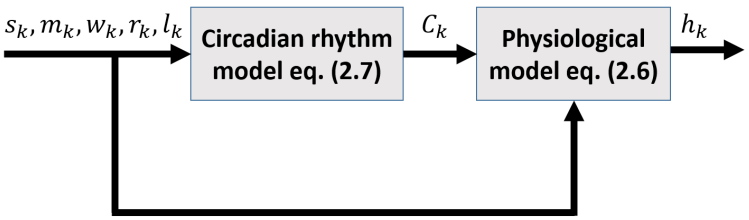

Figure 2.8: Structure scheme of the generic model (2.6), (2.7)

assumes that the instantaneous values of s_k, m_k, r_k, ℓ_k and w_k can be used for this decision); $\epsilon_k \in \mathbb{R}$ is the disturbance representing additional uncertain influencing forces and approximation errors (it is assumed that this term is sufficiently small if the model has been well identified); $\theta \in \mathbb{R}^q$, $q > 0$ is the vector of constant parameters of the model (2.6), and $F : \mathbb{R}_+^{\nu+6\mu+6+q} \to \mathbb{R}_+$ is a function defining the physiological model structure; $\xi_k \in \mathbb{R}^p$ is the state of the circadian oscillator (2.7); the functions $G : \mathbb{R}^{p+3\mu+3} \to \mathbb{R}^p$ and $D : \mathbb{R}^p \to \mathbb{R}$ define the structure of the circadian rhythm model (2.7). The model (2.7) assumes that circadian oscillations are entrained by the external cues s_k, m_k and w_k (some of them depending on the type of the rhythm under consideration, see below). The structural scheme of the model is given in Fig. 2.8.

The identification procedure consists in selecting an appropriate structure for the physiological model $F(\cdot)$ and the circadian model $G(\cdot)$, $D(\cdot)$, with posterior calculation of the corresponding vector of parameters θ.

Further, in this section two problems are considered. First, the issue of circadian rhythms modeling is discussed and a solution is proposed. Second, an ARMAX structure is selected for $F(\cdot)$ and the corresponding model is designed.

2.3.1 Models of circadian clocks

A rhythm in chronobiology is a biological process that displays an endogenous and self-sustained oscillation with a period of about 24 hours, for instance the circadian rhythm. These rhythms are driven by an internal clock, *i.e.* by a biochemical embedded mechanism. Their main properties are the generation of periodic rhythms, endogeneity, adaptability to a local environment by external forces called zeitgebers (the most important one being daylight for terrestrial animals), and robustness over a range of physiological temperatures. Rhythms have been observed in almost all forms of living organisms, from cyanobacteria and plants to mammals. The science of biological temporal rhythms, such as solar and lunar related rhythms, is called chronobiology [113][49].

2.3.1.1 Hypothesis on clocks

There exist many mathematical models of clock mechanisms [75, 95, 135]. Different hypotheses on the nature of clocks presented in oysters [145] have been issued, but not yet supported by a mathematical model. First, as many animals, the oysters may have circadian oscillations with the period of 24 hours synchronized by sunlight (*i.e.* *circadian* clock). Second, as animals living in a tidal ecosystem, they may also have a second rhythm with the period 12.4 hours and entrained by the tides, which may be driven by a *circatidal* clock. Third, the oyster rhythms may be regulated by the moon with the period 24.8 hours under the control of *circalunidian* clocks. The diversity of hypotheses follows the variety of the habitation areas of bivalves, e.g. arctic zones (where the sunlight may have approximately constant intensity during several months), open ocean conditions with strong tides or Mediterranean bays, where tides are almost negligible. Finally, this motivates the fourth hypothesis: a unique "circadian/circatidal" clock, synchronized by sunlight and tides, generating a bimodal rhythm running from 12.4 to 24.8 hours depending on the local biotope conditions. Among several different cases regarding the nature of the circadian clock, two hypotheses have been considered, namely:

1. Hypothesis 1 (H1): The rhythm of the oysters is governed mostly by a circadian clock in response to sunlight.

2. Hypothesis 2 (H2): The rhythm of the oysters is governed mostly by a circatidal clock and a circadian clock in response to the tide level and sunlight simultaneously.

The structural scheme of the model for the two different hypotheses is given in Fig. 2.9. Based on these two hypotheses, the corresponding mathematical models are developed below.

Conventional models of oscillators [75, 95, 135] have different complexity. There exist also methods to design generic oscillating systems [54] of any complexity. However, as it was observed in [57, 63] any oscillating system on the limit cycle can be fully characterized by its current phase and the form of limit cycle (*i.e.* amplitude of oscillations). Therefore, if an exact genetic or biochemical nature of oyster oscillations is not clear, then in order to preserve the model simplicity, the oyster rhythm can be represented by any oscillator, and a particular attention has to be paid to a relation of the phase of this oscillator and environmental rhythms. In [20, 63] variants of Van der Pol oscillator [93] have been used for modeling circadian rhythms in different animals. The Van der Pol oscillator has a simple planar mathematical model with just two parameters that allows

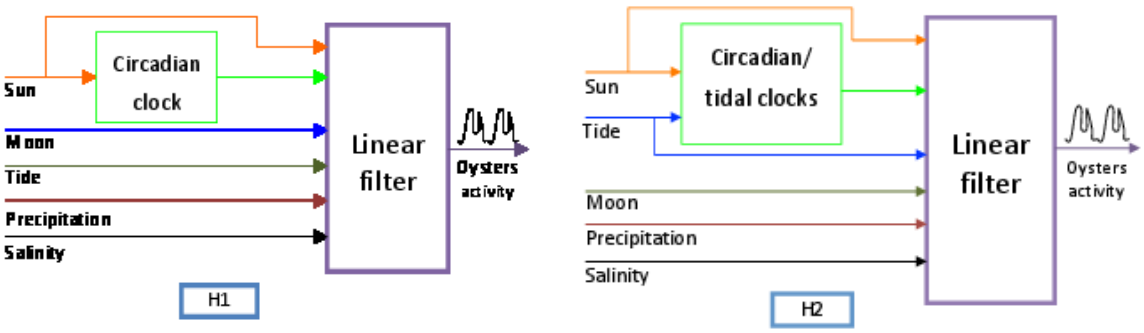

Figure 2.9: Structure scheme of the model for H1 and H2

the form of the limit cycle and the period of oscillations to be tuned:

$$\begin{aligned}\dot{\xi}_1 &= \alpha\left[\xi_2 + \mu\left(\xi_1 - \frac{4}{3}\xi_1^3\right) + u\right],\\ \dot{\xi}_2 &= -\alpha\xi_1,\end{aligned} \tag{2.8}$$

where $\xi_1 \in \mathbb{R}$ and $\xi_2 \in \mathbb{R}$ are the model states, $\alpha > 0$ determines the model oscillation velocity (adjustment of this parameter regulates the period of oscillation for the model); $\mu > 0$ is a parameter to determine the shape of oscillations ($\mu \approx 0$ for almost harmonic oscillations, $\mu \geq 2$ leads to a nonlinear profile); $u \in \mathbb{R}$ is the model input that can be used for the entrainment. In our case, the parameter α has to be selected in order to ensure the period of oscillations of 24 hours for the first hypothesis and 24.8 for the third one, for instance. The form of oscillations on the limit cycle, *i.e.* the value of parameter μ, is less important since in the model (2.6), (2.7) the shape of c_k can be taken into account later in the function $F(\cdot)$ and by tuning the parameters θ (the value $\mu = 2$ is used in this chapter for all computations). Therefore, the functions $G(\cdot)$ and $D(\cdot)$ in (2.7) can be defined based on Van der Pol equations discretized using the Euler method:

$$\begin{aligned}\xi_{1,k} &= \xi_{1,k-1} + T\alpha\left[\xi_{2,k-1} + \mu\left(\xi_{1,k-1} - \frac{4}{3}\xi_{1,k-1}^3\right) + u_k\right],\\ \xi_{2,k} &= \xi_{2,k-1} - T\alpha\xi_{1,k-1},\\ c_k &= \max\{0, \xi_{1,k}\},\end{aligned} \tag{2.9}$$

where $T = 1$ hour is the sampling time, c_k is the positive part of ξ_1 and u_k is the resetting input, which has to be specified.

The entrainment regulates the phase of oscillations (it synchronizes the exogenous cues and endogenous rhythms), the mechanism of entrainment and phase resetting can

be well analyzed using the Phase Response Curve approach [51, 57]. For example, for the first hypothesis, we select $u_k = \rho \max\{0, s_k\} / \max_{1 \le k \le L} |s_k|$, where $\rho > 0$ is the scaling parameters that is selected to harmonize the amplitude of the input u_k and the dimension of the limit cycle. The selection $\max\{0, s_k\}$ is applied since for the oyster rhythm the daylight is the principal zeitgeber, and the light is emitted when the sun is above the horizon only. For the first hypothesis, $u_k = s_k$, is the position of the sun, while for the second hypothesis, u_k has the following form:

$$u_k = [\lambda_s \ \lambda_w] \ [s_k \ w_k]^T \tag{2.10}$$

where λ_s and λ_w are the weights regulating the influence of the sun position s_k and the tide level w_k on the circadian oscillation. For the second hypothesis, in addition to the sunlight, we have also the tide/water level as zeitgeber. In order to harmonize the amplitude of the water level, we have selected w_k as $w_k = \rho w_k / \max_{1 \le k \le L} |w_k|$.

To generate the signal c_k using the proposed model it is necessary to properly assign the initial phase of the oyster clock model (the initial position on the limit cycle), which has to be coordinated with the current zeitgebers activity. A possible solution is to apply to the model the input patterns extracted from the first month of the experiment (or the last one in our case, since the experiment duration is 1 year and the inputs-sun position, moon position and the tide level have annual periodicity) several times in order to entrain the oscillator.

2.3.2 ARMAX model

The ARMAX (auto-regressive–moving-average with exogenous inputs) model is one of the most popular structures used for identification in various fields of science [103, 114, 147]. Its advantages include linearity with respect to all signals and parameters, different effective methods for calculation of the parameters, simplicity of stability analysis of the obtained model, robustness and sensitivity with respect to perturbations. Therefore, the function $F(\cdot)$ in (2.6) is selected in the following form:

$$\begin{aligned} F(\cdot) = &\sum_{i=1}^{\nu} \theta_i^h h_{k-i} + \sum_{j=0}^{\mu} \theta_i^s \tilde{s}_{k-j} + \sum_{j=0}^{\mu} \theta_i^m \tilde{m}_{k-j} + \sum_{j=0}^{\mu} \theta_i^w w_{k-j} + \sum_{j=0}^{\mu} \theta_i^r r_{k-j} \\ &+ \sum_{j=0}^{\mu} \theta_i^\ell \ell_{k-j} + \sum_{j=0}^{\mu} \theta_i^c c_{k-j}, \end{aligned} \tag{2.11}$$

$$\theta = [\theta_1^h, \ldots, \theta_\nu^h, \theta_0^s, \ldots, \theta_\mu^s, \theta_0^m, \ldots, \theta_\mu^m, \theta_0^w, \ldots, \theta_\mu^w, \theta_0^r, \ldots, \theta_\mu^r, \theta_\mu^\ell, \ldots, \theta_\mu^\ell, \theta_0^c, \ldots, \theta_\mu^c]^T,$$

where the positive values $\tilde{s}_k = \max\{0, s_k\}$ and $\tilde{m}_k = \max\{0, m_k\}$ of the signals s_k and m_k respectively are used to model the influence of the sunlight and moonlight (the sun and the moon are above the horizon and deliver the light when s_k and m_k are positive only). Formally the proposed function $F(\cdot)$ is nonlinear with respect to its arguments s_k and m_k (it contains $\max\{\cdot\}$). The nonlinear model under consideration, including the effect of circadian clock has the NARX structure (2.6), (2.7) for the selected $F(\cdot)$ and $G(\cdot)$, $D(\cdot)$. A summary of NARX type model can be found in [103].

2.4 Hypothesis selection, verification and analysis

Using the Least Square method [103, 114, 147], the estimates $\hat{\theta}$ of the parameters θ have been calculated for the dataset collected at the Eyrac pier, the Bay of Arcachon, France, 2007:

$$\hat{\theta} = (\Phi^T\Phi)^{-1}\Phi^T\Upsilon, \tag{2.12}$$

where $\Upsilon = [h_{\nu+1}, \ldots h_L]^T$ and the jth row of the matrix Φ,

$$\begin{aligned}\Phi_j \;=\; & [h_{j+\nu-1}, \ldots, h_j, \tilde{s}_{j+\nu}, \ldots, \tilde{s}_{j+\nu-\mu}, \tilde{m}_{j+\nu}, \ldots, \tilde{m}_{j+\nu-\mu}, w_{j+\nu}, \ldots, w_{j+\nu-\mu}, \\ & r_{j+\nu}, \ldots, r_{j+\nu-\mu}, \ell_{j+\nu}, \ldots, \ell_{j+\nu-\mu}, c_{j+\nu}, \ldots, c_{j+\nu-\mu}]\end{aligned}$$

for all $1 \leq j \leq L - \nu$.

2.4.1 Hypothesis selection

In 2.3.1.1, we have considered two different hypotheses, namely H1 & H2. A performance comparison of models based on H1 and H2 with experimental data can be seen in Fig. 2.10. From these results, no definitive conclusion can be drawn regarding the superiority or inferiority of any individual hypothesis. Both of them are almost identical. We are working with oysters living in real-life situation, *i.e.* in the sea, therefore oysters behaviors are influenced by a multitude of factors (and not only by the sun and moon position or water tide or precipitation or water salinity level). Hence, our suggestion in this case is that the effect of different cyclic inputs on oysters, like circadian clocks, might be better observed if we can place them in a controlled laboratory environment. In that case, we can experiment with individual inputs and will be able to observe the

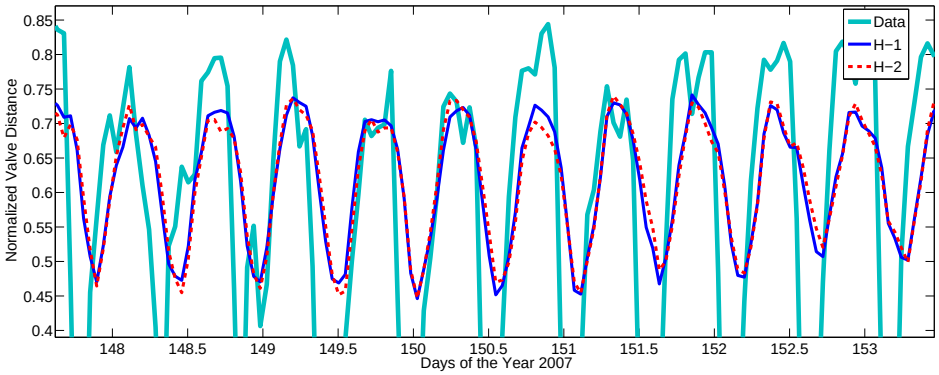

Figure 2.10: Comparative performance of two different hypotheses based model with actual data

response of oysters to that input. However, in our current situation we think that the second hypothesis is more realistic than the first one as it involves both sunlight and tide at the same time. For marine animals, to consider the effect of the tide along with sunlight on internal clocks is a very natural choice. So, for further analysis, we have selected the model based on hypothesis 2.

In hypothesis 2, the internal clock of oysters is influenced by sunlight and tide at the same time. So, a natural question is: what is the impact of individual inputs (sunlight and tide) on the behavior of oysters? To attempt to answer this question, we have considered three different situations. First, in case 1, we assumed that both inputs have equal weights *i.e.* $\lambda_s = \lambda_w = 0.5$. Second, in case 2, more weights on tide level were considered ($\lambda_w = 0.75$, $\lambda_s = 0.25$). Finally, in case 3, more weights on sunlight were imposed ($\lambda_w = 0.25$, $\lambda_s = 0.75$). The impact of these three cases on oysters can be seen in Fig. 2.11. From this figure, it can be seen that the performance of the model based on equal weights has better performance than the other two cases. Following this observation, we have considered equal weights on both sunlight and tide level for further analysis and verification.

2.4.2 Verification

To evaluate the obtained accuracy of the designed model, two performance costs J_ϵ and J_p have been calculated. The cost J_ϵ estimates the average amplitude of ϵ_k (the approximation errors in the model): $\epsilon_j = h_{j+\nu} - \hat{h}_{j+\nu}$, $\hat{h}_{j+\nu} = \Phi_j^T \hat{\theta}$, $1 \leq j \leq L - \nu$ and

$$J_\epsilon = \sqrt{\frac{\sum_{j=1}^{L-\nu} \epsilon_j^2}{L - \nu}}.$$

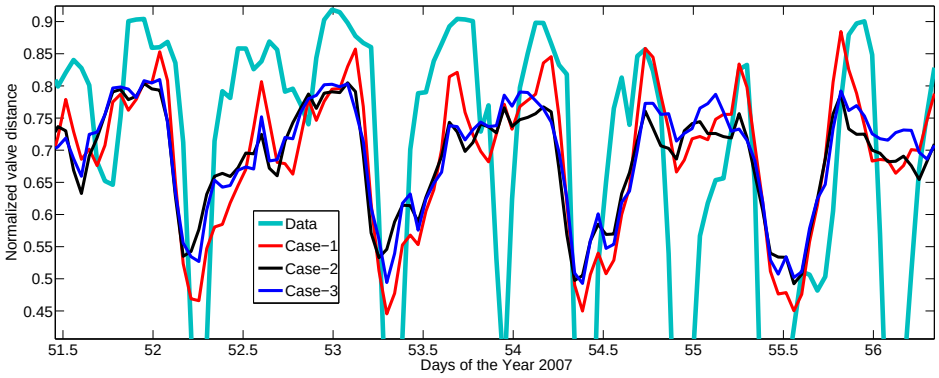

Figure 2.11: Impact of sunlight & tide level on the behavior of oysters

The cost J_p evaluates the prediction quality of the model on an infinite time interval: $e_j = h_{j+\nu} - \tilde{h}_{j+\nu}$, $1 \leq j \leq L - \nu$ and

$$J_p = \sqrt{\frac{\sum_{j=1}^{L-\nu} e_j^2}{L-\nu}} \quad \text{where}$$

$$\begin{aligned}
\tilde{h}_k &= h_k, \quad 1 \leq k \leq \nu, \\
\tilde{h}_{\nu+j} &= \sum_{i=1}^{\nu} \theta_i^h \tilde{h}_{\nu+j-i} + \sum_{z=0}^{\mu} \theta_i^s \tilde{s}_{\nu+j-z} + \sum_{z=0}^{\mu} \theta_i^m \tilde{m}_{\nu+j-z} + \sum_{z=0}^{\mu} \theta_i^w w_{\nu+j-z} \\
&\quad + \sum_{z=0}^{\mu} \theta_i^r r_{\nu+j-z} + \sum_{z=0}^{\mu} \theta_i^\ell \ell_{\nu+j-z} + \sum_{z=0}^{\mu} \theta_i^c c_{\nu+j-z}, \quad 1 \leq j \leq L - \nu
\end{aligned}$$

are the estimates of the valve positions h_k generated independently by the designed model in the presence of the same inputs. Examples of the obtained estimates $\hat{h}_k$ and $\tilde{h}_k$ (for $\nu = \mu = 72$, *i.e.* the oysters have 3 days of memory) for the second hypothesis are shown in Fig. 2.12, with performance costs $J_\epsilon = 0.08$ and $J_p = 0.19$. We conclude from this example that the model demonstrates a sufficiently good accuracy of representation of the physiological behavior of oysters.

2.4.3 Application to ecological monitoring

As it has been noted in chapter 1, ecological monitoring is in some part expensive and invasive of the environment under study (an extensive or poorly planned monitoring carries a risk of environmental degradation). This fact may be critical in wilderness areas or those that are averse to human presence. Some monitoring techniques may be

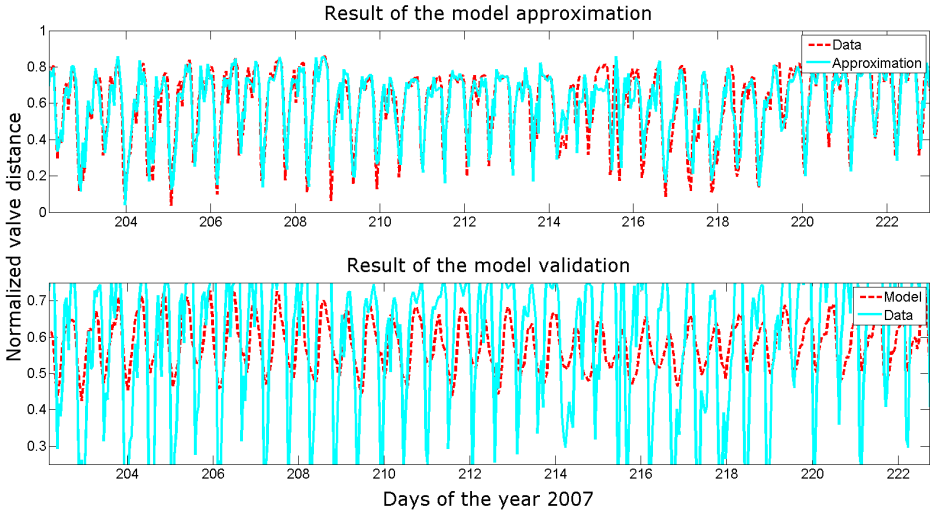

Figure 2.12: The results of the model numerical verification

very damaging, at least to the local population and can also degrade public trust in scientists carrying out the monitoring. That is why remote sensing and mathematical modeling become very important. Obviously, the application of a far-reaching mathematical modeling can reduce the cost of monitoring, while improving its safety and accuracy.

The area of population of bivalves is rather large, and the developed physiological model can serve for water quality monitoring, if we would compare the real measurements h_k obtained by an embedded electronic unit on a bay and the estimates provided by the model $\tilde{h}_k$. For example, the following daily monitoring residual can be computed:

$$r_k = \frac{1}{24} \sum_{z=0}^{23} |h_{k-z} - \tilde{h}_{k-z}| \tag{2.13}$$

for all $24 \leq k \leq L$, where an averaging on 24 hours is used to decrease sensitivity of the residual with respect to measurement noises. For the data set collected at the Eyrac pier in 2007, the obtained residual r_k is shown in Fig. 2.13. It is worth to stress that the Eyrac pier in the Bay of Arcachon is located in a fairly clean and well-protected area, but as we can see, the residual presented a peek value at the beginning of the December 2007. In fault detection literature [87, 154], the peak is known as a fault (*i.e.* a deviation from normal behavior). So, the detection of this fault is equivalent to the detection of pollution. The peak actually corresponds to a time period of heavy rain. Since the output of a storm sewer is located at about 10-15 meters from the oysters and as there was no change of salinity at that precise time (Fig. 2.6 bottom), we suggest

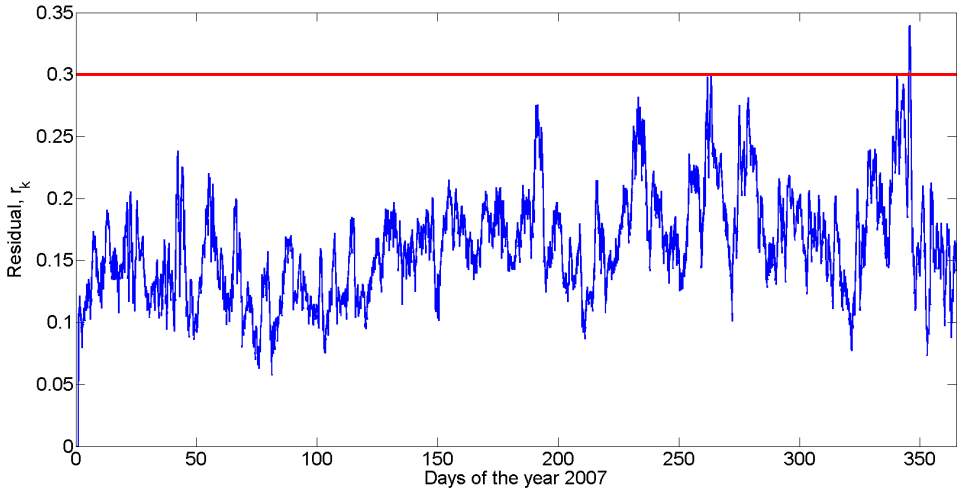

Figure 2.13: Residual for water quality monitoring

that some unknown contaminant, washed by the rain, could have reached them. This simple case study justifies the utility of the developed approach in automated systems tracking silent pollution.

2.5 Conclusion

This chapter presents the first development of a dynamical physiological model for oysters, which takes into account an influence of external cycles (daylight, moonlight and tides), externally influencing factors (like precipitation and water salinity level) and internal clocks as well. A generic "black-box" modeling approach has been used, and NARX structure of the model has been selected. It properly fits the idea that the clock mechanism in oysters is driven by tide and sunlight simultaneously. The obtained model has been successfully applied to automatically and fast detecting an abnormal deviation of behavior which occurred after a rainy period in Arcachon, France.

Chapter 3

Automatic detection of spawning in oysters: a fault detection approach

3.1 Introduction

In this chapter, we are interested in a particular behavior of oysters, *i.e.* their behavior during reproduction also known as spawning. Spawning is characterized by rapid and rhythmic contraction and relaxation of the valves to expel eggs in the water. Spawning observation is important in domains like aquaculture, ecology, *etc.* In Chapter 2, it was shown that the deviation of valve activity from normal behavior (*i.e.* slow and non rhythmic contraction and relaxation of valve) can be used as an automatic tool to suspect pollution in surrounding water. Spawning behavior is a deviation from normal behavior but not caused by pollution, so it is necessary to distinguish spawning from any other behavior. The motivation of the current chapter comes from this necessity. Here, the work is based on the valve activity dataset of the MolluSCAN-eye project recorded in the Bay of Arcachon, France in 2007, 2013 and 2014. Details about the data collection procedure have been described in Section 2.2.

Our goal in this chapter is to develop an algorithm that can automatically detect spawning in oysters using the valves movements data (*i.e.* the distance between the two valves of the oyster). In [68], P. S. Galtsoff did this detection by visual inspection under laboratory conditions. Due to various technical limitations (for example, unavailability of appropriate sensors in 1938), the recording of valve movements were limited in order to measure the data. This type of approach required constant attention, labor and experience to analyze and detect some spawning behavior, as it occurs once or twice a year. An increasing number of online measurements for different populations of oysters makes this manual detection approach unpractical due to a big amount of data to be

permanently analyzed visually by an expert. Therefore a solution is an automatic detection of the spawning that can save a lot of time and resources. In this perspective, spawning can be then considered as a deviated behavior or as a fault [27, 87, 154]. This chapter proposes the algorithm to detect this phenomenon.

The novelty and the relevance of this chapter lie on a new application of the fault detection theory for the analysis of bivalve physiology and for an automatic recognition of spawning. In this case, spawning is considered as a deviation from the normal behavior, then it can be interpreted as a "fault" of the system, which has to be detected. Introducing several differentiation algorithms as software sensors of valve movement velocity, the analytical redundancy approach is applied for this biological system. In general, in biological or medical applications, it is rather difficult to apply an engineering approach due to lack of measured information and mathematical models. However, in the considered application the valve distance measurements are available with a required frequency that makes possible the use of control engineering tools in the new setting. In addition, we hope that, the reported application of detection of complex oscillatory behavior is of interest by itself, for the control engineering community.

The outline of this chapter is as follows: spawning behavior of oysters are summarized in section 3.2 while the detection of spawning is presented in section 3.3. Section 3.4 contains the results and the discussion. The conclusion of this work can be found in Section 3.5.

3.2 Spawning of Oysters

For oysters, the experimental study of spawning dates back to 1938, when American biologist Paul S. Galtsoff published his seminal work on the physiology of reproduction of oysters [68]. Based upon laboratory observation, spawning is a specific/particular type of shell/valve activity of female oysters [23, 85]. In [68], an ostreograph was used to measure the valve activity and that data was later used to study spawning. Under normal environmental conditions shell/valve movements are characterized by long relaxation periods which may vary from a few minutes to hours and are often interrupted by secondary contractions. While during spawning (see Fig. 3.1 or Fig. 3.2, oysters N° 1 and N° 3), it can be seen that a series of rapid contractions and relaxations are occurring following one after another with remarkable regularity and continuing for about $30-40$ minutes. Consistency in the amplitude of the relaxation curve, especially during the first half of the reaction and the remarkable rhythmicity of the contractions are the most distinctive features of the sexual reaction of a female. This phenomenon does

not occur under any other circumstance. Burst of valve activity can be seen in other cases as well as under the influence of some external excitation (for example pollution or chemical injection) but (1) their frequency is never so regular, (2) will last for shorter period of time and (3) will have longer relaxation period. It was also known that spawning propagates from one to another and eventually over a large fraction of the oyster community [68]. Hence, any rhythmic behavior to be considered as spawning should have certain characteristics. For example:

1. regularity in rhythm and consistency in amplitude;
2. happening for $30-40$ minutes with short relaxation period;
3. simultaneous spawning in the population and so on.

In this chapter, we considered only this type of spawning that is clearly distinguishable. However, spawning can happen with mild characteristics also. For example, instead of $30-40$ minutes duration, it can last $10-20$ minutes. **We will focus in this chapter on detecting any spawning behavior with strong characteristics or clearly distinguishable**. Therefore, the spawning behavior can be considered as a deviation from normal behavior. In Fault Detection literature [27, 87], this is known as fault (*i.e.* deviation from normal behavior). So, the detection of this fault is equivalent to the detection of spawning.

In the experiment of MolluSCAN-eye project, they have collected the data of 16 oysters recorded in 2007, 2013 and 2014 respectively. They are denoted as dataset 1, 2 and 3 respectively. Two types of oyster data were collected: diploid oysters and triploid oysters. Triploid oysters are genetically modified and have three sets of chromosome while diploid oysters are not genetically modified and have two sets of chromosome. Diploids oysters normally spawn in the Summer while triploids cannot spawn because of the genetic modification. For details, the reference [10] can be consulted. Dataset 1 contains only diploid oysters while dataset 2 and 3 contains both diploid and triploid oysters. An equal number of diploid and triploid oysters were available, *i.e.* 8 diploids and 8 triploids respectively in dataset 2 and 3. In these datasets, we also found similar behavior as reported in [68]. In our case, for the first dataset, the oysters happened to spawn on the 15th of July, 2007. The data of 4 oysters including both spawning and non-spawning oysters can be seen in Fig. 3.1. A close look on oyster N° 3 and 15, can be seen in Fig. 3.2, where we can clearly check that oyster N° 3 fulfills all the criteria to call its rhythmic behavior as female spawning according to [68] (regular rhythmicity, consistency in the amplitude during rhythmic behavior, happening for about $30-40$

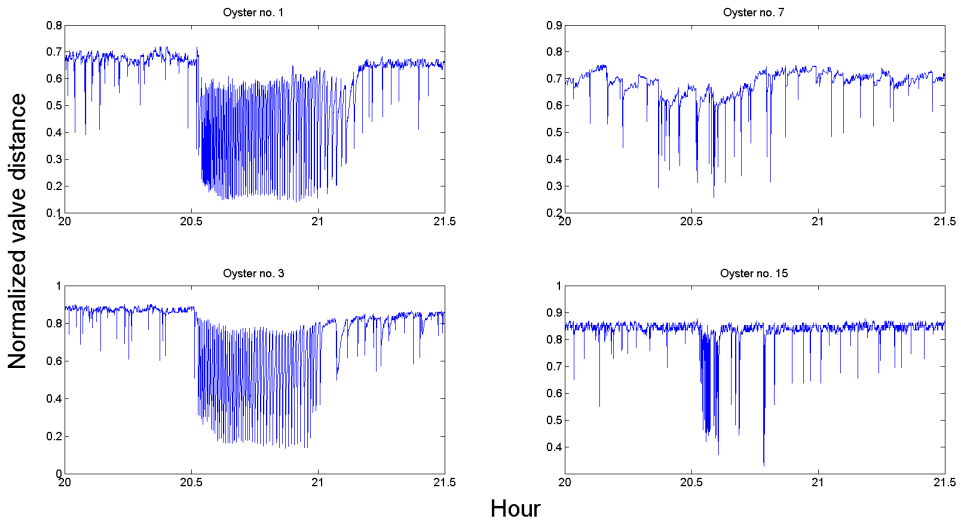

Figure 3.1: Spawning (left column) and non-spawning (right column) behavior of oysters

min., contraction followed by relaxation or vice-versa with short relaxation period, *etc.*). However, if we look at oyster N° 15, it is evident from its behavior that it is not spawning with very visible characteristics (like $30-40$ minutes duration, very regular contraction and relaxation, *etc.*) although some rhythmicity can be seen. So, oyster N° 15 is not showing the type of spawning we are interested in this chapter. Similarly, we can say that oyster N° 1 is spawning and N° 7 is not spawning in Fig. 3.1.

3.3 Automatic Detection of Spawning

In the previous Section, details about a spawning behavior were discussed. One point to be noted in this regard is that the detection of spawning is totally manual until now. In Chapter 2, we have tried to establish a relation between water quality and abnormal valve activity [6]. There, we have showed that the deviation of valve activity from normal behavior, if it occurs in the whole animal group can be used as an indicator for change in water quality. Since the spawning behavior is a total deviation from normal behavior, according to [6], it could also be considered as an indicator for change in water quality. However, in reality this is a totally normal behavior having little to do with the occurrence of poor water quality. By automatic spawning detection, we will be able to differentiate spawning behavior with numerous other abnormal motions. Moreover, it will save time and labor of visually analyzing the data to find the period of spawning. So, automatic detection of spawning can be very useful.

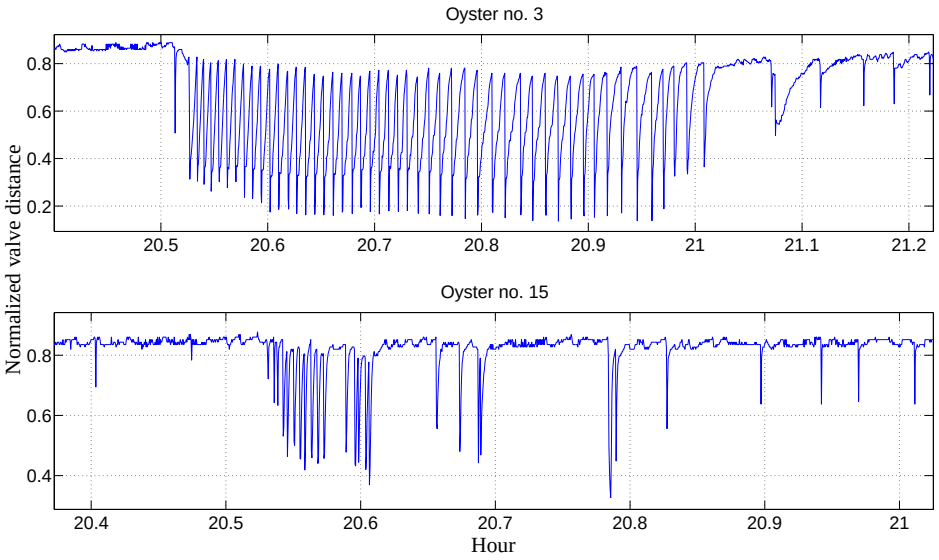

Figure 3.2: Behavior of oyster N° 3 and 15 (zoomed)

A typical pattern of a spawning behavior (see figures 3.1 and 3.2) is a series of contractions and relaxations of valves. In other words, the velocity of valve movement is fluctuating in a regular rhythmic manner. Since the kinetic energy is related to the velocity, it will also fluctuate very rapidly and regularly. By passing this high frequency kinetic energy like signal through a specially designed low-pass filter, we can expect to extract some features related to spawning. They can then be used for the detection of spawning.

The main idea of our spawning detection algorithm is first to estimate the velocity of valve movement. Velocity is the time derivative of the measured distance. Once the velocity is estimated, this information can be used to calculate the energy (square of velocity). Then by passing this energy through a low-pass filter and comparing the value with some pre-defined thresholds, we can detect spawning which is a typical approach used for fault detection [154]. We have chosen the energy signal as the marker because it is easier to obtain a pattern from the square of a velocity signal (having higher amplitude during spawning) than the velocity itself because of the amplitude. However, first we would like to process the raw data to reduce the computational burden. The idea is described in section 3.3.1. The details of the spawning detection algorithm are given below.

3.3.1 Rhythmicity Information Calculation

During the spawning, the valve movement maintains a very periodic nature. A first step in identifying this pattern of behavior from others is to calculate the minimum and maximum of the signal amplitude for a certain interval (for example 1000 data points). This difference of the minimum and maximum value of the amplitude in this interval has a lower bound or threshold during spawning. If at current sampling instant, the difference of the minimum and maximum value of the amplitude in the interval of the signal exceeds the threshold, we will proceed further, otherwise we can say that spawning is not happening. Since the signal amplitude for different oysters varies widely just by using this criteria we may ignore a lot of potential spawning oysters. In the next step, we will calculate the frequency in this interval. If the frequency crosses a certain threshold, we will proceed to the rest of our algorithm which will use a velocity based detection of spawning. These two criteria will help us to eliminate a lot of data points which will in turn reduce the computational burden. The two criteria can be briefly described as:

- Amplitude criterion:

$$\begin{aligned} A_{\text{int}} &= \max(y_{i-1000,j} : y_{i,j}) - \min(y_{i-1000,j} : y_{i,j}), \\ A_{\text{int}} &\geq A_{\text{th}}, \end{aligned} \tag{3.1}$$

  where i is the current sampling instant, j is the oyster number, A_{th} is the amplitude threshold and the interval we are considering is from $i - 1000$ to i, *i.e.* total 1001 datapoints.

- Frequency criterion:

$$f_{\text{int}} \geq f_{\text{th}}$$

  where f_{int} is the frequency of contraction of the interval and f_{th} is the frequency threshold.

3.3.2 Velocity Estimation

Since velocity is the time derivative of valve distance activity, we need to differentiate the valve distance to get the velocity. A common technique is to use the Euler method that can be described as the difference between the current and previous sample divided by the sample time. However, this method does not work well in the presence of noise which is our case. There exist various effective methods to estimate the time derivative of noisy signals. For example, [108] proposed a numerical differentiation scheme based

on an algebraic method. Homogeneous finite-time differentiation scheme can be found in [123] while non-homogeneous higher order sliding mode (HOSM) based differentiator was proposed in [55]. Out of various methods available, we have chosen the techniques proposed in the aforementioned references because of their simplicity, effectiveness and noise compensation [7]. In fault detection literature, hardware redundancy is a very well-known approach, where information from multiple hardware is passed through a voting scheme to detect the fault. We will use the same approach but from the software point of view which is known as analytical redundancy. We will use three different velocity estimation techniques and at the end the information obtained by different techniques will be passed through a voting scheme. This approach will help to minimize false detection and increase the rate of correct detection. The three differentiation schemes are summarized below:

3.3.2.1 Algebraic Differentiator

The algebraic time derivative estimation is based on concepts of differential algebra and operational calculus. A more detailed description of the approach can be found in [108, 146]. A moving horizon version of this technique is summarized below adapted from the mentioned references. For a real-valued signal $y(t)$, analytic on some time interval, the first-order time derivative estimate can be written as:

$$\widehat{\dot{y}}(t) = \frac{6}{T^3} \int_0^T (T - 2\tau)\, y(t - \tau) d\tau. \tag{3.2}$$

where $T > 0$ is the arbitrary constant time window length. The effect of the time integral, presented in equation (3.2), is obviously to dampen the impact of the measurement noise on the estimate. This noise dampening effect can also be used to filter out the noise from the original signal $y(t)$.

3.3.2.2 A non-homogeneous HOSM differentiator

Let us consider an unknown signal $y(t)$. To calculate the derivative of this signal, consider an auxiliary equation $\dot{x} = u$ where $x(t)$ denotes the estimate of the original signal $y(t)$. The control law u is designed to drive the estimation error, *i.e.* $e(t) = x(t) - y(t)$, to zero. The work [55] proposes a variant of a super-twisting finite-time control u that ensures vanishing the error $e(t)$ and its derivative $\dot{e}(t)$. Thus it can be used to provide a derivative estimate. It has also been shown that the obtained estimate is robust against a non-differentiable noise of any amplitude. Now if we consider a noisy version of the

original signal, *i.e.* $\tilde{y}(t) = y(t) + \nu(t)$, where $\nu(t)$ is a bounded measurement noise, then the differentiator is given by [55]:

$$\begin{aligned} \dot{x}_1 &= -\alpha\sqrt{|x_1 - \tilde{y}(t)|}\text{sign}\,(x_1 - \tilde{y}(t)) + x_2, \\ \dot{x}_2 &= -\beta\text{sign}\,(x_1 - \tilde{y}(t)) - \chi\text{sign}\,(x_2) - x_2, \end{aligned} \tag{3.3}$$

where $x_1, x_2 \in \mathbb{R}$ are the state variables of the system (3.3), α, β and χ are the tuning parameters with $\alpha > 0$ and $\beta > \chi \geq 0$. The variable $x_1(t)$ serves as an estimate of the function $y(t)$ and $x_2(t)$ converges to $\dot{y}(t)$, *i.e.* it provides the derivative estimate. Therefore the system (3.3) has $\tilde{y}(t)$ as the input and $x_2(t)$ as the output.

3.3.2.3 Homogeneous finite-time differentiator

Consider a chain of integrators,

$$\begin{aligned} \dot{z}_i &= z_{i+1}, \text{ for } i = 1, \ldots, n-1, \\ \dot{z}_n &= u, \\ y &= z_1, \end{aligned} \tag{3.4}$$

where $z \in \mathbb{R}^n$ is the state, $y \in \mathbb{R}$ is the output and $u \in \mathbb{R}$ is the input.

For the system (3.4), the following homogeneous finite-time differentiator can be proposed :

$$\begin{aligned} \dot{x}_1 &= x_2 - k_1\lfloor x_1 - y\rceil^{\alpha}, \\ \dot{x}_i &= x_{i+1} - k\lfloor x_1 - y\rceil^{i\alpha-(i-1)}, \text{ for } i = 2, \ldots, n-1, \\ \dot{x}_n &= -k_n\lfloor x_1 - y\rceil^{n\alpha-(n-1)} + u. \end{aligned} \tag{3.5}$$

where $\lfloor x\rceil^{\alpha} = \text{sign}\,(x).|x|^{\alpha}, \alpha > 0$. For details, [123] can be consulted.

3.3.3 Filtering of energy signal and spawning detection

From the normalized valve distance data $p_{i,j}$, using equations (3.2), (3.3) and (3.5), we can easily estimate the velocity $v_{i,j}(k)$, where $k = 1, 2, 3$ represents algebraic differentiator, non-homogeneous HOSM differentiator and homogeneous finite-time differentiator respectively. Analytic expressions for three different cases are given below:

Using algebraic differentiator (Section 3.3.2.1):

$$v_{i,j}(1) = \frac{6}{M^2 T_s} \sum_{l=0}^{M} \left(1 - 2\frac{l}{M}\right) p_{i-l,j} \tag{3.6}$$

Using non-homogeneous HOSM differentiator (Sec. 3.3.2.2) and applying Euler discretization, the equation (3.3) can be written as

$$\begin{aligned} x_1(i,j) &= x_1(i-1,j) + T_s\{-\alpha\sqrt{|x_1(i-1,j) - p(i-1,j)|}\text{sign}(x_1(i-1,j) \\ &\quad -\tilde{y}(i-1,j)) + x_2(i-1,j)\} \\ x_2(i,j) &= x_1(i-1,j) + T_s\{-\beta\text{sign}(x_1(i-1,j) - p(i-1,j)) \\ &\quad -\chi\text{sign}\left(x_2(i-1,j)\right) - x_2(i-1,j)\} \end{aligned} \tag{3.7}$$

where $x_1(i,j)$ is the estimate of $p_{i,j}$ and $x_2(i,j)$ is the estimated velocity $v_{i,j}(2)$.

Using homogeneous finite-time differentiator (Section 3.3.2.3) and applying Euler discretization, the equation (3.5) for calculating first order derivative can be written as

$$\begin{aligned} x_1(i,j) &= x_1(i-1,j) + T_s\left(x_2(i,j) - k_1\lceil x_1(i-1,j) - p(i-1,j)\rfloor^{\alpha}\right), \\ x_2(i,j) &= x_2(i-1,j) + T_s\left(-k_2\lceil x_1(i-1,j) - p(i-1,j)\rfloor^{2\alpha-1}\right), \end{aligned} \tag{3.8}$$

where $x_1(i,j)$ is the estimate of $p_{i,j}$ and $x_2(i,j)$ is the estimated velocity $v_{i,j}(3)$.

Notice that equations (3.6), (3.7) and (3.8) are in discrete form since in our case only discrete measurements are available.

From the estimated velocity, the kinetic energy like signal can be calculated just by taking square of the velocity signal $v_{i,j}(k)$:

$$E_{i,j}(k) = v_{i,j}^2(k),$$

where $E_{i,j}(k)$ is the energy. This signal will be passed through the following low-pass like filter:

$$f_{i+1,j}(k) = f_{i,j}(k) + T_s\left(\min(\gamma, E_{i,j}(k)) - \mu f_{i,j}(k)\right) \tag{3.9}$$

where $f_{i,j}(k)$ is the filtered signal, $Ts = 1.6$ sec. is the sampling period and μ and γ are the parameters of the filters. The filtered signal obtained through (3.9) will then be passed through another typical low-pass filter to eliminate the remaining high frequency fluctuation of the energy signal. A typical discrete first order low pass filter has the

following form:

$$\overline{f}_{i,j} = \alpha \overline{f}_{i-1,j} + (1-\alpha) f_{i,j} \tag{3.10}$$

where $\overline{f}_{i,j}$ is the filtered signal, $f_{i,j}$ is the original signal, $\alpha = \frac{\tau_f}{\tau_f + T_s}$, τ_f is the time constant of the filter and T_s is the sampling time. This doubly filtered energy signal $\overline{f}_{i,j}(k)$ will then be used for the detection of the spawning. If the signal exceeds some threshold, it will be considered as spawning, otherwise no spawning:

$$\mathrm{F}_{i,j}(k) = \begin{cases} 1, & \overline{f}_{i,j}(k) \geq \beta, : k = 1,2,3 \\ 0, & \text{otherwise} \end{cases} \tag{3.11}$$

where β is the threshold for spawning.

3.3.4 Decision rule

The last step is to come to a final decision about spawning from the 3 different flags obtained through (3.11). Since no prior information is available about the performance of individual detection scheme, no weight was associated with each flag of the (3.11). There are two popular choices for un-weighted voting (*i.e.* unanimity and majority), and here a majority based voting technique was used to determine whether spawning is happening at the current sampling instant or not. If at least two flags of (3.11) have value 1 then it is spawning, otherwise not. The expression is given below:

$$\mathrm{Spawning}_{i,j} = \begin{cases} 1, & \sum_{k=1}^{3} \mathrm{F}_{i,j}(k) \geq 2 \\ 0, & \text{otherwise} \end{cases} \tag{3.12}$$

The flow chart of the whole process can be seen in Fig. 3.3. The parameters of the algorithm were tuned on a trial and error basis since establishing some tuning rule is very difficult because of the wide variations of behavior among different animals. In this chapter, we have done the detection offline, however, the algorithm is designed for online detection, which is planned for the future.

3.4 Results and Discussions

As mentioned in Section 3.2, by visual inspection of the dataset, the spawning oysters can be identified. After such an expert evaluation, for dataset 1, the oysters 1, 3, 4, 10,

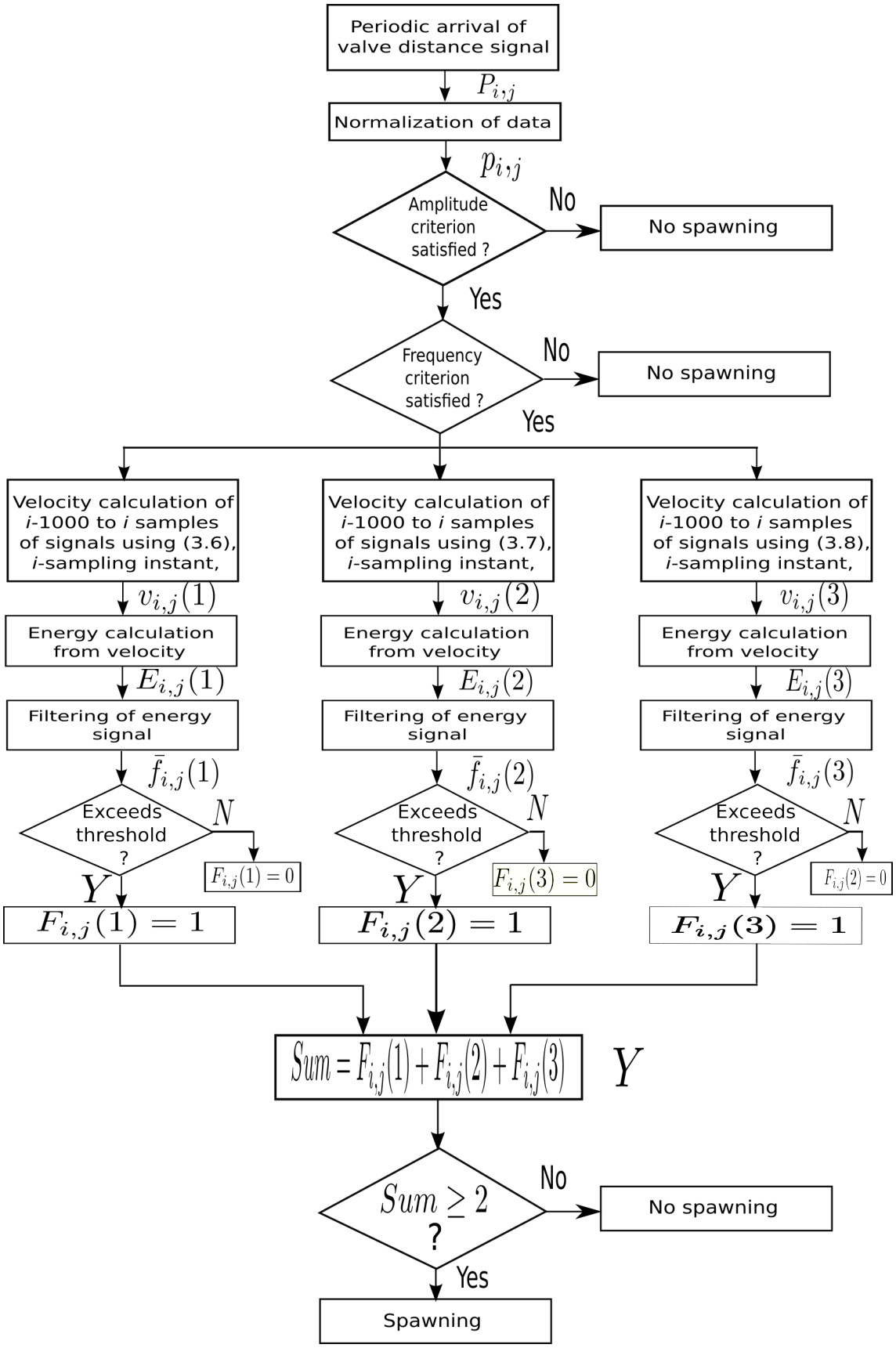

Figure 3.3: Flow chart of spawning detection process

11, 12, 13 and 16 were classified as clearly visible spawning oysters with spawning period of about 30 – 40 minutes and having very regular rhythmic contraction and relaxation of valves. So, the algorithm is supposed to find these spawning oysters. Next, the proposed algorithm has been applied. For example, the data of oysters 1 and 5 can be seen in Fig. 3.4. According to the criteria mentioned in Section 3.2, oyster 1 is classified as a typical spawner while 5 appears to exhibit a much lesser typical burst of contraction. Note that to know if 5 was really spawning or not would require the ability to check if it produces eggs or not which was out of the scope of the present work. The final output of our algorithm for dataset 1 can be seen in Fig. 3.5. Horizontal axis of all the figures in this Section are in hour format.

For dataset 2, we have first applied our algorithm to find spawning oysters and then we have asked expert evaluation to validate the effectiveness of our algorithm. We found that the oysters 1, 4, 5, 6 and 7 were spawning on September 6, 2013 between 8 – 10 a.m. All the spawning oysters were diploid. No triploid oysters showed clearly distinguishable spawning behavior. Expert evaluation confirmed our result. It is to be noted here that for dataset 2, spawning happened almost 2 months later than for dataset 1. Detection result for dataset 2 can be seen in Fig. 3.6.

In dataset 3, we have found that spawning happened two times unlike one time in dataset 1 and 2. The first time, spawning happened on the 15th of July, 2014 which is the same date as in dataset 1 while second spawning happened on the 11th of August. So, there is a gap of almost 1 month. Like dataset 2, in this case also only diploid oysters showed clearly distinguishable spawning behavior and not the triploids. In July 15, the oysters 2, 3, 5, 6 and 8 were spawning while in August 11, the oysters 1, 2, 6 and 8 were spawning. Detection results for July 15 case can be seen in Fig. 3.7 and in Fig. 3.8 for August 11.

From figures 3.5, 3.6, 3.7 and 3.8, it is clear that our algorithm can successfully detect the start and end of spawning. We can also see that our algorithm can detect the spawning for all the clear cut spawning oysters. There is no false alarm and zero misdetection. This proves the effectiveness of our algorithm. However, in some cases we can see a little delayed detection. This delay comes from the filtering and differentiation process and it is very common.

As mentioned in Section 3.2, according to [68], spawning may propagate from one to another and then induces an increased burst activity that eventually spread to most individuals. This is a very important criteria to check if the oysters are really spawning, which may tolerate the effect of wrong detection from the algorithm for certain oysters. If they are really spawning, we would see the spawning propagating, otherwise not. One

way to check this criteria is to calculate the number of oysters simultaneously spawning at a given time. The number of simultaneously spawning oysters in dataset 1 can be seen in Fig. 3.9 where we can notice that the spawning spread from one oyster to another and then eventually spread to the entire community. At the peak of spawning, all female oysters were spawning. This is a very strong proof of spawning and also tells the effectiveness of the spawning detection algorithm. Moreover, we can see that it took very short time to propagate spawning from the first spawning oyster to the second one and much less for the rest of the oysters.

The number of simultaneously spawning oysters in dataset 2 can be seen in Fig. 3.10. In both cases (1 and 2), we have seen simultaneous spawning that confirmed the effectiveness of our detection algorithm.

The proposed algorithm was compared with a FFT (Fast Fourier Transformation) based technique. A lot of false detection were observed in the FFT based case. Unlike rotating machineries, the fault frequencies are different for different oysters which leads to significant false detection. Results with FFT based techniques are omitted for the purpose of brevity.

3.5 Conclusions

This chapter presents an algorithm to automatically detect the start and the end of the spawning period of a population of oysters that is to detect individual spawning events and the day of spawning. The developed algorithm is based on the estimation of velocity of valve movement. The algorithm was then tested on three different populations to approve its effectiveness. The obtained results are very promising and open up the scope of real-time spawning detection of oyster population in marine environment.

In future, the algorithm can be tested on new measurement sites and different bivalves species. Very noisy/faulty measurement detection system can also be included into the algorithm to prevent any false/early/late detection. Once a spawning day has been automatically identified, it is a solid working base for an expert to screen the records and classify the atypical bursts of contractions. Different parameters of the algorithm were chosen on a trial and error basis. In future, establishing a numerical procedure for the tuning of the parameters will also be considered.

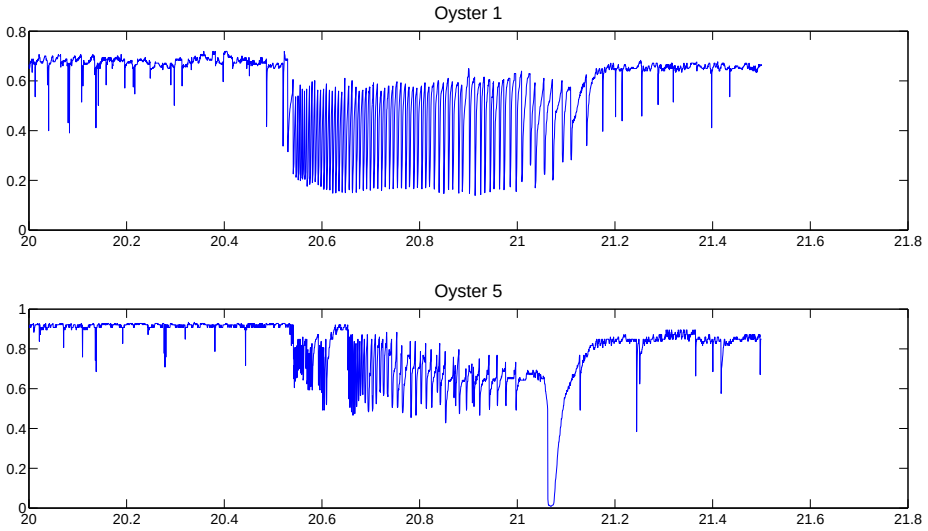

Figure 3.4: Valve activity of oyster 1 and 5 (x-axis is in hour and y-axis is normalized valve distance)

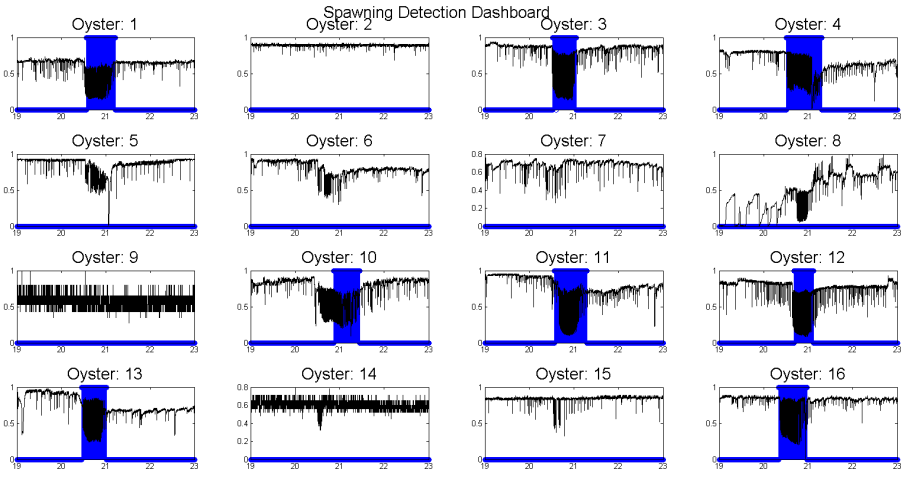

Figure 3.5: Spawning detection for the population of dataset 1 (2007)

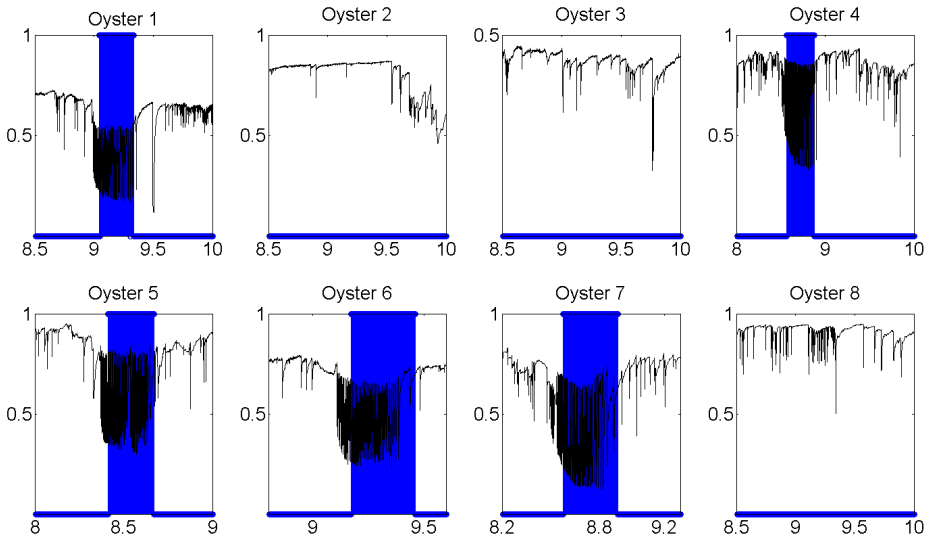

Figure 3.6: Spawning detection result for dataset 2

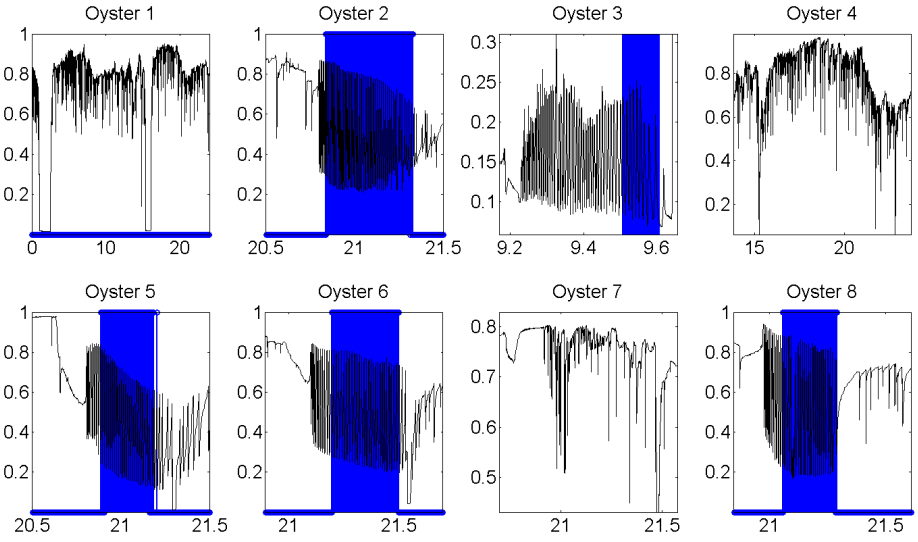

Figure 3.7: Spawning detection result for July 15 case (dataset 3)

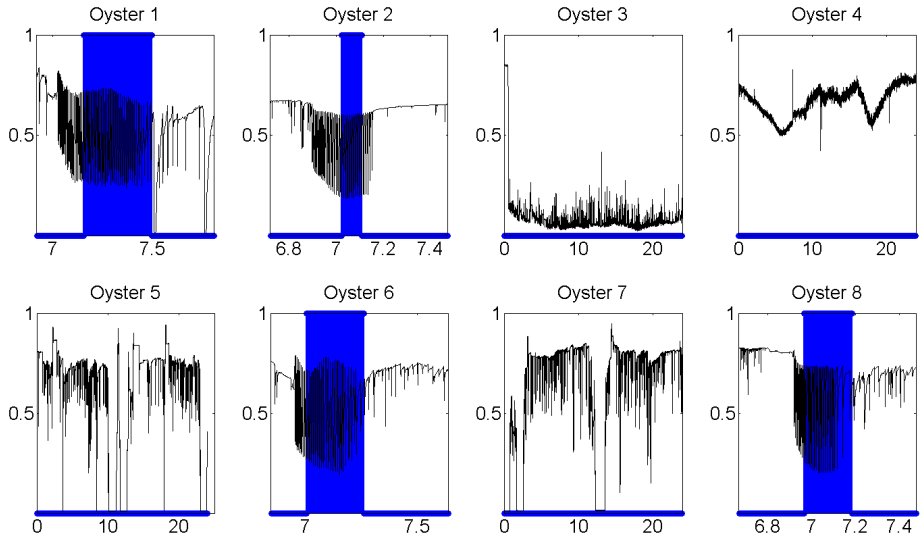

Figure 3.8: Spawning detection result for August 11 case (dataset 3)

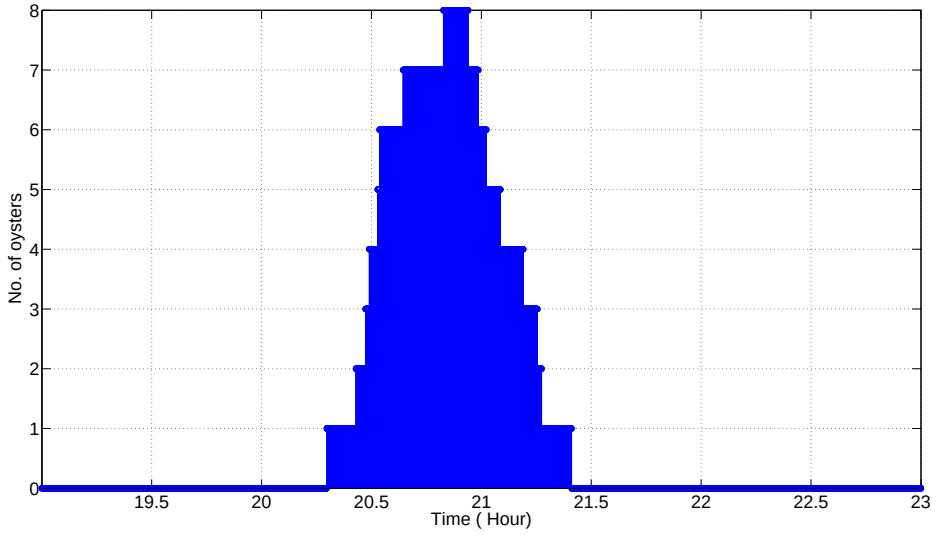

Figure 3.9: Number of simultaneously spawning oysters

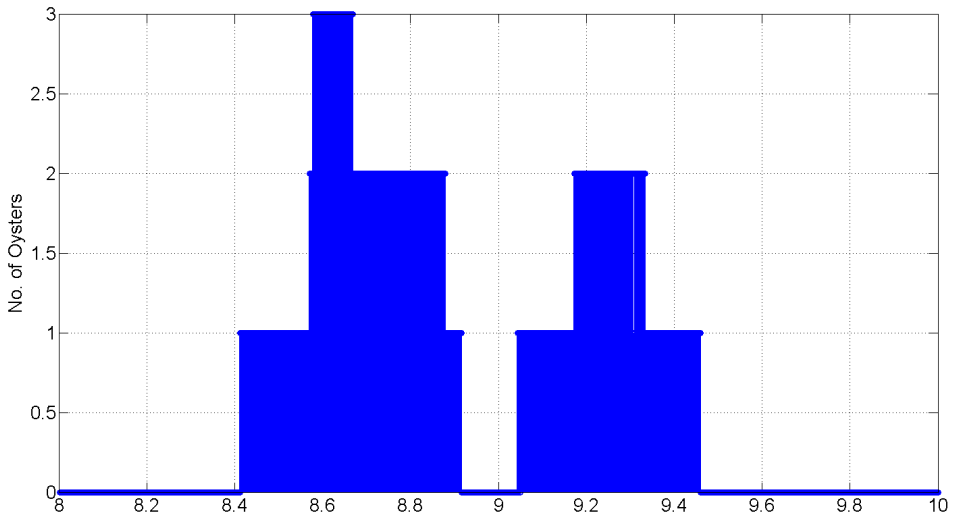

Figure 3.10: Number of simultaneously spawning oysters in dataset 2

Part II

Synchronization of oscillations

Chapter 4

Robustness of Phase Resetting to Cell Division under Entrainment

4.1 Introduction

The interest in the analysis and synthesis of genetic oscillators is continuously growing these last decades ([81, 98, 140, 148]). Any sinusoidal type periodic oscillation is characterized by its frequency (or frequency spectrum), phase and amplitude. The amplitude and frequency are mainly governed by external stimulus applied to oscillators, a phenomenon called *entrainment* ([88, 126]), while the phase value is dependent on properties of the oscillator and characteristics of entrainment. This phase feature has attracted the attention of many researchers and in particular, the phase synchronization phenomenon studies are very popular ([88, 126]). Phase synchronization is frequently observed in networks of oscillators, like a colony of the smallest free-living eukaryotes, the mammalian circadian pacemaker neural network ([21, 150]) or networks of neural oscillators ([34, 134, 140]), to mention a few. Controlled phase resetting has been studied in [22, 44, 51, 57] and for a population of oscillators in [53].

A simple but effective approach for analysis of phase resetting and dynamics for a single oscillator is based on PRC ([73, 79, 88]). The infinitesimal PRC map is calculated for the system linearized around the limit cycle and inputs with small amplitudes. If the entraining input is a series of pulses, then a Poincaré phase map based on PRC can be calculated to predict the phase behavior ([88]). Such a reduced phase model has been used in [57] and [53] for pulse amplitude and timing calculation for a controlled phase resetting.

Another interesting problem has emerged recently in [77], it concerns the influence of cell division on the behavior of genetic oscillators. It has been observed that oscillations

persist across cell divisions in *Repressilator* ([60]), similarly for circadian oscillations in cyanobacteria cells ([109]). In [112], the persistence of circadian oscillations in culture fibroblasts under cell division has been demonstrated, and it has been noted that cell division can shift the phase in circadian cycle. A rapid phase decorrelation between daughter cells has been remarked in [72] for oscillations in the p53/Mdm2[1] system. Moreover, experimental study that demonstrated synchronization of budding yeast cells using periodic cyclins and its validation with a complex stochastic model can be found in [36] and [117] respectively. Since cell division introduces a discontinuity in the oscillator dynamics (that is usually described by a system of nonlinear differential equations), then the analysis of division influence leads to the study of a hybrid or impulsive nonlinear oscillating system, which is a rather complicated problem ([40, 56]). In [77], this problem has been investigated using a stochastic simulation approach, and in [143], the geometric phase approach has been adopted from quantum mechanics.

The goal of this chapter is to analyze the phase behavior and synchronization under cell division in genetic oscillators using the PRC formalism. A motivating example given by a simple biological model of circadian oscillations in *Neurospora*, is studied in Section 4.2. The analysis of cell division influence on the phase dynamics is presented in Section 4.3. An illustration by simulations of the obtained results is given in Section 4.4. General results about phase dynamics are summarized in the Appendix A.

4.2 Motivating example

Let us consider a simple biological model of circadian oscillations in *Neurospora* in the following form [100]:

$$\begin{aligned}
\dot{M}(t) &= (v_s + u(t))\,\frac{K_I^n}{K_I^n + F_N^n(t)} - v_m \frac{M(t)}{K_m + M(t)},\\
\dot{F}_C(t) &= k_s M(t) - v_d \frac{F_c(t)}{K_d + F_C(t)} - k_1 F_C(t) + k_2 F_N(t),\\
\dot{F}_N(t) &= k_1 F_C(t) - k_2 F_N(t),
\end{aligned} \tag{4.1}$$

where $M(t)$, $F_C(t)$ and $F_N(t)$ are the concentrations (defined with respect to the total cell volume) of the *frq* mRNA, the cytosolic and nuclear forms of FRQ, respectively. The parameter v_s defines the rate of *frq* transcription (this parameter increases in the

[1]Mouse double minute 2 homolog (MDM2) also known as E3 ubiquitin-protein ligase Mdm2 is a protein that in humans is encoded by the MDM2 gene.

light phase) while the influence of light (the external entraining input in the model (4.1)) is denoted by $u(t) \geq 0$. A description of the other parameters appearing in these equations can be found in [100]. The following values of parameters are proposed there: $v_m = 0.505nMh^{-1}$, $v_d = 1.4nMh^{-1}$, $k_s = 0.5h^{-1}$, $k_1 = 0.5h^{-1}$, $k_2 = 0.6h^{-1}$, $K_m = 0.5nM$, $K_I = 1nM$, $K_d = 0.13nM$, $n = 4$ and $1 \leq v_s + u(t) \leq 2.5$.

For all these values, the system (4.1) for $u(t) = 0$ has single unstable equilibrium and globally attractive limit cycle that represents a rhythmic behavior of the circadian rhythm in *Neurospora* with a period $T > 0$. It is a continuous-time dynamical system that for any initial conditions $M(0) > 0$, $F_C(0) > 0$ and $F_N(0) > 0$ has a continuous positive solution for all $t \geq 0$. To model the cell division in (4.1), it is necessary to introduce an increasing series of time instants $t_k > 0$, $k = 1, 2, \ldots$ with a division at each t_k. During the division, the state variables are reset ([77]), *i.e.* $M(t_k^+) = \lambda_k^M M(t_k)$, $F_C(t_k^+) = \lambda_k^{F_C} F_C(t_k)$ and $F_N(t_k^+) = \lambda_k^{F_N} F_N(t_k)$, where $M(t_k^+)$ is the value of the concentration M after division at instant t_k; $\lambda_k^M > 0$, $\lambda_k^{F_C} > 0$ and $\lambda_k^{F_N} > 0$ are parameters.

The cell division cycle can be larger than the period of oscillations T ([143]) or similar, as in proliferating human cells ([24]) where the circadian clock is a major synchronizing factor, which orchestrates daily rhythms regulating the cell division cycle; or two times faster as in cyanobacteria ([111]). The values λ_k^M, $\lambda_k^{F_C}$, $\lambda_k^{F_N}$ have been selected around 0.5 in [77] (for the Goodwin model), but in [43] it has been observed *in vivo* that concentrations do not jump significantly after cell division. In this chapter, we will adopt the latter hypothesis by taking λ_k^M, $\lambda_k^{F_C}$, $\lambda_k^{F_N}$ close to 1.

The modeling of such a hybrid oscillator corresponds to a mother cell in the population, then after each division the daughter cells have a similar dynamics and forthcoming divisions augment the population. It is assumed that division instants t_k for each cell are different, then the phase synchronization behavior in a population (suppose that there is no interconnection between cells) can be analyzed using (4.1). If the phase converges to a steady-state in this hybrid system under some conditions, then the population will be phase synchronized in some sense. In this chapter, we have considered in-phase synchronization. For details about various kinds of phase synchronization (anti-phase, in-phase, arbitrary phase locking) consult [125].

Taking the previously mentioned parameter values and $v_s = 1.11$, the period of the autonomous oscillation of (4.1) is obtained as $T = 19.25$ hours. For these values of parameters and for the case $u(t) = 0$ and $t_k = k\,(T - \upsilon_k)$, $k \geq 1$, where $\upsilon_k \in [0.15T, 0.30T]$ is a uniformly distributed random variable, the results of the *Neurospora's* circadian oscillation model simulation for the same initial conditions and different realizations of

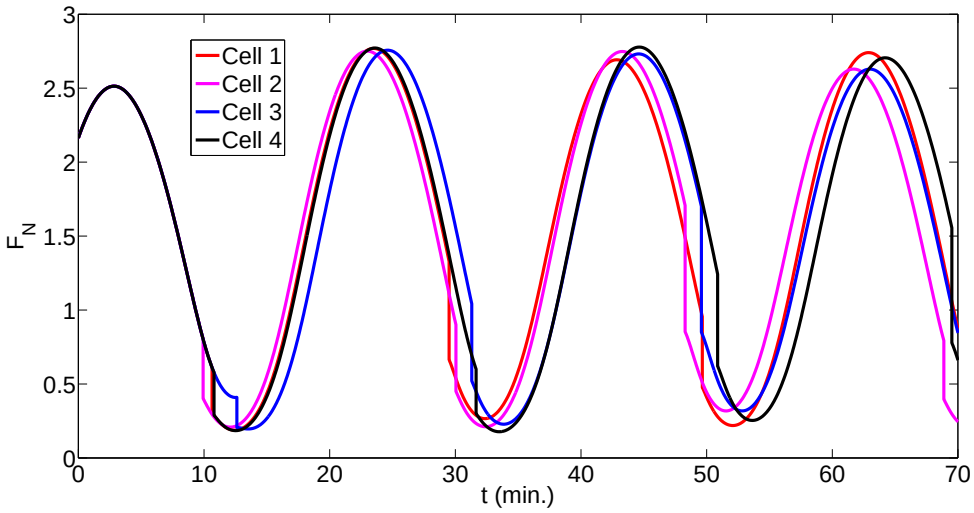

Figure 4.1: Oscillations of different single cells with cell divisions and without any common input

v_k for 4 different cells undergoing divisions can be seen in Fig. 4.1. As we can conclude from these results the phase is diverging as it has been noted in [72, 112] and in some experiments of [77]. Next, by taking $u(t) = \max\{0,\, 0.2\sin(\omega t)\}(\omega = 2\pi T^{-1})$ as the common external entraining input and repeating the same experiments, the results are given in Fig. 4.2. From this figure, it is evident that the oscillations converge to a common entrained mode.

The robustness of this common entrained mode can be checked through simulation of a large population of cells. This can be seen in Fig. 4.3. The population consists of 100 cells, the transcription rate represented by the uniformly distributed random variable, $v_s \in [1.1, 1.3]$ and the cell division time parameters $v_k \in [0.15T, 0.3T]$. Histograms of v_k and v_s can be seen in Fig. 4.3 (bottom). From Fig. 4.3, it is evident that the oscillations converge to a common entrained mode in the case of a large population well despite of simultaneous variations in the cell division time and transcription rate. So, from the simulation experiments it can be seen that the common entrained mode is quite robust.

In this chapter, we will try to find conditions providing both these two types of phase behavior (Fig. 4.2 and 4.1) using the PRC phase model for small inputs *i.e.* inputs with small amplitude.

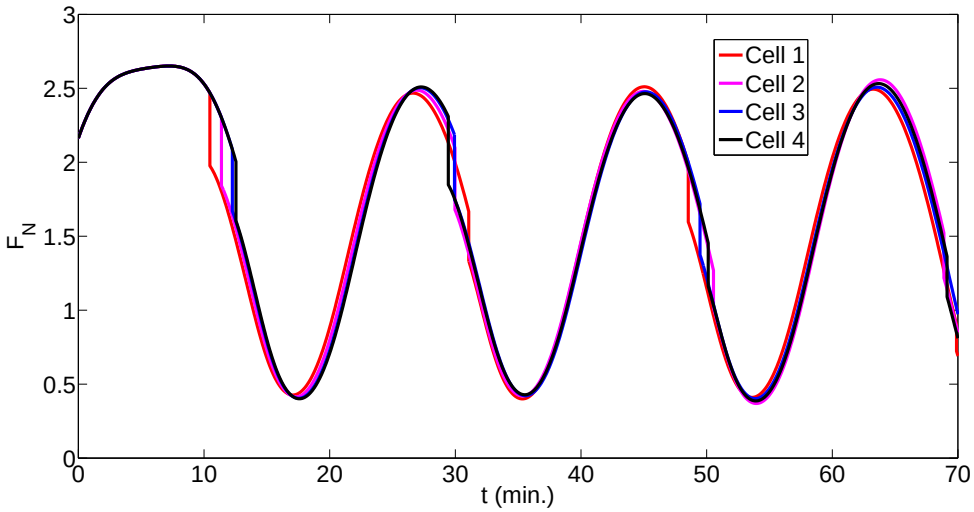

Figure 4.2: Oscillations of different single cells with cell divisions and common external entraining input

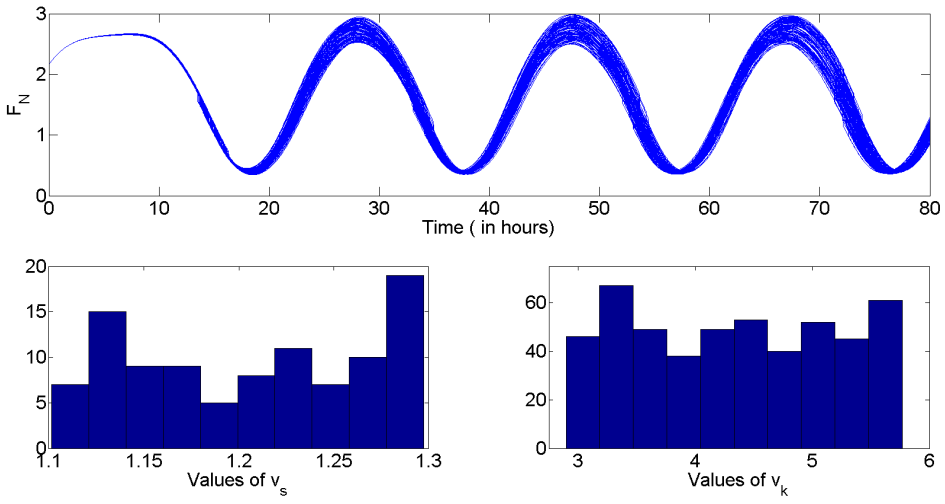

Figure 4.3: Top - oscillations of 100 single cells with cell divisions and common external entraining input, bottom - histogram of v_k (in hours) and v_s

4.3 PRC-based phase model for an oscillator with cell division

This Section begins with the introduction of the formalized problem statement. Next, the reduced PRC model is introduced and the phase synchronization analysis is presented.

Details of the standard procedure for a phase model derivation for an oscillator can be found in [53, 88, 126]. According to the references, the reduced order phase model of an oscillator can be written as:

$$\theta(t) = \omega t + \theta(0) + \mathrm{PRC}[\theta(0)] \tag{4.2}$$

where $\theta(t)$ is the asymptotic phase at time t, ω is the frequency of the oscillator, the map $\mathrm{PRC}(\theta)$, $\theta \in [0, 2\pi)$ is defined for the particular pulse w (by definition $-\pi \leq \mathrm{PRC}(\theta) < \pi$ for all $\theta \in [0, 2\pi)$), it tabulates the phase shift by the pulse w ([88, 126]). A summary on the derivation of the model (4.2) is given in the Appendix A. For further reading of this chapter, readers are requested to consult Appendix A first to be familiar with the notions that will be used later in this chapter.

4.3.1 *Problem statement*

Let us consider a population of $N > 0$ cells (genetic oscillators) with $s = 1, 2, \ldots, N$:

$$\begin{aligned} \dot{x}_s(t) &= f_s(x_s(t), u(t)) \quad t \in [t_{s,k}, t_{s,k+1}),\ k \geq 0; \\ x_s(t^+_{s,k+1}) &= \Lambda_{s,k,n} x_s(t_{s,k+1}) \quad k \geq 1, \end{aligned} \tag{4.3}$$

where $x_s(t) \in \mathbb{R}^n$ is the state (concentrations of different products) of the s^{th} cell and the input $u(t)$ is a periodical train of pulses

$$u(t) = \sum_{i=0}^{+\infty} w(t - i\mathbb{T}),$$

with a pulse $w(t)$, $w(t) = 0$ for all $t \geq \mathcal{T}$ or $t \leq 0$, $\sup_{0 \leq t \leq \mathcal{T}} |w(t)| \leq W < +\infty$ and $\mathcal{T} < \mathbb{T}$ where $\mathbb{T} > 0$ is the period of u; $t_{s,0} = 0$ and $t_{s,k}$, $k \geq 0$ is a strictly increasing sequence of impulses (discontinuous jumps in (4.3)) for all $s = 1, 2, \ldots, N$, $\Lambda_{s,k,n} = \mathrm{diag}[\lambda_{s,k,1}, \ldots, \lambda_{s,k,n}] \in \mathbb{R}^{n \times n}$ with $\lambda_{s,k,1} \in [1 - \varepsilon, 1]$ for some $\varepsilon > 0$ sufficiently small. The periodical input $u(t)$ models the common entrainment for all cells and the discontinuities at instants $t_{s,k}$, $k \geq 1$ represent the cell division, the diagonal matrix $\Lambda_{s,k,n}$ determines changes in the state vector (in concentrations) after division. The

instants of division $t_{s,k}$ and the concentration changes $\Lambda_{s,k,n}$ may be different for each cell.

Remark 4.1. Note that, formally, at each $t_{s,k}$, $k \geq 1$, the population should be augmented by a daughter cell, that has dynamics similar to mother one. Then, the number N is continuously growing. In this chapter, we will consider a fixed size of the population N, since as it will be shown below (and due to similarity of dynamics for newborn cells and initial conditions), the problem of phase synchronization can be analyzed using the model even for a single cell.

It is necessary to establish conditions (restrictions on f_s, u and $t_{s,k}$ or $\Lambda_{s,k,n}$) under which there exists a synchronization phenomenon in the cell population (4.3).

4.3.2 Reduced phase model under cell division

The presence of divisions can be alternatively modeled by an additional impulsion input:

$$\dot{x}_s(t) = f_s(x_s(t), u(t)) + \sum_{k=1}^{+\infty} \chi_{s,k}\, \delta(t - t_{s,k}), \tag{4.4}$$

where $\delta(t)$ is a delta-impulse function,

$$\chi_{s,k} = (\Lambda_{s,k,n_s} - I_{n_s})\, x_s(t_{s,k+1})$$

and I_{n_s} is the identity matrix of dimension n_s, $s = 1, 2, \ldots, N$.

Assumption 4.2. *For each $s = 1, 2, , N$, the s^{th} subsystem in (4.3), with $u = 0$ and $\Lambda_{s,k,n_s} = I_{n_s}$ for all $k \geq 0$, has a limit cycle $\Gamma_s \subset \mathcal{A}_s$ with an open set of attraction $\mathcal{A}_s \subset \mathbb{R}^{n_s}$, and with period $T_s > 0$, $\omega_s = 2\pi T_s^{-1}$.*

This assumption says that if there is no entrainment u and cell division, then each cell in the population is an oscillator with the limit cycle Γ_s and period T_s. Under Assumption 4.2 and using the theory presented in Appendix A, for each cell in (4.3) it is possible to define its asymptotic phase $\theta_s \in [0, 2\pi)$. Under additional restrictions that ε and W are sufficiently small, we can design a phase dynamical model of (4.3) in some vicinity of Γ_s as in Appendix A. Since the model derived in (A.4) is based on the first order approximation and in the system (4.4) there are two inputs (u and the train of impulses), by superposition principle, (A.4) takes the form in this case for $s = 1, 2, \ldots, N$:

$$\dot{\theta}_s = \omega_s + Q_s(t + \theta_{s,0}\omega_s^{-1})\, b_s(t + \theta_{s,0}\omega_s^{-1})\, u(t) + Q_s(t + \theta_{s,0}\omega_s^{-1}) \sum_{k=1}^{+\infty} \chi_{s,k}\delta(t - t_{s,k}), \tag{4.5}$$

where

$$b_s(t+\theta_{s,0}\omega_s^{-1}) = \left.\frac{\partial f_s(x_s,u)}{\partial u}\right|_{x_s=\gamma_s(t+\theta_{s,0}\omega_s^{-1})}$$

and $\gamma_s(t+\theta_{s,0}\omega_s^{-1})$ is a trajectory of the s^{th} cell in (4.3) for $u=0$ and $\Lambda_{s,k,n_s} = I_{n_s}$ for all $k \geq 0$ with initial conditions in Γ_s with the initial phase $\theta_{s,0} \in [0, 2\pi]$, $Q_s(t)$ is the infinitesimal PRC derived in the Appendix A. This model is constructed around the base trajectory $\gamma_s(t+\theta_{s,0}\omega_s^{-1})$ under the assumption that the perturbed trajectory with $u \neq 0$ and $\Lambda_{s,k,n_s} \neq I_{n_s}$ stays close to that one ([53]). Since such a closeness assumption is rather restrictive and may be invalid on a sufficiently long time interval (the excited trajectory can belong to a small vicinity of Γ_s for sufficiently small ε and W, but moving away from $\gamma_s(t+\theta_{s,0}\omega_s^{-1})$ due to a phase shift induced by external inputs), then it is better to recalculate the phase of base trajectory $\gamma_s(t+\theta_{s,0}\omega_s^{-1})$ after a period $\mathbb{T}$, for example (that is the idea of Poincaré phase map approach, [88]). In this case, by recurrent integration of (4.5), the phase shift over the interval $[i\mathbb{T}, (i+1)\mathbb{T}]$ can be evaluated as follows:

$$\theta_{s,i+1} = \omega_s(\mathbb{T} - T_s) + \theta_{s,i} + \mathrm{PRC}_s(\theta_{s,i}) + \Delta_{s,i}, \tag{4.6}$$

with

$$\mathrm{PRC}_s(\theta) = \int_0^{\mathcal{T}} Q_s(t+\theta\omega_s^{-1})\, b_s(t+\theta\omega_s^{-1})\, w(t)dt,$$
$$\Delta_{s,i} = \sum_{k\in\mathbb{K}_{s,i}} \chi_{s,k} Q_s(t_{s,k} + \theta_{s,i}\omega_s^{-1})$$

for all $s = 1, 2, \ldots, N$, where

$\mathbb{K}_{s,i} = \{k \geq 1 \mid t_{s,k} \in [i\mathbb{T}, (i+1)\mathbb{T}]\}$ is the set of indexes whose impulses happen in the interval $[i\mathbb{T}, (i+1)\mathbb{T}]$, $\mathrm{PRC}_s : [0, 2\pi) \to [0, 2\pi)$ is the PRC of the s^{th} oscillator for the pulse w and $\Delta_{s,i} \in \mathbb{R}$ is the phase perturbation imported by cell division on the interval $[i\mathbb{T}, (i+1)\mathbb{T}]$.

Remark 4.3. Formally, the set $\mathbb{K}_{s,i}$ can be decomposed on two parts:

$$\mathbb{K}_{s,i} = \mathbb{K}^1_{s,i} \cup \mathbb{K}^2_{s,i},$$
$$\mathbb{K}^1_{s,i} = \{k \geq 1 \mid t_{s,k} \in [i\mathbb{T}, i\mathbb{T} + \mathcal{T}]\},$$
$$\mathbb{K}^2_{s,i} = [i\mathbb{T} + \mathcal{T}, (i+1)\mathbb{T}],$$

where $\mathbb{K}^1_{s,i}$ characterizes the impulses arrived for $u(t) \neq 0$ and $\mathbb{K}^2_{s,i}$ is for $u(t) = 0$ on the

interval $[i\mathbb{T}, (i+1)\mathbb{T}]$. Then the model (4.6) can be rewritten as follows:

$$\theta_{s,i+1} = \omega_s(\mathbb{T} - T_s) + \theta_{s,i} + \mathrm{PRC}_s(\theta_{s,i} + \Delta^1_{s,i}) + \Delta_{s,i},$$
$$\Delta_{s,i} = \Delta^1_{s,i} + \Delta^2_{s,i},$$
$$\Delta^j_{s,i} = \sum_{k \in \mathbb{K}^j_{s,i}} \chi_{s,k} Q_s(t_{s,k} + \theta_{s,i}\omega_s^{-1}),\ j = 1, 2.$$

The difference with respect to (4.6) is that the perturbation caused by cell division appears nonlinearly in the last model. For brevity of consideration only the case of (4.6) is studied below.

4.3.3 Phase synchronization

The model (4.6) for each $s = 1, 2, \ldots, N$ is a scalar nonlinear integrator-like discrete-time system (that is a considerable advantage with respect to (4.3)) with the state $\theta_{s,i}$ and external input $\omega_s(\mathbb{T} - T_s) + \Delta_{s,i}$, where the constant part represents the influence of entrainment and $\Delta_{s,i}$ is the perturbation originated by cell division.

Assume that there is no common entrainment and $u(t) = 0$, then the model (4.6) can be simplified to a pure integrator over the interval $[i\mathbb{T}, (i+1)\mathbb{T}]$ as:

$$\theta_{s,i+1} = \theta_{s,i} + \Delta_{s,i}.$$

If $\Delta_{s,i}$ are different for each $s = 1, 2, \ldots, N$ and have not a zero mean, then the phase $\theta_{s,i}$ will be drifting in a unique manner for each $s = 1, 2, \ldots, N$. Thus, there is no phase synchronization. This is the case presented in Fig. 4.1 and also observed in [72, 112].

Therefore, the synchronous properties of (4.6) depend critically on the nonlinear function PRC_s. In this chapter, as in [44, 53, 57], we assume that the PRC map has particular properties (similar to type II PRC from [84], where either an advance or delay in phase can be produced depending upon the timing of the perturbation ([33])).

Assumption 4.4. *For all $s = 1, 2, \ldots, N$, the map PRC_s is continuously differentiable and there exist $0 < \beta_s \leq 1$ and $\Theta_s \in [0, 2\pi)$ such that the equation $\mathrm{PRC}_s(\theta^0_s) = \omega_s(T_s - \mathbb{T})$ has a solution $\theta^0_s \in [0, 2\pi)$ with*

$$-2 + \beta_s \leq \frac{\partial\, \mathrm{PRC}_s(\theta)}{\partial\theta} \leq -\beta_s \quad \forall\theta \in [\theta^0_s - \Theta_s, \theta^0_s + \Theta_s].$$

Obviously, for $\Delta_{s,i} = 0$ (no cell division), θ^0_s corresponds to a stable equilibrium of the system (4.6) for given s with the domain of attraction $[\theta^0_s - \Theta_s, \theta^0_s + \Theta_s]$ ([88]).

Lemma 4.5. *For each $s = 1, 2, \ldots, N$, under the Assumption 4.4, if $|\theta_{s,0} - \theta_s^0| \leq \Theta_s - \beta_s^{-1}\overline{\Delta_s}$ where $\overline{\Delta_s} = \sup_{i\geq 0} |\Delta_{s,i}| < +\infty$, then*

$$|\theta_{s,i} - \theta_s^0| \leq \Theta_s \quad \forall i \geq 0, \ \lim_{i\to+\infty} |\theta_{s,i} - \theta_s^0| \leq \beta_s^{-1}\overline{\Delta_s}. \tag{4.7}$$

Proof. Taking into account definition of θ_s^0, the model (4.6) can be rewritten as follows:

$$\theta_{s,i+1} = \theta_{s,i} + \mathrm{PRC}_s(\theta_{s,i}) - \mathrm{PRC}_s(\theta_s^0) + \Delta_{s,i}.$$

Using the Mean value theorem (PRC_s is continuously differentiable by Assumption 4.4), we obtain:

$$\theta_{s,i+1} = \theta_{s,i} + \frac{\partial \mathrm{PRC}_s(\theta'_{s,i})}{\partial \theta'_{s,i}}(\theta_{s,i} - \theta_s^0) + \Delta_{s,i},$$

where $\theta'_{s,i} = \mu\theta_{s,i} + (1-\mu)\theta_s^0$ for some $\mu \in [0,1]$. Define the phase error $e_{s,i} = \theta_{s,i} - \theta_s^0$, then

$$e_{s,i+1} = \left(1 + \frac{\partial \mathrm{PRC}_s(\theta'_{s,i})}{\partial \theta'_{s,i}}\right) e_{s,i} + \Delta_{s,i}.$$

By Assumption 4.4, $-2 + \beta_s \leq \frac{\partial \mathrm{PRC}_s(\theta'_{s,i})}{\partial \theta'_{s,i}} \leq -\beta_s$ provided that $|e_{s,i}| \leq \Theta_s$. Then taking Lyapunov function $V(e) = |e|$, we have:

$$\begin{aligned} V(e_{s,i+1}) - V(e_{s,i}) &= \left|\left(1 + \frac{\partial \mathrm{PRC}_s(\theta'_{s,i})}{\partial \theta'_{s,i}}\right) e_{s,i} + \Delta_{s,i}\right| \\ &\qquad - |e_{s,i}| \\ &\leq \left(\left|1 + \frac{\partial \mathrm{PRC}_s(\theta'_{s,i})}{\partial \theta'_{s,i}}\right| - 1\right) |e_{s,i}| + |\Delta_{s,i}| \\ &\leq -\beta_s V(e_{s,i}) + |\Delta_{s,i}|, \end{aligned}$$

that implies

$$|e_{s,i}| \leq (1-\beta_s)^i |e_{s,0}| + \beta_s^{-1}\overline{\Delta_s} \quad i \geq 0$$

under assumption that $|e_{s,i}| \leq \Theta_s$ for all $i \geq 0$. However, if $|e_{s,0}| \leq \Theta_s - \beta_s^{-1}\overline{\Delta_s}$ then $|e_{s,i}| \leq \Theta_s$ for all $i \geq 0$ as needed, and $\lim_{i\to+\infty} |e_{s,i}| \leq \beta_s^{-1}\overline{\Delta_s}$. □

Consequently, if the influence of cell division quantified by $\overline{\Delta_s}$ is sufficiently small and the initial phase $\theta_{s,0}$ lies sufficiently close to θ_s^0, then the phase $\theta_{s,i}$ stays in the domain of attraction of θ_s^0 and asymptotically converges to a vicinity of that equilibrium. Since all cells in population (4.3) yield this kind of behavior, then under these conditions, the phases are asymptotically synchronized with the error of synchronization proportional

to superposition of $\max\{\beta_{s_1}^{-1}\overline{\Delta_{s_1}}, \beta_{s_2}^{-1}\overline{\Delta_{s_2}}\}$ and $|\theta_{s_1}^0 - \theta_{s_2}^0|$ for any $1 \le s_1 \ne s_2 \le N$.

Theorem 4.6. *Let assumptions 4.2, 4.4 be satisfied and ε, w be sufficiently small in (4.3). If $|\theta_{s,0} - \theta_s^0| \le \Theta_s - \beta_s^{-1}\overline{\Delta_s}$ for all $s = 1, 2, \dots, N$, then for any $1 \le s_1 \ne s_2 \le N$*

$$|\theta_{s_1,i} - \theta_{s_2,i}| \le |\theta_{s_1}^0 - \theta_{s_2}^0| + \Theta_{s_1} + \Theta_{s_2} \quad \forall i \ge 0,$$
$$\lim_{i\to+\infty} |\theta_{s_1,i} - \theta_{s_2,i}| \le |\theta_{s_1}^0 - \theta_{s_2}^0| + \beta_{s_1}^{-1}\overline{\Delta_{s_1}} + \beta_{s_2}^{-1}\overline{\Delta_{s_2}}.$$

Proof. If Assumption 4.2 holds and ε, W are sufficiently small, then the results presented in Appendix A imply that a first order approximation of (4.3) can be used for analysis of the population behavior, and the reduced PRC model (4.6) can be derived for each $s = 1, 2, \dots, N$. Next, since all conditions of Lemma 4.5 are satisfied, then the relations (4.7) are valid for all $s = 1, 2, \dots, N$. Consider the phase difference $\theta_{s_1,i} - \theta_{s_2,i}$ of any two oscillators with $1 \le s_1 \ne s_2 \le N$. Since

$$\theta_{s_1,i} - \theta_{s_2,i} = \theta_{s_1,i} - \theta_{s_1}^0 - \theta_{s_2,i} + \theta_{s_2}^0 + \theta_{s_1}^0 - \theta_{s_2}^0$$

from (4.7):

$$\begin{aligned} |\theta_{s_1,i} - \theta_{s_2,i}| &\le |e_{s_1,i} - e_{s_2,i}| + |\theta_{s_1}^0 - \theta_{s_2}^0| \\ &\le |\theta_{s_1}^0 - \theta_{s_2}^0| + \Theta_{s_1} + \Theta_{s_2} \end{aligned}$$

and

$$\begin{aligned} \lim_{i\to+\infty} |\theta_{s_1,i} - \theta_{s_2,i}| &\le \lim_{i\to+\infty} |e_{s_1,i} - e_{s_2,i}| + |\theta_{s_1}^0 - \theta_{s_2}^0| \\ &\le |\theta_{s_1}^0 - \theta_{s_2}^0| + \beta_{s_1}^{-1}\overline{\Delta_{s_1}} + \beta_{s_2}^{-1}\overline{\Delta_{s_2}} \end{aligned}$$

as required. □

This theorem establishes phase-lock behavior in the population (4.3), which may be composed by different cells. If all cells are identical, then the following synchronization conditions can be obtained.

Corollary 4.7. *Let all conditions of Theorem 4.6 be satisfied and $\mathrm{PRC}_s(\theta) = \mathrm{PRC}(\theta)$ for all $s = 1, 2, \dots, N$ and all $\theta \in [0, 2\pi)$ (then also $\theta_s^0 = \theta^0$, $\Theta_s = \Theta$ and $\beta_s = \beta$). If $|\theta_{s,0} - \theta^0| \le \Theta - \beta^{-1}\overline{\Delta_s}$ for all $s = 1, 2 \dots N$, then*

$$|\overline{\theta}_i - \theta^0| \le \Theta, \quad \forall i \ge 0, \ \lim_{i\to+\infty} |\overline{\theta}_i - \theta^0| \le \frac{1}{N\beta}\sum_{s=1}^{N}\overline{\Delta_s},$$

where $\overline{\theta}_i = N^{-1}\sum_{s=1}^{N}\theta_{s,i}$ *is the average phase of the population.*

Proof. The result follows from Lemma 4.5 and Theorem 4.6 under assumption that all PRC_s are identical. □

If there is no cell division, then

$$\frac{1}{N\beta}\sum_{s=1}^{N}\overline{\Delta_s} = 0$$

and we recover a well-known result on phase synchronization under a periodical entrainment ([53, 88]).

4.4 Examples

Let us illustrate the theoretical findings obtained in the previous Section.

4.4.1 Circadian oscillations in *Neurospora*

Consider a population of circadian oscillators in *Neurospora* (4.1). Take all cells in the population identical with the values of parameters given in Section 4.2. Then the Assumption 4.2 is satisfied for $T_s = T = 19.25$ hours ($\omega = 2\pi T^{-1}$). Select

$$w(t) = \begin{cases} \max\{0, W\sin(\omega t)\} & \text{if } 0 \le t \le T \\ 0 & \text{otherwise} \end{cases}$$

with $W = 0.02$. Setup the same $\Lambda_{s,k,n}$ for all s and n as Λ_k defined by:

$$\Lambda_k = \mathrm{diag}[0.99\ 0.98\ 0.98]$$

with $t_k = k\,(T - \upsilon_k)$, $k \ge 1$, where $\upsilon_k \in [0.15T, 0.30T]$ is a uniformly distributed random variable as before. The values ε, W are chosen sufficiently small. For this pulse $w(t)$, the obtained $\mathrm{PRC}(\theta)$ and $\mathrm{PRC}'(\theta) = \frac{\partial\,\mathrm{PRC}(\theta)}{\partial\theta}$ are shown in Fig. 4.4. From these plots, $\theta^0 = 2.34$, $\Theta = 1.04$ and $\beta = 0.05$, and the Assumption 4.4 is also satisfied. Thus, all conditions of Theorem 4.6 are verified.

Simulated phase behavior of (4.1) is shown in Fig. 4.5 by the blue curve (the phase value was computed by finding the closest point on the limit cycle at instants iT for $i \ge 0$ and by assigning the phase of that point as θ_i). The values of phase obtained by the model (4.6) are presented in the same figure by the red curve. As we can see, both

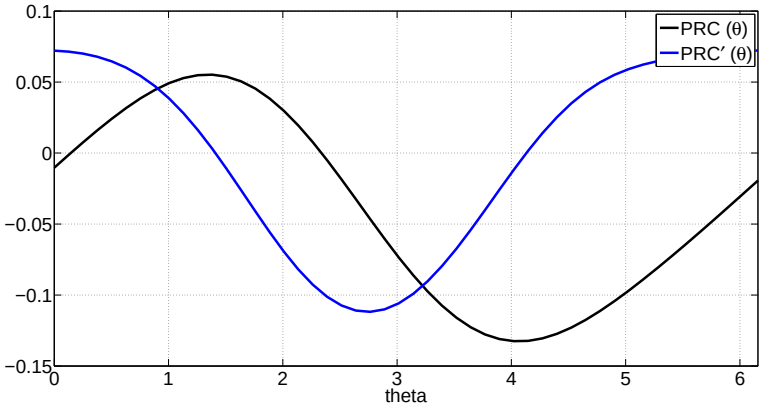

Figure 4.4: PRC(θ) and PRC'(θ) for the input $w(t)$ for *Neurospora* model.

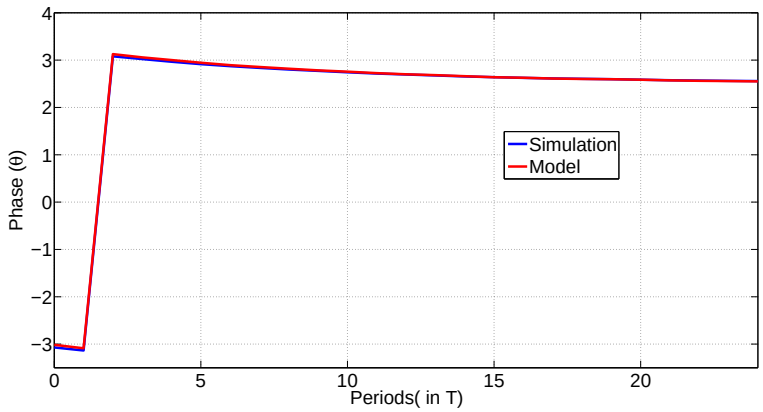

Figure 4.5: Phase behavior of (4.1)

curves are very close and that confirms all theoretical developments presented in this chapter, and phase asymptotically converges to a vicinity of θ^0, then synchronization of phase would be observed for a population of circadian oscillators of *Neurospora* (4.3) as in [77] for the Goodwin model.

4.4.2 The Repressilator

The *repressilator* ([60]) is a very simple genetic oscillator consisting of three genes, which can be modeled as below ([77]):

$$\begin{aligned}
\dot{M}_1(t) &= \alpha_0 + \alpha_1 \frac{K^n}{K^n + P_3^n(t)} - \delta M_1(t) + u(t) \\
\dot{M}_2(t) &= \alpha_0 + \alpha_1 \frac{K^n}{K^n + P_1^n(t)} - \delta M_2(t) \\
\dot{M}_3(t) &= \alpha_0 + \alpha_1 \frac{K^n}{K^n + P_2^n(t)} - \delta M_3(t) \\
\dot{P}_1(t) &= \beta M_1(t) - \gamma P_1(t) \\
\dot{P}_2(t) &= \beta M_2(t) - \gamma P_2(t) \\
\dot{P}_3(t) &= \beta M_3(t) - \gamma P_3(t)
\end{aligned} \tag{4.8}$$

where the variables $M_i(t)$ and $P_i(t)$ (with $i = 1, 2, 3$) represent the concentrations of mRNA and protein of the three components of the *repressilator* respectively and $u(t) \geq 0$ represents the external entraining input. Details about other parameters of the model can be found in [77]. We will consider the following values for (4.8): $\alpha_1 = 1min^{-1}$, $\alpha_0 = 0.01min^{-1}$, $K = 1$, $n = 2$ and $\delta = \beta = \gamma = 0.1min^{-1}$. With these values, this model has a single equilibrium and one limit cycle and the period of autonomous oscillation is obtained as $T = 116.6$ minutes. In this chapter we have not consider the robustness of the *repressilator* model with respect to variation in its various parameters, however it can be done following the idea presented in [39] through Monte-Carlo simulation.

Now, let us consider a population of identical *repressilators* with the previously mentioned parameters. The Assumption 4.2 is satisfied for $T_s = T = 116.6\text{min}$ ($\omega = 2\pi T^{-1}$). Select

$$w(t) = \begin{cases} \max\{0, W \sin(\omega t)\} & \text{if } 0 \leq t \leq T \\ 0 & \text{otherwise} \end{cases}$$

with $W = 0.002$. As seen previously, set:

$$\Lambda_k = \text{diag}[0.99\ 0.98\ 0.98]$$

with $t_k = k\,(T - \upsilon_k)$, $k \geq 1$, where $\upsilon_k \in [0.15T, 0.30T]$ is a uniformly distributed random variable as before. The values ε, W are chosen sufficiently small. For this pulse $w(t)$ the obtained $\text{PRC}(\theta)$ and $\text{PRC}'(\theta) = \frac{\partial\,\text{PRC}(\theta)}{\partial\theta}$ are shown in Fig. 4.6, from these plots $\theta^0 = 3.9$ (which is -2.4 in a scale between $-\pi$ to π), $\Theta = 1.6$ and $\beta = 0.01$, and Assumption 4.4 is also satisfied. Thus, all conditions of Theorem 4.6 are verified.

Simulated phase behavior of (4.8) is shown in Fig. 4.7 by the blue curve (the phase value was computed by finding the closest point on the limit cycle at instants iT for

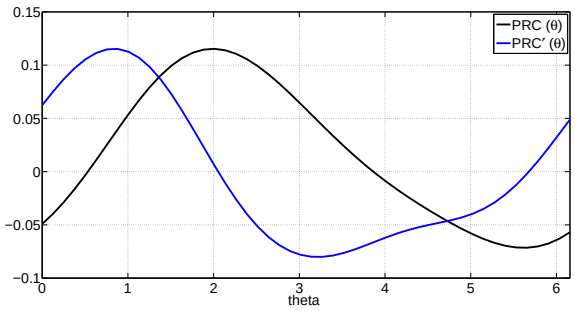

Figure 4.6: PRC(θ) and PRC'(θ) for the input $w(t)$ for the *repressilator* model.

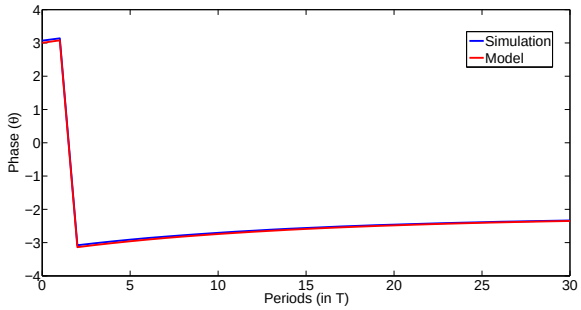

Figure 4.7: Phase behavior of (4.8)

$i \geq 0$ and by assigning the phase of that point as θ_i). The values of phase obtained by the model (4.6) are presented in the same figure by the red curve. As we can see, both curves are very close and that confirms all theoretical developments presented in this chapter, and phase asymptotically converges to a vicinity of θ^0, then synchronization of phase would be observed for a population of *repressilator* model (4.3) as in [77].

4.5 Conclusion

The influence of cell division on the dynamics of a population of genetic oscillators is analyzed. As it has been observed *in vivo* ([60, 72, 109, 112]), oscillations in cells are frequently quite resilient to cell division. Recently, this phenomenon has been analyzed by a stochastic simulation in [77], where phase synchronization in the population has been observed. Modeling cell division by impulses places the dynamics of population in the class of hybrid systems. In this chapter, analytical conditions are established for phase synchronization applying PRC model approach for small inputs. The results are illustrated by numerical experiments with two different circadian/genetic oscillator models.

Chapter 5

Robust synchronization for multistable systems

5.1 Introduction

Over the last decades, the synchronization of complex dynamical systems and/or network of systems has attracted a great attention from multidisciplinary research communities thanks to their pervasive presence in nature, technology and human society [119, 124, 139]. A collective behavior occurs in the interconnection of dynamical systems and it has several potential application domains. For instance, transient stability in power network, cooperative multitasking and formation control. The core of synchronization is the collective objective of agents in a network to reach a consensus about certain variables of interest.

The existing literature on the synchronization problem is very vast and covers many areas. In [70], the problem of formation control is investigated in swarms within the framework of output regulation in nonlinear systems. A detailed study regarding the control and synchronization of chaos can be found in [76]. The paper [101] extends optimal control and adaptive control design methods to multi-agent nonlinear systems on communication graphs. Recent advances in various aspects of cooperative control of multi-agent systems can be found in [132]. The theoretical framework for design and analysis of distributed flocking algorithms can be found in [118].

In this chapter, we consider the synchronization problem for multistable systems based on the framework of Input-to-State Stability (ISS). This is a very well established method for the study of stability and robustness of nonlinear systems. The ISS property provides a natural framework of stability analysis with respect to input perturbations (see [46] and references therein). The classical definition allows to formulate and

characterize stability properties with respect to arbitrary compact invariant sets (and not simply equilibria). Nevertheless, the implicit requirement that these sets should be simultaneously Lyapunov stable and globally attractive, makes the basic theory not applicable for a global analysis of many dynamical behaviors of interest, having multistability [16, 19, 71] or periodic oscillations [138], just to name a few, and only local analysis remains possible [37]. Some attempts were made to overcome such limitations by introducing the notions of almost global stability [128] and almost input-to-state stability [13], *etc.*

Recently, the authors in [14] have proposed that the most natural way of relaxing ISS condition for systems with multiple invariant sets is equivalent to relax the Lyapunov stability requirement [52] (rather than the global nature of the attractivity property). Using this relatively mild conditions in [14], they have generalized the ISS theory as well as the related literature on time invariant autonomous dynamical systems on compact spaces [116] for multistable systems. Multistability accounts for the possible coexistence of various oscillatory regimes or equilibria in the phase space of the system for the same set of parameters. Any system that exhibits multistability is called a multistable system. For a multistable system, it is frequently very difficult to predict the asymptotic regime on which this system will attain asymptotically for the given set of initial conditions and inputs [59]. In this chapter, the results presented in [14] are applied to provide sufficient conditions for the existence of robust synchronization for multistable systems in the presence of external inputs. The conditions obtained in this chapter are global.

The rest of this chapter is organized as follows. Some preliminaries about decomposable sets and notions of robustness that are related to this work can be consulted from the Appendix C. Our main results and the family of nonlinear systems being considered in this chapter can be found in Section 5.2. In Section 5.3, numerical simulation examples are given to illustrate these results. Concluding remarks in Section 5.4 close this chapter.

5.2 Synchronization of multistable systems

The following family of nonlinear systems is considered in this section:

$$\dot{x}_i(t) = f_i\left(x_i(t), u_i(t), d_i(t)\right), \ i = 1, \ldots, N, \ N > 1, \tag{5.1}$$

where the state $x_i(t) \in M_i$, with M_i an n_i-dimensional $\mathcal{C}^2$ connected and orientable Riemannian manifold without a boundary, the control $u_i(t) \in \mathbb{R}^{m_i}$ and the external

disturbance $d_i(t) \in \mathbb{R}^{p_i}$ ($u_i(\cdot)$ and $d_i(\cdot)$ are locally essentially bounded and measurable signals) for $t \geq 0$ and the map $f_i : M_i \times \mathbb{R}^{m_i} \times \mathbb{R}^{p_i} \to T_{x_i}M_i$ is $\mathcal{C}^1$, $f_i(0,0,0) = 0$. Denote the common state vector of (5.1) as $x = [x_1^T, \ldots, x_N^T]^T \in M = \prod_{i=1}^N M_i$, so M is the corresponding Riemannian manifold of dimension $n = \sum_{i=1}^N n_i$ where the family (5.1) behaves and $d = [d_1^T, \ldots, d_N^T]^T \in \mathbb{R}^p$ with $p = \sum_{i=1}^N p_i$ is the total exogenous input. For further reading of this chapter, readers are requested to consult Appendix C first to be familiar with the notions that will be used later in this chapter.

Assumption 5.1. *For all $i = 1, \ldots, N$, each system in (5.1) has a compact invariant set $\mathcal{W}_i$ containing all $\alpha-$ and $\omega-$ limit sets of $\dot{x}_i(t) = f_i(x_i(t), 0, 0)$, $\mathcal{W}_i$ is decomposable in the sense of Definition C.7 (given in Appendix C), and the system enjoys the AG property with respect to inputs u_i and d_i as in Definition C.8 (given in Appendix C).*

Under this assumption, from Theorem C.12 (given in Appendix C), there exist $\mathcal{C}^1$ ISS-Lyapunov functions $V_i : M_i \to \mathbb{R}$ with $\mathcal{K}_\infty$ functions $\alpha_{1i}, \alpha_{2i}, \alpha_{3i}, \gamma_{ui}$ and γ_{di} such that

$$\begin{aligned} \alpha_{1i}(|x_i|_{\mathcal{W}_i}) \leq V_i(x_i) \leq \alpha_{2i}(|x_i|_{\mathcal{W}_i} + c_i),\ c_i \geq 0, \\ DV_i(x_i) f_i(x_i, u_i, d_i) \leq -\alpha_{3i}(|x_i|_{\mathcal{W}_i}) + \gamma_{ui}(|u_i|) + \gamma_{di}(|d_i|) \end{aligned} \tag{5.2}$$

for all $i = 1, \ldots, N$. Define also the invariant set of disconnected and unperturbed ($u_i = d_i = 0$) family $\mathcal{W} = \prod_{i=1}^N \mathcal{W}_i \subset M$ ($0 \in \mathcal{W}$). Then, by definition, there exist functions $\nu_1, \nu_2 \in \mathcal{K}_\infty$ such that

$$\nu_1(|x|_{\mathcal{W}}) \leq \sum_{i=1}^N |x_i|_{\mathcal{W}_i} \leq \nu_2(|x|_{\mathcal{W}}) \tag{5.3}$$

for all $x \in M$. Since the set $\mathcal{W}$ is compact, then there are functions $\nu_3, \nu_4 \in \mathcal{K}_\infty$ and a scalar $c_0 \geq 0$ such that for all $x \in M$,

$$|x| \leq \nu_3(|x|_{\mathcal{W}}) + c_0,\ |x|_{\mathcal{W}} \leq \nu_4(|x|). \tag{5.4}$$

Hence, we will consider in this chapter, the family (5.1) under Assumption 5.1, *i.e.* a family of robustly stable nonlinear systems. In general, the sets $\mathcal{W}_i$ include equilibrium (at the origin, for instance) and limit cycles of agents in (5.1). There are several works devoted to synchronization and design of consensus protocols for such a family or oscillatory network [102, 127, 151]. The goal of this chapter is to find a condition under which the existence of a global synchronization/consensus protocol for $d = 0$ implies robust synchronization in (5.1) for a bounded $d \neq 0$.

Let a $\mathcal{C}^1$ function $y(x) : M \to \mathbb{R}^q$, $y(0) = 0$ be a synchronization measure for (5.1). We say that the family (5.1) is synchronized (or reached the consensus) if $y(x(t)) \equiv 0$ for all $t \geq 0$ on the solutions of the network (5.1) under properly designed control actions

$$u_i(t) = \varphi_i[y(x(t))] \tag{5.5}$$

($\varphi_i : \mathbb{R}^q \to \mathbb{R}^{m_i}$ is a $\mathcal{C}^1$ function, $\varphi_i(0) = 0$) for $d(t) \equiv 0$, $t \geq 0$. In this case the set $\mathcal{A} = \{x \in \mathcal{W} \mid y(x) = 0\}$ contains the synchronous solutions of the unperturbed family in (5.1) and the problem of synchronization of "natural" trajectories is considered since $\mathcal{A} \subset \mathcal{W}$. Due to the condition $\varphi_i(0) = 0$, the convergence of y (synchronization/consensus) implies that the solutions of the interconnection belong to $\mathcal{W}$, the conditions of convergence of the synchronizing/consensus output y can be found in [102, 127, 151].

The proposed synchronization protocol is output based, as in [102, 127, 151]. The synchronization measure y in general depends on some elements of the vectors x_i for all $i = 1, \ldots, N$. In addition, since y is a vector, then different topology of interconnection can be imposed, see examples in Section 5.3.

Assumption 5.2. *The set $\mathcal{A}$ is compact, it contains all $\alpha-$ and $\omega-$ limit sets of (5.1), (5.5) for $d = 0$, and it is decomposable.*

Therefore, it is assumed that the controls $\varphi_i(y)$ ensure the network global synchronization, while decomposability in general follows from Assumption 5.1. We will show that in the setup as above, by selecting the shapes of φ_i, it is possible to guarantee robust synchronization of (5.1) for any measurable and essentially bounded input d.

By continuity arguments, there exist functions $\eta_1, \eta_2, \mu_i \in \mathcal{K}_\infty$ with a scalar $\eta_0 \geq 0$ such that for all $x \in M$:

$$\begin{gathered} |y(x)| \leq \eta_0 + \eta_1(|x|_{\mathcal{W}}),\ |y(x)| \leq \eta_2(|x|), \\ |\varphi_i(y)| \leq \mu_i(|y|) \end{gathered} \tag{5.6}$$

(note that the first two inequalities are related through (5.4)). Then the intermediate result below can be proven under Assumption 5.1 for (5.1), (5.5).

Proposition 5.3. *Let Assumption 5.1 be satisfied for (5.1). Then there exist φ_i, $i = 1, \ldots, N$ in (5.5) such that the interconnection (5.1), (5.5) has pGS property with respect to the set $\mathcal{W}$.*

Proof. Consider a Lyapunov function candidate $S(x) = \sum_{i=1}^N V_i(x_i)$, where the functions V_i are given in (5.2). From (5.3), there exist two functions $\underline{\alpha}, \overline{\alpha} \in \mathcal{K}_\infty$ and a scalar $g \geq 0$

such that for all $x \in M$:

$$\underline{\alpha}(|x|_{\mathcal{W}}) \leq S(x) \leq \overline{\alpha}(|x|_{\mathcal{W}} + g).$$

Taking the derivative of S with respect to equations in (5.1), (5.5) we obtain:

$$\dot{S} \leq \sum_{i=1}^{N}[-\alpha_{3i}(|x_i|_{\mathcal{W}_i}) + \gamma_{ui}(|\varphi_i(y)|) + \gamma_{di}(|d_i|)].$$

From (5.3) and (5.6), we deduce:

$$\begin{aligned}
\sum_{i=1}^{N} \alpha_{3i}(|x_i|_{\mathcal{W}_i}) &\geq 2\alpha_4(|x|_{\mathcal{W}}),\\
\sum_{i=1}^{N} \gamma_{ui}(|\varphi_i(y)|) &\leq \sum_{i=1}^{N} \gamma_{ui} \circ \mu_i(|y|)\\
&\leq \sum_{i=1}^{N} \gamma_{ui} \circ \mu_i(\eta_0 + \eta_1(|x|_{\mathcal{W}}))\\
&\leq h + \sum_{i=1}^{N} \gamma_{ui} \circ \mu_i(2\eta_1(|x|_{\mathcal{W}})),
\end{aligned}$$

for some $\alpha_4 \in \mathcal{K}_\infty$ and where $h = \sum_{i=1}^{N} \gamma_{ui} \circ \mu_i(2\eta_0)$. By optimizing the shape of φ_i, it is possible to adjust the form of μ_i. In particular, providing that

$$\mu_i(s) \leq \gamma_{ui}^{-1}\left[N^{-1}\alpha_4 \circ \eta_1^{-1}(0.5s)\right]$$

for all $i = 1, \ldots, N$ we guarantee the relation $\gamma_{ui} \circ \mu_i(2\eta_1(s)) \leq \frac{1}{N}\alpha_4(s)$, then

$$\sum_{i=1}^{N} \gamma_{ui}(|\varphi_i(y)|) \leq h + \sum_{i=1}^{N} \frac{1}{N}\alpha_4(s) \leq h + \alpha_4(s).$$

Substituting the obtained terms in the inequality derived for $\dot{S}$, we obtain

$$\dot{S} \leq -\alpha_4(|x|_{\mathcal{W}}) + h + \gamma_d(|d|),$$

where γ_d is a function from class $\mathcal{K}_\infty$ such that $\sum_{i=1}^{N} \gamma_{di}(|d_i|) \leq \gamma_d(|d|)$. Finally, $\alpha_4 \circ \overline{\alpha}^{-1}[S(x)] \leq \alpha_4(2|x|_{\mathcal{W}}) + \alpha_4(2g)$ and

$$\dot{S} \leq -\alpha_4 \circ \overline{\alpha}^{-1}(S) + h + \alpha_4(2g) + \gamma_d(|d|),$$

which by the standard arguments [136] implies that for all $t \geq 0$

$$S(t) \leq \beta(S(0), t) + r + \gamma'_d(\|d\|_\infty)$$

for some function $\beta \in \mathcal{KL}$, $\gamma'_d \in \mathcal{K}$ and a scalar $r \geq 0$. The pGS property follows taking in mind that $\underline{\alpha}(|x(t)|_{\mathcal{W}}) \leq S(t)$, $S(0) \leq [\overline{\alpha}(|x(0)|_{\mathcal{W}} + g)]$ and the properties of a function from the class $\mathcal{KL}$. □

Note that by definition of the set $\mathcal{A}$, $|x(t)|_{\mathcal{W}} \leq |x(t)|_{\mathcal{A}} \leq |x(t)|_{\mathcal{W}} + z$ for a scalar $z \geq 0$ for all $x \in M$, then the pGS property with respect to the set $\mathcal{A}$ has also been proven.

Therefore, in the setup used in this chapter the boundedness of trajectories (boundedness of $|x(t)|_{\mathcal{W}}$ implies the same property for $|x(t)|$ according to (5.4)) follows by a proper selection of the interconnection gain in (5.5), *i.e.* by decreasing the control gain a certain robustness of (5.1), (5.5) is inherited after individual systems as it is stated in Assumption 5.1.

Theorem 5.4. *There exist φ_i, $i = 1, \ldots, N$ in (5.5) such that the interconnection (5.1), (5.5) has AG property with respect to $\mathcal{A}$, provided that assumptions 5.1 and 5.2 are satisfied for (5.1), (5.5).*

Proof. Since all conditions of Proposition 5.3 are satisfied, by a proper selection of φ_i, the Lyapunov function S has the properties as in the proof above. From (5.6) $\alpha_4 \circ \eta_1^{-1}(0.5|y(x)|) \leq \alpha_4 \circ \eta_1^{-1}(\eta_0) + \alpha_4(|x|_{\mathcal{W}})$. Then

$$\dot{S} \leq -0.5\alpha_4(|x|_{\mathcal{W}}) - 0.5\alpha_5(|y(x)|) + h' + \gamma_d(|d|),$$

where $h' = h + 0.5\alpha_4 \circ \eta_1^{-1}(\eta_0)$ and $\alpha_5(s) = \alpha_4 \circ \eta_1^{-1}(0.5s)$. By the definition of the set $\mathcal{A}$, there exists $\theta \in \mathcal{K}_\infty$ such that $\alpha_4(|x|_{\mathcal{W}}) + \alpha_5(|y(x)|) \geq 2\theta(|x|_{\mathcal{A}})$ for all $x \in M$, then

$$\dot{S} \leq -\theta(|x|_{\mathcal{A}}) + h' + \gamma_d(|d|).$$

According to Proposition 5.3, the solutions are bounded. Hence, the system (5.1), (5.5) is forward complete. Following [18], for any forward complete system, there exists a smooth function $Q : M \to \mathbb{R}$ (the proof in [18] deals with Euclidean spaces, but similar arguments can be adopted here) such that for all $x \in M$ and $d \in \mathbb{R}^p$

$$\psi_1(|x|) \leq Q(x) \leq \psi_2(|x|), \ \dot{Q} \leq 1 + \rho(|d|)$$

for some $\psi_1, \psi_2, \rho \in \mathcal{K}_\infty$. Note that there exists $\nu_5 \in \mathcal{K}_\infty$ such that $|x|_{\mathcal{A}} \leq \nu_5(|x|)$ for all $x \in M$ similarly to (5.4). Let us introduce a practical ISS Lyapunov function $U(x) = Q(x) + S(x)$ for (5.1), (5.5), then for all $x \in M$ and $d \in \mathbb{R}^p$ we have

$$\begin{aligned} \underline{\alpha}'(|x|_{\mathcal{A}}) \leq U(x) \leq \overline{\alpha}'(|x|_{\mathcal{A}} + g'), \\ \dot{U} \leq -\theta(|x|_A) + h' + 1 + \gamma_d(|d|) + \rho(|d|) \end{aligned}$$

for properly defined $\underline{\alpha}', \overline{\alpha}' \in \mathcal{K}_\infty$ and a scalar $g' \geq 0$. Thus, U admits all requirements imposed on practical ISS Lyapunov functions, and under Assumption 5.2 the system (5.1), (5.5) possesses all properties in Theorem C.12 and it is ISS with respect to $\mathcal{A}$. □

Roughly speaking, this qualitative result states that if the synchronized output y is related with $|x|_{\mathcal{W}}$ as in (5.6) and each system in the network is robustly stable as in Assumption 5.1, then the system can be robustly synchronized by a sufficiently small bounded feedback proportional to y.

5.3 Examples and simulations

5.3.1 Application to nonlinear pendulums without friction

Consider a network of nonlinear identical pendulums for $i = 1, \ldots, N$, $N > 1$:

$$\begin{aligned} \dot{x}_{1i} &= x_{2i}, \\ \dot{x}_{2i} &= -\omega \sin(x_{1i}) + v_i + d_i, \end{aligned} \tag{5.7}$$

where the state $x_i = [x_{1i}, x_{2i}]$ takes values on the cylinder $M_i := \mathbb{S} \times \mathbb{R}$, the exogenous disturbance $d_i(t) \in \mathbb{R}$, the regulation input $u_i(t) \in \mathbb{R}$, and ω is a constant positive parameter. The unperturbed system is conservative with Hamiltonian $H(x_i) = 0.5x_{2i}^2 + \omega(1 - \cos(x_{1i}))$ and $\dot{H} = x_{2i}(v_i + d_i)$. The control v_i will have two parts, one to force controlled oscillations in (5.7) and one for the synchronization u_i:

$$v_i = -x_{2i}[H(x_i) - H^*] + u_i,$$

where $0 < H^* < 2\omega$ is the desired level of $H(x_i)$ that defines the attracting limit cycle $\Gamma_i = \{x \in M_i : H(x_i) = H^*\}$ in

$$\begin{aligned} \dot{x}_{1i} &= x_{2i}, \\ \dot{x}_{2i} &= -\omega \sin(x_{1i}) - x_{2i}[H(x_i) - H^*] + u_i + d_i. \end{aligned} \tag{5.8}$$

Despite of the limit cycle Γ_i, each unperturbed system admits also two equilibria $[0,0]$ and $[\pi,0]$, the latter being a saddle point. Thus $\mathcal{W}_i = \{[0,0] \cup [\pi,0] \cup \Gamma_i\}$. Clearly, $\mathcal{W}_i$ is compact and contains all α and ω limit sets of (5.8) for $u_i = d_i = 0$. Moreover, it is straightforward to check that $\mathcal{W}_i$ is decomposable in the sense of Definition C.7 (Appendix C).

Lemma 5.5. *For each $i = 1, \ldots, N$, the systems in (5.8) have AG property.*

Proof. The conditions of Theorem C.12 (given in Appendix C) are satisfied for the system (5.8) and $\mathcal{W}_i$, thus it is enough to check a practical AG in this case. First, $|x_{1i}(t)| \leq \pi$ for all $t \geq 0$ by definition, and it is necessary to show a pAG for the coordinate x_{2i} only. For this purpose, we consider $W(x_{2i}) = 0.5x_{2i}^2$. Hence:

$$\begin{aligned}
\dot{W} &= x_{2i}[-\omega \sin(x_{1i}) - x_{2i}[H(x_i) - H^*] + u_i + d_i] \\
&= x_{2i}[-\omega \sin(x_{1i}) - x_{2i}[0.5x_{2i}^2 + \omega(1 - \cos(x_{1i})) \\
&- H^*] + u_i + d_i] \\
&\leq \omega|x_{2i}| - x_{2i}^2[0.5x_{2i}^2 + \omega(1 - \cos(x_{1i})) \\
&- H^*] + 0.5x_{2i}^2 + 0.5(u_i + d_i)^2 \\
&\leq -0.5x_{2i}^4 + (0.5 + H^* + 2\omega)x_{2i}^2 + \omega|x_{2i}| \\
&+ 0.5(u_i + d_i)^2.
\end{aligned}$$

Since $0.5 + H^* + 2\omega > 0$ and $\omega > 0$, there exists $f_{max} > 0$ such that $-0.25x_{2i}^4 + (0.5 + H^* + 2\omega)x_{2i}^2 + \omega|x_{2i}| \leq f_{max}$ for all $x_{2i} \in \mathbb{R}$, then

$$\begin{aligned}
\dot{W} &\leq -0.25x_{2i}^4 + f_{max} + 0.5(u_i + d_i)^2 \\
&\leq -W^2 + f_{max} + 0.5(u_i + d_i)^2.
\end{aligned}$$

Next, applying standard arguments:

$$\begin{aligned}
&\limsup_{t \to +\infty} W(t) \leq \sqrt{f_{max} + 0.5(\|u_i\|_\infty + \|d_i\|_\infty)^2} \text{ and} \\
&\limsup_{t \to +\infty} |x_{2i}(t)|^2 \leq 2\sqrt{f_{max} + 0.5(\|u_i\|_\infty + \|d_i\|_\infty)^2}.
\end{aligned}$$

Take $|x_i| = \sqrt{x_{1i}^2 + x_{2i}^2}$ then

$$\limsup_{t \to +\infty} |x_i(t)| \leq \sqrt{\pi^2 + 2\sqrt{f_{max} + 0.5(\|u_i\|_\infty + \|d_i\|_\infty)^2}}$$

and the pAG property holds since $|x_i|_{\mathcal{W}_i} \leq |x_i|$. □

As a consequence, Assumption 5.1 is satisfied for (5.8) and we may select the synchronization measure y for the network. The synchronization problem for nonlinear pendulums has been widely considered previously [64, 65, 151] (usually for unperturbed systems without a limit cycle, for example, with $v_i = -\kappa x_{2i} + u_i$ for some $\kappa > 0$). In this chapter we will consider

$$y = Ax_2,$$

where $x_2 = [x_{21}, \dots, x_{2N}]^T$ and $A \in \mathbb{R}^{N\times N}$ is a Metzler matrix whose off-diagonal elements $A_{i,j} \in \{0, 1\}$ for all $1 \leq i \neq j \leq N$ and $\sum_{j=1}^{N} A_{ij} = 0$, $\sum_{j=1}^{N} |A_{ij}| \neq 0$ for all $i = 1, \dots, N$ (for example, $A = \begin{bmatrix} -1 & 1 \\ 1 & -1 \end{bmatrix}$ for $N = 2$). It is necessary to check (5.6) for this y: obviously the function η_2 exists. To evaluate the constant η_0 and the function η_1 it is necessary to calculate $|x_i|_{\mathcal{W}_i}$ (and $|x_i|_{\mathcal{W}}$). Note that $|y|^2 \leq \|A\|_2 \sum_{j=1}^{N} x_{2i}^2$, then it is enough to estimate a relation between x_{2i} and $|x_i|_{\mathcal{W}_i}$. There exist $\delta_1, \delta_2 \in \mathcal{K}_\infty$ such that for all $x \in M_i$

$$\delta_1(|x_i|_{\mathcal{W}_i}) \leq \Delta(x_i) \leq \delta_2(|x_i|_{\mathcal{W}_i})$$

where $\Delta(x_i) = \min\{\sin^2(x_{1i}) + 0.5x_{2i}^2, |H(x_i) - H^*|\}$. Then it is enough to establish the boundedness of x_{2i} by $\Delta(x_i)$, but a direct computation shows:

$$0.5x_{2i}^2 \leq \Delta(x_i) + H^*$$

and (5.6) is valid for y. Take

$$\varphi_i(y) = \epsilon \tanh(y_i),\ \epsilon > 0,$$

then we may suppose that Assumption 5.2 is satisfied for some sufficiently small ϵ. The results of simulations confirm this conclusion, see for example Fig. 5.1, where for $N = 4$ and

$$A = \begin{bmatrix} -2 & 1 & 1 & 0 \\ 0 & -2 & 1 & 1 \\ 1 & 0 & -2 & 1 \\ 1 & 1 & 0 & -2 \end{bmatrix},\ \omega = 2,\ H^* = 2,\ \epsilon = 0.1$$

the results for two scenarios are given: Fig. 5.1,a without disturbances and Fig. 5.1,b with disturbances as $[d_1, d_2, d_3, d_4]^T = [0.7\sin(2t), -0.25\sin(0.5t), -0.8\sin(10t), \sin(25t)]^T$.

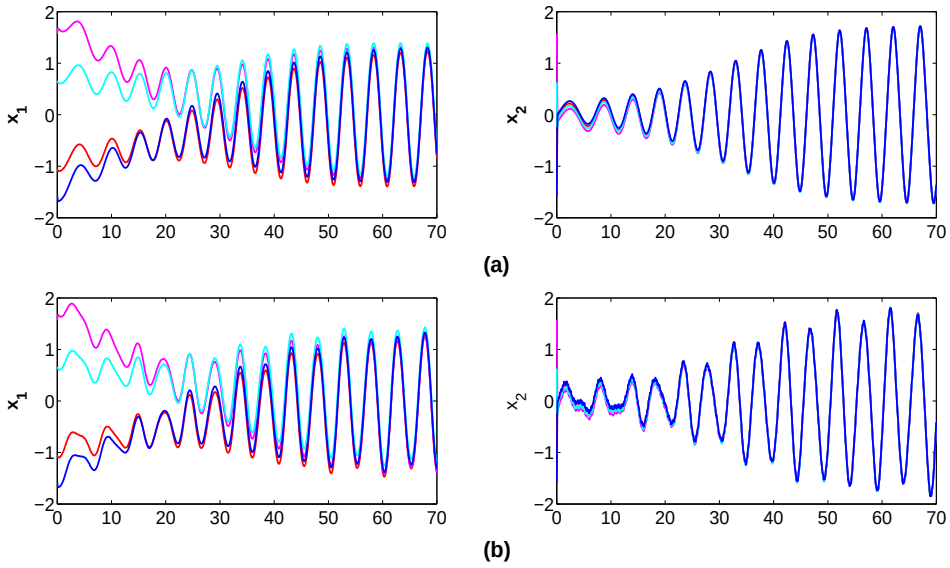

Figure 5.1: The results of simulation for (5.8)

5.3.2 Application to nonlinear pendulums with friction

This example is taken from [151]. Consider a network of nonlinear non-identical pendulums for $i = 1, \ldots, N$, $N > 1$:

$$\begin{aligned} \dot{x}_{1i} &= x_{2i}, \\ \dot{x}_{2i} &= -\Omega_i^2 \sin(x_{1i}) - \kappa x_{2i} + d_i, \end{aligned} \tag{5.9}$$

where the state $x_i = [x_{1i}, x_{2i}]$ takes values on the cylinder $M_i := \mathbb{S}^1 \times \mathbb{R}$, the exogenous disturbance $d_i(t) \in \mathbb{R}$, κ is a constant parameter and Ω_i^2 is the angular frequency of individual pendulums. The unperturbed system has a Hamiltonian $H(x_i) = 0.5x_{2i}^2 + \Omega_i^2(1 - \cos(x_{1i}))$ and $\dot{H} = x_{2i}d_i - \kappa x_{2i}^2$. Each unperturbed system has two equilibria $[0, 0]$ and $[\pi, 0]$ (the former is attractive and the later one is a saddle-point), thus $\mathcal{W}_i = \{[0, 0] \cup [\pi, 0]\}$ is a compact set containing all α- and ω-limit sets of (5.9) for $d_i = 0$. In addition, it is easy to check that $\mathcal{W}_i$ is decomposable in the sense of Definition C.7 (Appendix C) [4].

Lemma 5.6. *[58] For each $i = 1, \ldots, N$, the systems in (5.9) is ISS with respect to the set $\mathcal{W}_i$.*

As a consequence, Assumption 5.1 is satisfied for (5.9) (remark that admitting an ISS Lyapunov function is equivalent to enjoying AG property by Theorem C.12 (Appendix C)) and we may select the synchronization measure y for the network. Since in [151],

the authors have considered the first coordinate as synchronization measure, we follow here the same idea:

$$y = A\sin(x_1),$$

where $x_1 = [x_{11}, \ldots, x_{1N}]^T$ and $A \in \mathbb{R}^{N\times N}$ is a Metzler matrix as in the first example.

Since the global boundedness of trajectories of (5.9) for bounded inputs is proven in Lemma 5.6, then a local analysis around equilibria is sufficient to show the synchronization measure convergence. It is straightforward to check that linearized around equilibria dynamics has $y = 0$ as a stable and attractive manifold. By this, the convergence of y is guaranteed locally. Then by taking,

$$\varphi_i(y) = \beta y_i, \beta > 0,$$

we may suppose that Assumption 5.2 is satisfied for some sufficiently small β. The results of simulations confirm this conclusion, see Fig. 5.2 where a) is the disturbance free case and b) represents the simulation result with disturbances. The simulation parameters are $N = 5$, $\Omega_i^2 = 0.02i$, $\beta = 0.1$, the disturbance inputs are $[\phi_1, \ldots, \phi_5]^T = [0.1\sin(t), -0.15\sin(t), -0.2\sin(t), 0.15\sin(t), 0.2\sin(t)]^T$ and

$$A = \begin{bmatrix} -3 & 1 & 1 & 0 & 1 \\ 1 & -3 & 1 & 1 & 0 \\ 1 & 1 & -3 & 1 & 0 \\ 0 & 1 & 1 & -3 & 1 \\ 1 & 0 & 0 & 1 & -2 \end{bmatrix}.$$

5.4 Conclusions

In this chapter, sufficient conditions for robust synchronization have been derived based on an extension of the ISS framework to systems evolving on a (non-compact) manifold and with multiple invariant sets. The condition imposed on the controller ($\varphi_i(0) = 0$) ensures that the convergence of the synchronization measure implies that the trajectory belongs to the decomposable set $\mathcal{W}$. Practical global stability analysis of the interconnection has been done with respect to $\mathcal{W}$. The asymptotic gain property of the interconnection with respect to the set of synchronous solutions $\mathcal{A}$ ($\mathcal{A} \subset \mathcal{W}$) has been also proved.

Numerical simulations demonstrated the effectiveness of our method to network of both identical and nonidentical nodes. Remark that the results obtained in this chapter

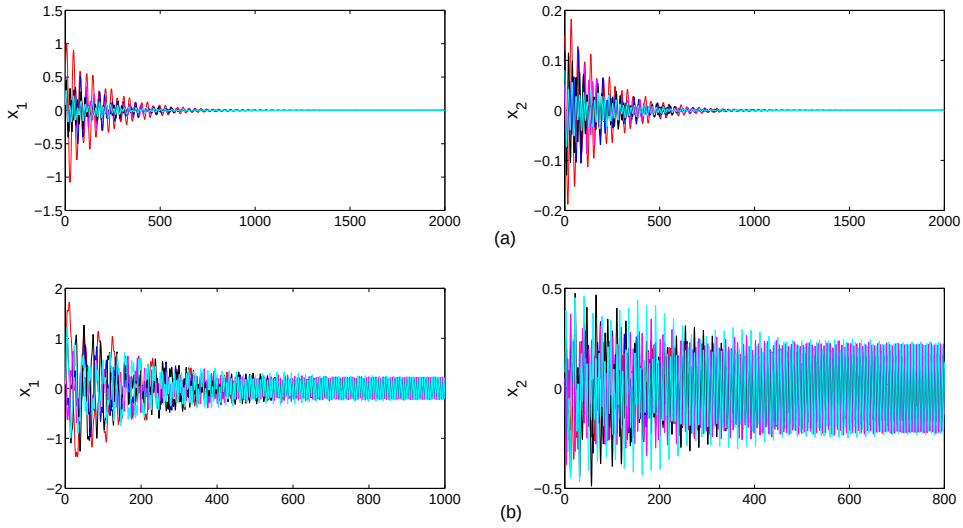

Figure 5.2: The result of simulation for (5.9)

are applicable only to systems that allow decomposition without cycles.

Chapter 6

General Conclusion and future works

6.1 General conclusion

In this thesis, the problems of modeling and synchronization of biological rhythms have been studied with applications in domains like environmental monitoring, phase synchronization of cell population, *etc.*

Chapter 2 recalls the problems associated with existing environmental monitoring solution using bivalves as bio-sensors. The methods reported in the literature rely heavily on chemical analysis and provide local monitoring solution. To overcome these problems, an intelligent autonomous large scale monitoring solution has been proposed in Chapter 2 using oysters valve movement activity model. The model takes into account the biological rhythms (*i.e.* circadian and circatidal) along with various other external factors. The proposed method works on identifying abnormal valve movement activity using residuals.

Chapter 3 considers the detection of a particular abnormal valve movement activity *i.e.* spawning which is not related to pollution. Spawning is characterized by rapid and rhythmic contractions and relaxation of the valves to expel eggs in the water. Since this behavior is very oscillatory in nature, then an online fault detection algorithm has been developed by considering spawning as fault *i.e.* deviation from normal behavior. The proposed algorithm estimates the velocity of valve movement followed by associated signal processing techniques. Moreover, the reported application of detection of complex oscillatory behavior is of interest for the control engineering community also.

Chapter 4 considers the problem of phase synchronization in a population of genetic oscillators undergoing cell division. Cell division introduces discontinuities in the

dynamics of genetic oscillators. If the period of cell division varies widely, then the mother-daughter cells lost synchronization after cell division. This chapter provided analytical conditions that guarantee phase synchronization after cell division by considering common entrainement. The conditions have been obtained based on Phase Response Curve (PRC) formalism. The analytical conditions reported in this chapter correspond to stochastic simulation results reported recently in the literature.

Chapter 5 deals with the problem of synchronization of multi-stable systems evolving on manifolds within Input-to-State Stability (ISS) framework. Based on a recent generalization of the classical ISS theory to multistable systems, a robust global synchronization protocol is designed with respect to a compact invariant set of the unperturbed system. The invariant set is assumed to admit a decomposition without cycles, that is, with neither homoclinic nor heteroclinic orbits. The results obtained in this chapter has been applied to a recently proposed oscillator model and is given in the Appendix.

6.2 Future works

Modeling and synchronization of biological rhythms are vast topics. Various ideas have been presented in this work. There exists still a large scope to extend the work presented in this thesis. In particular, the following research directions can be considered for the future:

- Part I of this thesis proposed the application of mathematical modeling, estimation and detection techniques to detect abnormal behavior in oysters. The results that have been obtained until now allow the detection of an abnormal behavior (related to the presence of toxic substances or not). An interesting future research direction would be to find out/isolate the reasons behind abnormal behaviors. A possible solution would be to consider engineering approach. For example, in the case of electric motor fault detection, engineers first artificially create a particular type of fault that they wish to detect in a healthy motor. Then they analyze various time/frequency domain characteristics of the faulty motor to obtain some features that can be used for the detection of that particular fault. Similar approach may be useful for isolating the source of toxic substances behind oysters abnormal behavior.

- In Part II, one of the considered problems was the synchronization of Brockett oscillators. Through experimental validation, we showed that Brockett model of oscillator is not just only a pure mathematical concept but also has the potential

to be applied for practical problems. However, until now no practical application has been reported in the literature. So, in future a very promising research direction will be to apply it for practical problems. For example, as an alternative of Van der Pol oscillator. Moreover, although experimental results showed robust synchronization property but this is yet to be supported theoretically. This could be an interesting problem to be considered in the near future.

References

[1] Aguilar, C., Montalvo, C., Rodriguez, L., Ceron, J., and Ceron, R. (2012). American oyster (crassostrea virginica) and sediments as a coastal zone pollution monitor by heavy metals. *International Journal of Environmental Science and Technology*, 9(4):579–586.

[2] Ahmed, H., Ushirobira, R., and Efimov, D. (2015a). On robustness of phase resetting to cell division under entrainment. *Journal of theoretical biology*, 387:206–213.

[3] Ahmed, H., Ushirobira, R., and Efimov, D. (2016a). On the robust synchronization of Brockett oscillators. *IFAC-PapersOnLine*, 49(14):142–147.

[4] Ahmed, H., Ushirobira, R., Efimov, D., and Perruquetti, W. (2015b). On conditions of robust synchronization for multistable systems. In *Control Conference (ECC), 2015 European*, pages 181–185. IEEE.

[5] Ahmed, H., Ushirobira, R., Efimov, D., and Perruquetti, W. (2016b). Robust synchronization for multistable systems. *Automatic Control, IEEE Transactions on*, 61(6):1625–1630.

[6] Ahmed, H., Ushirobira, R., Efimov, D., Tran, D., and Massabuau, J.-C. (2014). Dynamical model identification of population of oysters for water quality monitoring. In *Control Conference (ECC), 2014 European*, pages 152–157.

[7] Ahmed, H., Ushirobira, R., Efimov, D., Tran, D., and Massabuau, J.-C. (2015c). Velocity estimation of valve movement in oysters for water quality surveillance. *IFAC-PapersOnLine*, 48(11):333–338.

[8] Ahmed, H., Ushirobira, R., Efimov, D., Tran, D., Sow, M., Ciret, P., and Massabuau, J. C. (2016c). Monitoring biological rhythms through the dynamic model identification of an oyster population. *IEEE Transactions on Systems, Man, and Cybernetics: Systems (to appear)*.

[9] Ahmed, H., Ushirobira, R., Efimov, D., Tran, D., Sow, M., Payton, L., and Massabuau, J.-C. (2016d). A fault detection method for automatic detection of spawning in oysters. *Control Systems Technology, IEEE Transactions on*, 24(3):1140–1147.

[10] Allen, S. K., Gaffney, P. M., and Ewart, J. W. (1993). *Genetic improvement of the eastern oyster for growth and disease resistance in the Northeast*. Northeastern Regional Aquaculture Center, University of Massachusetts, Dartmouth.

[11] Ananthasubramaniam, B. and Herzel, H. (2014). Positive feedback promotes oscillations in negative feedback loops. *PloS one*, 9(8):e104761.

[12] Andronov, A., Vitt, A., and Khaikin, A. (1987). *Theory of oscillators*. Dover, reprint edition.

[13] Angeli, D. (2004). An almost global notion of input-to-state stability. *IEEE Trans. Automatic Control*, 49:866–874.

[14] Angeli, D. and Efimov, D. (2013). On input-to-state stability with respect to decomposable invariant sets. In *52nd IEEE Conference on Decision and Control*, pages 5897–5902. IEEE.

[15] Angeli, D. and Efimov, D. (2015). Characterizations of input-to-state stability for systems with multiple invariant sets. *Automatic Control, IEEE Transactions on*, 60(12):3242–3256.

[16] Angeli, D., Ferrell, J., and Sontag, E. (2004). Detection of multistability, bifurcations and hysteresis in a large class of biological positive-feedback systems. *Proc. Natl. Acad. Sci. USA*, 101:1822–1827.

[17] Angeli, D. and Praly, L. (2011). Stability robustness in the presence of exponentially unstable isolated equilibria. *IEEE Trans. Automatic Control*, 56:1582–1592.

[18] Angeli, D. and Sontag, E. (1999). Forward completeness, unboundedness observability, and their Lyapunov characterizations. *Syst. Control Lett.*, 38(4-5):209–217.

[19] Angeli, D. and Sontag, E. (2004). Multi-stability in monotone input/output systems. *Systems&Control Lett.*, 51:185–202.

[20] Antle, M., Foley, D., Foley, N., and Silver, R. (2003). Gates and oscillators: a network model of the brain clock. *Journal of Biological Rhythms*, 18(4):339–350.

[21] Antle, M., Foley, N., Foley, D., and Silver, R. (2007). Gates and oscillators II: zeitgebers and the network model of the brain clock. *Journal of Biological Rhythms*, 22:14–25.

[22] Bagheri, N., Stelling, J., and Doyle, F. (2007). Circadian phase entrainment via nonlinear model predictive control. *Int. J. Robust and Nonlinear Control*, 17:1555–1571.

[23] Bernard, I. (2011). *Ecologie de la reproduction de l'huitre creuse, Crassostrea gigas, sur les cotes atlantiques francaises: vers une explication de la variabilite du captage.* PhD thesis, University of La Rochelle.

[24] Bernard, S. and Herzel, H. (2006). Why do cells cycle with a 24 hour period? *Genome Inform.*, 17:72–79.

[25] Beyene, A., Awoke, A., and Triest, L. (2014). Validation of a quantitative method for estimating the indicator power of, diatoms for ecoregional river water quality assessment. *Ecological Indicators*, 37:58–66.

[26] Bhatia, N. and Szegö, G. (1970). *Stability Theory of Dynamical Systems.* Springer-Verlag, Berlin.

[27] Blanke, M. and Schroder, J. (2006). *Diagnosis and fault-tolerant control*, volume 2. Springer.

[28] Borcherding, J. (1992). *The Zebra Mussel Dreissena Polymorpha: Ecology, Biological Monitoring and First Applications in the Water Quality Management*, chapter Another early warning system for the detection of toxic discharges in the aquatic environment based on valve movements of the freshwater mussel Dreissena polymorpha, pages 127–146. Gustav Fischer Verlag, NY.

[29] Borcherding, J. (2006). Ten years of practical experience with the dreissena-monitor, a biological early warning system for continuous water quality monitoring. *Hydrobiologia*, 556(1):417–426.

[30] Brockett, R. (2013). Synchronization without periodicity. In Huper, K. and Trumpf, J., editors, *Mathematical Systems Theory, A Volume in Honor of U. Helmke*, pages 65–74. CreateSpace.

[31] Cabecinha, E., Cortes, R., and Cabral, J. A. (2004). Performance of a stochastic-dynamic modelling methodology for running waters ecological assessment. *Ecological modelling*, 175(3):303–317.

[32] Cabecinha, E., Silva-Santos, P., Cortes, R., and Cabral, J. A. (2007). Applying a stochastic-dynamic methodology (stdm) to facilitate ecological monitoring of running waters, using selected trophic and taxonomic metrics as state variables. *Ecological Modelling*, 207(2):109–127.

[33] Canavier, C. (2006). Phase response curve. *Scholarpedia*, 1(12):1332.

[34] Canavier, C. and Achuthan, S. (2010). Pulse coupled oscillators and the phase resetting curve. *Math Biosci.*, 226(2):77–96.

[35] Chambon, C., Legeay, A., Durrieu, G., Gonzalez, P., Ciret, P., and Massabuau, J. (2007). Influence of the parasite worm polydora sp. on the behaviour of the oyster crassostrea gigas: A study of the respiratory impact and associated oxidative stress. *Mar. Biol.*, 152:329–338.

[36] Charvin, G., Cross, F., and Siggia, E. (2009). Forced periodic expression of g1 cyclins phase-locks the budding yeast cell cycle. *Proceedings of the National Academy of Sciences*, 106(16):6632–6637.

[37] Chaves, M., Eissing, T., and Allgower, F. (2008). Bistable biological systems: A characterization through local compact input-to-state stability. *IEEE Trans. Automatic Control*, 45:87–100.

[38] Chen, W.-Y., Jou, L.-J., Chen, S.-H., and Liao, C.-M. (2012). A real-time biomonitoring system to detect arsenic toxicity by valve movement in freshwater clam corbicula fluminea. *Ecotoxicology*, 21(4):1177–1187.

[39] Cho, K.-H., Shin, S.-Y., Kolch, W., and Wolkenhauer, O. (2003). Experimental design in systems biology, based on parameter sensitivity analysis using a monte carlo method: A case study for the tnfα-mediated nf-κ b signal transduction pathway. *Simulation*, 79(12):726–739.

[40] Churilov, A., Medvedev, A., and Mattsson, P. (2014). Periodical solutions in a pulse-modulated model of endocrine regulation with time-delay. *IEEE Transactions on Automatic Control*, 59(3):728–733.

[41] Clayton, D., Hills, M., and Pickles, A. (1993). *Statistical models in epidemiology*, volume 161. IEA.

[42] Conrad, E. D. (1999). Mathematical models of biochemical oscillations.

[43] Cookson, N., Cookson, S., Tsimring, L., and Hasty, J. (2010). Cell cycle-dependent variations in protein concentration. *Nucleic Acids Research*, 38(8):2676–2681.

[44] Danzl, P. and Moehlis, J. (2008). Spike timing control of oscillatory neuron models using impulsive and quasi-impulsive charge-balanced inputs. In *Proc. 29th American Control Conference (ACC2008)*, pages 171–176, Seattle, USA.

[45] Das, A. and Lewis, F. L. (2010). Distributed adaptive control for synchronization of unknown nonlinear networked systems. *Automatica*, 46(12):2014–2021.

[46] Dashkovskiy, S., Efimov, D., and Sontag, E. (2011). Input to state stability and allied system properties. *Automation and Remote Control*, 72(8):1579–1614.

[47] Ding, S. (2008). *Model-based fault diagnosis techniques*. Springer.

[48] Doherty, F. G., Cherry, D. S., and Cairns Jr, J. (1987). Valve closure responses of the asiatic clam corbicula fluminea exposed to cadmium and zinc. *Hydrobiologia*, 153(2):159–167.

[49] Dunlap, J. C., Loros, J. J., and DeCoursey, P. J. (2004). *Chronobiology: biological timekeeping*. Sinauer Associates.

[50] Efimov, D. (2009). On global Lyapunov characterization of multi-stable nonlinear systems. In *Proc. IEEE CDC 2009*, pages 6299–6304.

[51] Efimov, D. (2011). Phase resetting control based on direct phase response curve. *Journal of Mathematical Biology*, 63(5):855–879.

[52] Efimov, D. (2012). Global lyapunov analysis of multistable nonlinear systems. *SIAM Journal on Control and Optimization*, 50(5):3132–3154.

[53] Efimov, D. (2015). Phase resetting for a network of oscillators via phase response curve approach. *Biological cybernetics*, 109(1):95–108.

[54] Efimov, D. and Fradkov, A. (2008). Yakubovich's oscillatority of circadian oscillations models. *Mathematical Biosciences*, 216:187–191.

[55] Efimov, D. and Fridman, L. (2011). A hybrid robust non-homogeneous finite-time differentiator. *Automatic Control, IEEE Transactions on*, 56(5):1213–1219.

[56] Efimov, D., Perruquetti, W., and Shiriaev, A. (2014). On existence of oscillations in hybrid systems. *Nonlinear Analysis: Hybrid Systems*, 12(5):104–116.

[57] Efimov, D., Sacre, P., and Sepulchre, R. (2009). Controlling the phase of an oscillator: a phase response curve approach. In *Proc. IEEE CDC 2009*, pages 7692–7697. IEEE.

[58] Efimov, D., Schiffer, J., and Ortega, R. (2016). Robustness of delayed multistable systems with application to droop-controlled inverter-based microgrids. *International Journal of Control*, 89(5):909–918.

[59] Egorov, E. and Koronovskii, A. (2004). Dynamical control in multistable systems. *Technical Physics Letters*, 30(3):186–189.

[60] Elowitz, M. and Leibler, S. (2000). A synthetic oscillatory network of transcriptional regulators. *Nature*, 403:335–338.

[61] Englund, V. and Heino, M. (1994). Valve movement of anodonta anatina and unio tumidus (bivalvia, unionidae) in a eutrophic lake. In *Annales Zoologici Fennici*, volume 31, pages 257–262.

[62] Englund, V. P. and Heino, M. P. (1996). Valve movement of the freshwater mussel anodonta anatina: a reciprocal transplant experiment between lake and river. *Hydrobiologia*, 328(1):49–56.

[63] Forger, D. and Kronauer, R. (2002). Reconciling mathematical models of biological clocks by averaging on approximate manifolds. *SIAM Journal on Applied Mathematics*, 62(4):1281–1296.

[64] Fradkov, A., Andrievsky, B., and Boykov, K. (2005). Control of the coupled double pendulums system. *Mechatronics*, 15(10):1289–1303.

[65] Fradkov, A. L. and Andrievsky, B. (2007). Synchronization and phase relations in the motion of two-pendulum system. *International Journal of Non-Linear Mechanics*, 42(6):895–901.

[66] Freeman, M. (2000). Feedback control of intercellular signalling in development. *Nature*, 408(6810):313–319.

[67] Galang, G., Bayliss, C., Marshall, S., and Sinnott, R. O. (2012). Real-time detection of water pollution using biosensors and live animal behaviour models. In *eResearch Australasia: emPower eResearch*, Sydney, Australia.

[68] Galtsoff, P. S. (1938). Physiology of reproduction of ostrea virginica i. spawning reactions of the female and male. *The Biological Bulletin*, 74(3):461–486.

[69] Garcia-March, J., Sanchis Solsona, M., and GarciaCarrascosa, A. (2008). Shell gaping behavior of pinna nobilis l., 1758: Circadian and circalunar rhythms revealed by in situ monitoring. *Marine Biology*, 153:689–698.

[70] Gazi, V. and Passino, K. M. (2011). *Swarm Stability and Optimization*. Springer.

[71] Gelig, A., Leonov, G., and Yakubovich, V. (1978). *Stability of nonlinear systems with non unique equilibrium*. Nauka, Moscow. [in Russian].

[72] Geva-Zatorsky, N., Rosenfeld, N., Itzkovitz, S., Milo, R., Sigal, A., Dekel, E., Yarnitzky, T., Liron, Y., Polak, P., Lahav, G., and Alon, U. (2006). Oscillations and variability in the p53 system. *Mol. Syst. Biol.*, 2:0033.

[73] Glass, L., Nagai, Y., Hall, K., Talajic, M., and Nattel, S. (2002). Predicting the entrainment of reentrant cardiac waves using phase resetting curves. *Physical Rev. E*, 65:65–74.

[74] Goldbeter, A. (1996). *Biochemical oscillations and cellular rhythms*. Cambridge University Press.

[75] Goldbeter, A. (2002). Computational approaches to cellular rhythms. *Nature*, 420:238–245.

[76] González-Miranda, J. M. (2004). *Synchronization and Control of Chaos: An Introduction for Scientists and Engineers*. Imperial College Press.

[77] Gonze, D. (2013). Modeling the effect of cell division on genetic oscillators. *Journal of Theoretical Biology*, 325(0):22–33.

[78] Gonze, D. and Abou-Jaoudé, W. (2013). The Goodwin model: behind the Hill function. *PloS one*, 8(8):e69573.

[79] Govaerts, W. and Sautois, B. (2006). Computation of the phase response curve: A direct numerical approach. *Neural Computation*, 18:817–847.

[80] Guckenheimer, J. and Holmes, P. (1988). Structurally stable heteroclinic cycles. *Math. Proc. Camb. Phil. Soc.*, 103:189–192.

[81] Guevara, M., Glass, L., and Shrier, A. (1981). Phase locking, period-doubling bifurcations, and irregular dynamics in periodically stimulated cardiac cells. *Science*, 214:1350–1353.

[82] Haberkorn, H., Tran, D., Massabuau, J.-C., Ciret, P., Savar, V., and Soudant, P. (2011). Relationship between valve activity, microalgae concentration in the water and toxin accumulation in the digestive gland of the pacific oyster crassostrea gigas exposed to alexandrium minutum. *Marine pollution bulletin*, 62(6):1191–1197.

[83] Ham, K. D. and Peterson, M. J. (1994). Effect of fluctuating low-level chlorine concentrations on valve-movement behavior of the asiatic clam (corbicula fluminea). *Environmental toxicology and chemistry*, 13(3):493–498.

[84] Hansel, D., Mato, G., and Meunier, C. (1995). Synchrony in excitatory neural networks. *Neural Comput.*, 7:307–337.

[85] His, E. (1976). *Contribution à l'étude biologique de l'huitre dans le bassin d'Arcachon. Activité valvaire de Crassostrea angulata et de Crasssotrea gigas ; application à la reproduction de l'huitre japonaise*. PhD thesis, University of Bordeaux 1.

[86] Hu, T. and Lin, Z. (2001). *Control systems with actuator saturation: analysis and design*. Springer Science & Business Media.

[87] Isermann, R. (2006). *Fault-diagnosis systems*. Springer.

[88] Izhikevich, E. (2007). *Dynamical Systems in Neuroscience: The Geometry of Excitability and Bursting*. The MIT press.

[89] James, I. (2002). Modelling pollution dispersion, the ecosystem and water quality in coastal waters: a review. *Environmental Modelling & Software*, 17(4):363–385.

[90] Jorgensen, S. (1990). A general model for the heavy metal pollution of aquatic ecosystems: Model development. *Environmental Software*, 5(3):136–141.

[91] Jou, L.-J., Lin, S.-C., Chen, B.-C., Chen, W.-Y., and Liao, C.-M. (2013). Synthesis and measurement of valve activities by an improved online clam-based behavioral monitoring system. *Computers and electronics in agriculture*, 90:106–118.

[92] Kádár, E., Salánki, J., Jugdaohsingh, R., Powell, J. J., McCrohan, C. R., and White, K. N. (2001). Avoidance responses to aluminium in the freshwater bivalve anodonta cygnea. *Aquatic Toxicology*, 55(3):137–148.

[93] Kanamaru, T. (2007). Van der pol oscillator. *Scholarpedia*, 2(1):2202.

[94] Khalil, H. (1992). *Nonlinear Systems*. Macmillan.

[95] Klerman, E. and St Hilaire, M. (2007). On mathematical modeling of circadian rhythms, performance, and alertness. *J Biol Rhythms*, 22(2):91–102.

[96] Kramer, K. J. M., Jenner, H. A., and De Zwart, D. (1989). The valve movement response of mussels: A tool in biological monitoring. *Hydrobiologia*, 188/189:433–443.

[97] Kröger, S. and Law, R. (2005). Sensing the sea. *Trends in Biotechnology*, 23:250–256.

[98] Kuramoto, Y. (1984). *Chemical Oscillations, Waves and Turbulence*. Springer, Berlin.

[99] LaSalle, J. P. (1960). Some extensions of Liapunov's second method. *Circuit Theory, IRE Transactions on*, 7(4):520–527.

[100] Leloup, J.-C., Gonze, D., and Goldbeter, A. (1999). Limit cycle models for circadian rhythms based on transcriptional regulation in drosophila and neurospora. *J. Biological Rhythms*, 14:433–448.

[101] Lewis, F., Zhang, H., Hengster-Movric, K., and Das, A. (2014). *Cooperative Control of Multi-Agent Systems*. Communications and Control Engineering. Springer.

[102] Li, Z., Duan, Z., Chen, G., and Huang, L. (2010). Consensus of multiagent systems and synchronization of complex networks: A unified viewpoint. *Circuits and Systems I: Regular Papers, IEEE Transactions on*, 57(1):213–224.

[103] Ljung, L. (1998). *System identification*. Springer.

[104] Lofberg, J. (2004). Yalmip : A toolbox for modeling and optimization in MATLAB. In *Proceedings of the CACSD Conference*, Taipei, Taiwan.

[105] Luna-Acosta, A., Budzinski, H., Le Menach, K., Thomas-Guyon, H., and Bustamante, P. (2015a). Persistent organic pollutants in a marine bivalve on the marennes-oleron bay and the gironde estuary (french atlantic coast)-part 1: Bioaccumulation. *Science of The Total Environment*, 514:500–510.

[106] Luna-Acosta, A., Bustamante, P., Budzinski, H., Huet, V., and Thomas-Guyon, H. (2015b). Persistent organic pollutants in a marine bivalve on the marennes–oléron bay and the gironde estuary (french atlantic coast)-part 2: Potential biological effects. *Science of The Total Environment*, 514:511–522.

[107] Marceau, F. (1909). Contraction of molluscan muscle. *Arch. Zool. Exp. Gen.*, 2:295–469.

[108] Mboup, M., Join, C., and Fliess, M. (2009). Numerical differentiation with annihilators in noisy environment. *Numerical Algorithms*, 50(4):439–467.

[109] Mihalcescu, I., Hsing, W., and Leibler, S. (2004). Resilient circadian oscillator revealed in individual cyanobacteria. *Nature*, 430:81–85.

[110] Mimendia, A., Gutierrez, J. M., Leija, L., Hernandez, P. R., Favari, L., Munoz, R., and Del Valle, M. (2010). A review of the use of the potentiometric electronic tongue in the monitoring of environmental systems. *Environmental Modelling & Software*, 25(9):1023–1030.

[111] Mori, T., Binder, B., and Johnson, C. (1996). Circadian gating of cell division in cyanobacteria growing with average doubling times of less than 24 hours. *Proc. Natl. Acad. Sci. U.S.A.*, 93:10183–10188.

[112] Nagoshi, E., Saini, C., Bauer, C., Laroche, T., Naef, F., and Schibler, U. (2004). Circadian gene expression in individual fibroblasts: Cell-autonomous and self-sustained oscillators pass time to daughter cells. *Cell*, 119(5):693–705.

[113] Naylor, E. (2010). *Chronobiology of marine organisms*. Cambridge University Press.

[114] Nelles, O. (2000). *Nonlinear System Identification*. Springer, Berlin.

[115] Nguyen, L. K. (2012). Regulation of oscillation dynamics in biochemical systems with dual negative feedback loops. *Journal of The Royal Society Interface*, 9(73):1998–2010.

[116] Nitecki, Z. and Shub, M. (1975). Filtrations, decompositions, and explosions. *American Journal of Mathematics*, 97(4):1029–1047.

[117] Oguz, C., Palmisano, A., Laomettachit, T., Watson, L. T., Baumann, W. T., and Tyson, J. J. (2014). A stochastic model correctly predicts changes in budding yeast cell cycle dynamics upon periodic expression of CLN2. *PLoS ONE*, 9(5):e96726.

[118] Olfati-Saber, R. (2006). Flocking for multi-agent dynamic systems: algorithms and theory. *Automatic Control, IEEE Transactions on*, 51(3):401–420.

[119] Osipov, G. V., Kurths, J., and Zhou, C. (2007). *Synchronization in Oscillatory Networks*. Springer.

[120] Palmer, T., Uehling, P., and Pollack, J. (2015). Using oyster tissue toxicity as an indicator of disturbed environments. *International Journal of Environmental Science and Technology*, 12(6):2111–2116.

[121] Pandey, L. K., Kumar, D., Yadav, A., Rai, J., and Gaur, J. (2014). Morphological abnormalities in periphytic diatoms as a tool for biomonitoring of heavy metal pollution in a river. *Ecological Indicators*, 36:272–279.

[122] Pemmaraju, S. and Skiena, S. (2003). Cycles, stars, and wheels. *Computational Discrete Mathematics Combinatiorics and Graph Theory in Mathematica*, pages 284–249.

[123] Perruquetti, W., Floquet, T., and Moulay, E. (2008). Finite-time observers: application to secure communication. *Automatic Control, IEEE Transactions on*, 53(1):356–360.

[124] Pikovsky, A. and Kurths, J. (2003). *Synchronization: A Universal Concept in Nonlinear Sciences*. Cambridge University Press.

[125] Pikovsky, A. and Rosenblum, M. (2007). Synchronization. *Scholarpedia*, 2(12):1459.

[126] Pikovsky, A., Rosenblum, M., and Kurths, J. (2001). *Synchronization. A Universal Concept in Nonlinear Sciences*. Cambridge University Press, Cambridge.

[127] Pogromsky, A. Y. (2008). A partial synchronization theorem. *Chaos*, 18:037107.

[128] Rantzer, A. (2001). A dual to Lyapunov's stability theorem. *Syst. Control Lett.*, 42:161–168.

[129] Robson, A., Wilson, R., and Garcia de Leaniz, C. (2007). Mussels flexing their muscles: A new method for quantifying bivalve behavior. *Marine Biology*, 151:1195–1204.

[130] Rose, K. A., McLean, R. I., and Summers, J. K. (1989). Development and monte carlo analysis of an oyster bioaccumulation model applied to biomonitoring data. *Ecological Modelling*, 45(2):111–132.

[131] Schmitt, F. G., De Rosa, M., Durrieu, G., Sow, M., Ciret, P., Tran, D., and Massabuau, J.-C. (2011). Statistical study of bivalve high frequency microclosing behavior: Scaling properties and shot noise analysis. *International Journal of Bifurcation and Chaos*, 21(12):3565–3576.

[132] Shamma, J. S. (2008). *Cooperative Control of Distributed Multi-Agent Systems*. Wiley-Interscience.

[133] Shumway, S. E. and Cucci, T. L. (1987). The effects of the toxic dinoflagellate protogonyaulax tamarensis on the feeding and behaviour of bivalve molluscs. *Aquatic Toxicology*, 10(1):9–27.

[134] Smeal, R., Ermentrout, G., and White, J. (2010). Phase-response curves and synchronized neural networks. *Phil. Trans. R. Soc. B*, 365:2407–2422.

[135] Smolen, P., Baxter, D., and Byrne, J. (2002). A reduced model clarifies the role of feedback loops and time delays in the drosophila circadian oscillator. *Biophysical Journal*, 83:2349–2359.

[136] Sontag, E. and Wang, Y. (2001). Lyapunov characterizations of input to output stability. *SIAM J. Control and Optimization*, 39:226–249.

[137] Sow, M., Durrieu, G., Briollais, L., Ciret, P., and Massabuau, J.-C. (2011). Water quality assessment by means of hfni valvometry and high-frequency data modeling. *Environmental monitoring and assessment*, 182(1-4):155–170.

[138] Stan, G.-B. and Sepulchre, R. (2007). Analysis of interconnected oscillators by dissipativity theory. *IEEE Trans. Automatic Control*, 52:256–270.

[139] Strogatz, S. H. (2004). *Sync: How Order Emerges from Chaos in the Universe, Nature, and Daily Life*. Hyperion.

[140] Tass, P. (1999). *Phase Resetting in Medicine and Biology. Stochastic Modeling and Data Analysis*. Springer Verlag, Berlin.

[141] Telfer, T., Atkin, H., and Corner, R. (2009). Review of environmental impact assessment and monitoring in aquaculture in europe and north america. In *Environmental impact assessment and monitoring in aquaculture*, Fish Aquac Tech Pap No. 527, pages 285–394, Rome. FAO, UN FAO.

[142] Tlili, S., Minguez, L., Giamberini, L., Geffard, A., Boussetta, H., and Mouneyrac, C. (2013). Assessment of the health status of donax trunculus from the gulf of tunis using integrative biomarker indices. *Ecological Indicators*, 32:285–293.

[143] Tourigny, D. S. (2014). Geometric phase shifts in biological oscillators. *Journal of Theoretical Biology*, 355(0):239–242.

[144] Tran, D., Ciret, P., Ciutat, A., Durrieu, G., and Massabuau, J.-C. (2003). Estimation of potential and limits of bivalve closure response to detect contaminants: application to cadmium. *Environmental Toxicology and Chemistry*, 22(4):914–920.

[145] Tran, D., Nadau, A., Durrieu, G., Ciret, P., Parisot, J. P., and Massabuau, J. C. (2011). Field chronobiology in molluscan bivalves: How moon and sun cycles interactions deeply drive oyster activity rhythms. *Chronobiol. Int.*, 28:307–317.

[146] Ushirobira, R., Perruquetti, W., Mboup, M., and Fliess, M. (2013). Algebraic parameter estimation of a multi-sinusoidal waveform signal from noisy data. In *Control Conference (ECC), 2013 European*, pages 1902–1907. IEEE.

[147] Walter, E. and Pronzato, L. (1997). Identification of parametric models. *Communications and Control Engineering*.

[148] Winfree, A. (1980). *The Geometry of Biological Time*. Springer Verlag, Berlin.

[149] Yakubovich, V. and Starzhinskii, V. (1975). *Linear differential equations with periodic coefficients*. Wiley.

[150] Zhao, G. (2010). Phase organization of circadian oscillators in extended gate and oscillator models. *J. Theoretical Biology*, 264(2):367–376.

[151] Zhao, J., Hill, D., and Liu, T. (2012). Global bounded synchronization of general dynamical networks with nonidentical nodes. *Automatic Control, IEEE Transactions on*, 57(10):2656–2662.

[152] Zhusubaliyev, Z. T., Medvedev, A., and Silva, M. M. (2014). Nonlinear dynamics in closed-loop anesthesia: Pharmacokinetic/pharmacodynamic model under pid-feedback. In *American Control Conference (ACC), 2014*, pages 5496–5501. IEEE.

[153] Zhusubaliyev, Z. T., Medvedev, A., and Silva, M. M. (2015). Bifurcation analysis of pid-controlled neuromuscular blockade in closed-loop anesthesia. *Journal of Process Control*, 25:152–163.

[154] Zolghadri, A., Henry, D., Cieslak, J., Efimov, D., and Goupil, P. (2014). *Fault Diagnosis and Fault-Tolerant Control and Guidance for Aerospace Vehicles*. Springer.

Appendix A

Phase Model in vicinity of a limit cycle

A.1 Linearized model

Consider a (smooth) dynamical system

$$\dot{x} = f(x,u), \quad x \in \mathbb{R}^n, \quad u \in [-U,U] \subset \mathbb{R},\ U > 0. \tag{A.1}$$

Denote by $x(t,x_0,u)$ a solution of (A.1) with the initial condition x_0 and input u and assume that for $u(t) \equiv 0$, $t \geq 0$ and some $x_0 \in \mathbb{R}^n$ the system (A.1) has (non-constant) T-periodic solution $x(t,x_0,0) = \gamma(t) = \gamma(t+T) \in \mathbb{R}^n$, $t \geq 0$. Then the corresponding limit cycle, described by the set $\Gamma = \{x \in \mathbb{R}^n \mid x = \gamma(t), 0 \leq t < T\}$, attracts a non-empty open bounded set of initial conditions $\mathcal{A} \subset \mathbb{R}^n$, $\Gamma \subset \mathcal{A}$, and the linearized system

$$\delta\dot{x}(t) = A(t)\,\delta x(t) + b(t)u(t) + d[\delta x(t), \gamma(t), u(t)], \tag{A.2}$$

$$A(t) = \left.\frac{\partial f(x,u)}{\partial x}\right|_{x=\gamma(t)}, \quad b(t) = \left.\frac{\partial f(x,u)}{\partial u}\right|_{x=\gamma(t)}$$

has $n-1$ multipliers strictly inside the unit cycle and one multiplier equals to 1 ([12, 149]), where $\delta x(t) = x(t) - \gamma(t)$, the matrix function A and the vector function b are T-periodic due to properties of γ; the function $d[\delta x(t), \gamma(t), u(t)]$ represents the higher order terms with respect to $\delta x(t)$ in the system (A.1) linearization and for all $x \in \mathcal{A}$ and $|u| \leq U$ there exist $d_1 > 0$, $d_2 > 0$ such that (the function d contains products of δx and u with

power 2 and higher):

$$|d(\delta x, \gamma, u)| \leq d_1 |\delta x|^2 + d_2\, u^2.$$

Multipliers are the eigenvalues of the monodromy matrix $M = \Phi(T)$ defined via the *fundamental matrix function* Φ of the system (A.2) and the solution of *adjoint* system Ψ:

$$\dot{\Phi}(t) = A(t)\Phi(t), \Phi(0) = I; \dot{\Psi}(t) = -A(t)^T \Psi(t), \Psi(0) = I,$$

where I is the identity matrix and $\Phi(t)^T \Psi(t) = I$.

A.2 Phase variables

Any point $x_0 \in \Gamma$ can be characterized by a scalar *phase* $\varphi_0 \in [0, 2\pi)$, that uniquely determines the position of the point x_0 on the limit cycle Γ (Γ is a one-dimensional closed curve in $\mathbb{R}^n$) ([88, 126]). The smooth bijective *phase map* $\vartheta : \Gamma \to [0, 2\pi)$ assigns to each point $x_0 \in \Gamma$ the corresponding phase $\varphi_0 = \vartheta(x_0)$. Any solution of the system (A.1) $x(t, x_0, 0)$ with $x_0 \in \Gamma$ satisfies $x(t, x_0, 0) = \gamma(t + \varphi_0 \omega^{-1})$, where $\omega = 2\pi T^{-1}$ is the system frequency, provided we choose the convention $\gamma(t) = x(t, \vartheta^{-1}(0), 0)$, then we can define $\vartheta^{-1}(\varphi) = \gamma(\varphi\omega^{-1})$. The *phase variable* $\varphi : \mathbb{R}_+ \to [0, 2\pi)$ is defined for the trajectories $x(t, x_0, 0)$, $x_0 \in \Gamma$ as $\varphi(t) = \vartheta\left(x(t, x_0, 0)\right) = \vartheta\left(\gamma(t + \varphi_0\omega^{-1})\right)$. Due to the periodic nature of $\gamma(t)$, the function $\varphi(t)$ is also periodic. Moreover the function ϑ can be defined providing $\varphi(t) = \omega t + \varphi_0$ and $\dot{\varphi}(t) = \omega$ ([88, 126]).

The notion of phase can be extended to any solution $x(t, x_0, 0)$ starting in the attraction set $\mathcal{A}$ of the limit cycle. By definition, for all $x_0 \in \mathcal{A}$ there exists an asymptotic phase $\theta_0 \in [0, 2\pi)$ such that

$$\lim_{t \to +\infty} |x(t, x_0, 0) - \gamma(t + \theta_0 \omega^{-1})| = 0.$$

Then there exists the *asymptotic phase map* $\upsilon : \mathcal{A} \to [0, 2\pi)$ connecting a point $x_0 \in \mathcal{A}$ and the corresponding phase θ_0, *i.e.* $\theta_0 = \upsilon(x_0)$ and by construction $\upsilon(x_0) = \vartheta(x_0)$ for all $x_0 \in \Gamma$. The *asymptotic phase variable* $\theta : \mathbb{R}_+ \to [0, 2\pi)$ is derived as $\theta(t) = \upsilon\left(x(t, x_0, 0)\right)$, $t \geq 0$. In the case $\varphi(t) = \omega t + \varphi_0$ we have $\theta(t) = \omega t + \theta_0$ and $\dot{\theta}(t) = \omega$, which implies time invariance of this map: if $\upsilon(x_1) = \upsilon(x_2)$, then $\upsilon\left(x(t, x_1, 0)\right) = \upsilon\left(x(t, x_2, 0)\right)$ for all $t \geq 0$ and $x_1, x_2 \in \mathcal{A}$ ([88]). The initial conditions $x_1, x_2 \in \mathcal{A}$ having the same asymptotic phase determine the *isochrone* curves ([88]).

The notion of asymptotic phase variable can be extended to a generic $u(t) \neq 0$, $t \geq 0$ provided that the corresponding trajectory $x(t, x_0, u)$ stays in the set $\mathcal{A}$ for all

$t \geq 0$. In this case, the asymptotic phase variable can be defined in a trivial way as $\theta(t) = \upsilon\left(x(t, x_0, u)\right)$, $t \geq 0$. Then the variable $\theta(t')$ at an instant $t' \geq 0$ evaluates the asymptotic phase of the point $x(t', x_0, u)$ if one would pose $u(t) = 0$ for $t \geq t'$. Dynamics of the asymptotic phase variable $\theta(t)$ in the generic case for $u(t) \neq 0$, $t \geq 0$ is difficult to derive. A local model obtained in a small neighborhood of the limit cycle for infinitesimal inputs is presented below ([53, 88]).

A.3 Infinitesimal PRC

Consider the case $u(t) = 0$ for $t \geq 0$, then by definition $\dot{\gamma}(t) = f(\gamma(t), 0)$, $\ddot{\gamma}(t) = A(t)\dot{\gamma}(t)$ and $\dot{\gamma}(t) = \Phi(t)\dot{\gamma}(0)$ for all $t \geq 0$. Therefore, $\dot{\gamma}(0) = f(\gamma(0), 0)$ is the left eigenvector of the matrix M for the eigenvalue equal to 1. There exists a right eigenvector $m \in \mathbb{R}^n$ such that $m^T M = m^T$ and $m^T \dot{\gamma}(0) = \omega$. Finally, define $Q(t) = m^T \Psi(t)^T$ then

$$\begin{aligned} Q(t) f(\gamma(t), 0) &= m^T \Psi(t)^T f(\gamma(t), 0) \\ &= m^T \Psi(t)^T \Phi(t) \dot{\gamma}(0) = m^T \dot{\gamma}(0) = \omega. \end{aligned}$$

From another side, $\theta(t) = \upsilon\left(\gamma(t)\right) = \omega t + \theta(0)$ and

$$\omega = \dot{\theta} = \left.\frac{\partial \upsilon(x)}{\partial x}\right|_{x=\gamma(t)} f(\gamma(t), 0).$$

Therefore $Q(t) = \left.\frac{\partial \upsilon(x)}{\partial x}\right|_{x=\gamma(t)} + \zeta(t)$, where $\zeta(t)$ is a row-vector orthogonal to $f(\gamma(t), 0)$. Since m is the eigenvector corresponding to the eigen value equal to 1 (or movement on the limit cycle), then $Q(t) = m^T \Psi(t)^T$ is independent of perturbations orthogonal to the limit cycle flow $f(\gamma(t), 0)$ and the convention

$$Q(t) = \left.\frac{\partial \upsilon(x)}{\partial x}\right|_{x=\gamma(t)} = m^T \Psi(t)^T \tag{A.3}$$

is adopted. The first equality in (A.3) explains the physical meaning of $Q(t)$, while the last equality in (A.3) is used for numerical calculation. The function $Q(t)$ is T-periodic by construction.

The function $Q(\phi\omega^{-1})$ for phase $\varphi \in [0, 2\pi)$ is called *infinitesimal* PRC ([88]), it serves as the phase response characteristics for a delta-impulse input.

A.4 Phase dynamics

Consider the case $u(t) \neq 0$ (we assume that $x(t, x_0, u) \in \mathcal{A}$ for all $t \geq 0$), then

$$\begin{aligned}\dot{\theta}(x(t)) &= \dot{\theta}(\gamma(t) + \delta x(t)) \\ &= \left.\frac{\partial \upsilon(x)}{\partial x}\right|_{x=\gamma(t)+\delta x(t)} f(\gamma(t) + \delta x(t), u(t)) \\ &= \left.\frac{\partial \upsilon(x)}{\partial x}\right|_{x=\gamma(t)} f(\gamma(t), u(t)) + r_1\left(\gamma(t), \delta x(t), u(t)\right)^T \delta x(t),\end{aligned}$$

where the term $r_1\left(\gamma(t), \delta x(t), u(t)\right)^T \delta x(t)$ corresponds to the powers of $\delta x(t)$ higher than one in the Taylor series of the function $\dot{\theta}(\gamma(t) + \delta x(t))$ with respect to the variable $\delta x(t)$. From above, the quantity $\dot{\theta}(t) = \omega$ should be satisfied for $u(t) = 0$, therefore $\left.\frac{\partial \upsilon(x)}{\partial x}\right|_{x=\gamma(t)} f(\gamma(t), 0) + r_1\left(\gamma(t), \delta x(t), 0\right)^T \delta x(t) = \omega$, which implies the property $r_1\left(\gamma(t), \delta x(t), 0\right) = 0$. Next,

$$\begin{aligned}\dot{\theta}(x(t)) = &\left.\frac{\partial \upsilon(x)}{\partial x}\right|_{x=\gamma(t)} f(\gamma(t), 0) \\ &+ \left.\frac{\partial \upsilon(x)}{\partial x}\right|_{x=\gamma(t)} \left.\frac{\partial f(\gamma(t), u)}{\partial u}\right|_{u=0} u(t) + g\left(\gamma(t), \delta x(t), u(t)\right), \\ g(\gamma, \delta x, u) = &\, r_1(\gamma, \delta x, u)^T \delta x + r_2(\gamma, u)\, u^2,\end{aligned}$$

where $r_2(\gamma, u)\, u^2$ represents the terms with powers two and higher for the Taylor series of the function

$$\left.\frac{\partial \upsilon(x)}{\partial x}\right|_{x=\gamma(t)} f(\gamma(t), u(t))$$

with respect to the control u. For all $x \in \mathcal{A}$ and $|u| \leq U$ there are $g_1 > 0$ and $g_2 > 0$ such that $|g(\gamma, \delta x, u)| \leq g_1 u^2 + g_2 |\delta x|^2$. Recalling the previously introduced designations, we obtain

$$\dot{\theta} = \omega + Q(t)\, b(t)\, u(t) + g\left(\gamma(t), \delta x(t), u(t)\right).$$

This model has been derived around the solution $\gamma(t)$, due to the periodicity of the solution $\gamma(t + \phi\omega^{-1})$, $\phi \in [0, 2\pi)$ and u, the model for $\gamma(t + \phi\omega^{-1})$ has a similar form

([53, 88]):

$$\dot{\theta} = \omega + Q(t + \phi\omega^{-1})\, b(t + \phi\omega^{-1})\, u(t) + g\left(\gamma(t + \phi\omega^{-1}), \delta x(t), u(t)\right).$$

Skipping the residual function g, we obtain the first order approximation of the phase model:

$$\dot{\theta} = \omega + Q(t + \phi\,\omega^{-1})\, b(t + \phi\omega^{-1})\, u(t). \tag{A.4}$$

Since the property $|g(\gamma, \delta x, u)| \leq g_1 u^2 + g_2 |\delta x|^2$ holds for all $x \in \mathcal{A}$ and $|u| \leq U$, such an approximation is rather accurate for a sufficiently small U.

Assume that the input $u(t) = w(t)$, where $w(t)$ has a pulse-like form, *i.e.* $|w(t)| \leq U$ for all $0 < t < \mathcal{T} < T$ and $w(t) = 0$ for all $t \geq \mathcal{T}$ or $t \leq 0$. Then integration of (A.4) yields for $t \geq \mathcal{T}$:

$$\begin{aligned} \theta(t) &= \omega t + \theta(0) + \int_0^t Q(\tau + \theta(0)\omega^{-1})\, b(\tau + \theta(0)\omega^{-1})\, u(\tau)\, d\tau \\ &= \omega t + \theta(0) + \mathrm{PRC}[\theta(0)], \\ \mathrm{PRC}(\theta) &= \int_0^{\mathcal{T}} Q(\tau + \theta\omega^{-1})\, b(\tau + \theta\omega^{-1})\, u(\tau)\, d\tau. \end{aligned} \tag{A.5}$$

The map $\mathrm{PRC}(\theta)$, $\theta \in [0, 2\pi)$ is defined for the particular pulse w (by definition $-\pi \leq \mathrm{PRC}(\theta) < \pi$ for all $\theta \in [0, 2\pi)$), it tabulates the phase shift by the pulse w ([88, 126]). For $w(t) = \delta(t - \eta)$ with $\eta \in (0, \mathcal{T})$ and $\delta(t)$ is the impulse input, we obtain the infinitesimal PRC

$$\mathrm{iPRC}(\theta) = Q(\eta + \theta\omega^{-1})\, b(\eta + \theta\omega^{-1}),$$

which defines the phase shift under an impulse input.

Appendix B

Robust synchronization of Brockett oscillators

B.1 Introduction

In the context of the synchronization of oscillators, R. Brockett has recently proposed the following model of an oscillator [30]:

$$\ddot{x} + \varepsilon \dot{x}\left(\dot{x}^2 + x^2 - 1\right) + x = \varepsilon^2 u, x \in \mathbb{R}^n, \varepsilon > 0 \tag{B.1}$$

Next, for $|\varepsilon|$ sufficiently small, but non-zero, let us consider the set

$$S_\varepsilon = \left\{(x, \dot{x}) \,|\, \left(\dot{x}^2 + x^2 - 1\right) + 2\varepsilon^2 x\dot{x}\,\mathrm{sign}\left(\dot{x}^2 + x^2 - 1\right) = \varepsilon\right\}$$

which contains two smooth closed contours: Γ_ε^+ lies outside the unit circle in the $(x, \dot{x})$-space and Γ_ε^- lies inside the unit circle. Both curves approach the unit circle as ε goes to zero. Then the main result of [30] is given below.

Theorem B.1. *Let $\Gamma_\varepsilon^\pm$ be as before. Then there exist $\varepsilon_0 > 0$ such that for all $0 < \varepsilon < \varepsilon_0$, the solutions of (B.1) beginning in the annulus bounded by Γ_ε^+ and Γ_ε^- remain in this annulus for all time, provided that $|u| \leq \sqrt{x^2 + \dot{x}^2}$.*

Theorem B.1 provides a local synchronization result which depends on a small parameter $\varepsilon \neq 0$. Moreover, the result is applicable to the synchronization of identical oscillators only. Thus, the goal of this appendix is to extend the result of [30] and to develop a protocol of global synchronization in the network of (B.1), for the case of identical and non-identical models of the agents. The proposed solution is based on the framework of Input-to-State Stability (ISS) of multistable systems.

In this appendix, the results presented in Chapter 5 along with the results of [15] are applied to provide sufficient conditions for the existence of robust synchronization for identical/non-identical Brockett oscillators in the presence of external inputs. In opposite to the local results of [30], the conditions obtained in this chapter are global.

The rest of this appendix is organized as follows. More details about Brockett oscillators and the synchronization of a family of oscillators can be found in Section B.2 and B.3 respectively. In Section B.4, numerical simulation examples and experimental results are given to illustrate these results. Concluding remarks in Section B.5 close this chapter.

B.2 The Brockett Oscillator

Let us consider the Brockett oscillator [30]:

$$\ddot{\xi} + b\dot{\xi}\left(\dot{\xi}^2 + \xi^2 - 1\right) + \xi = au, \tag{B.2}$$

where $\xi \in \mathbb{R}$, $\dot{\xi} \in \mathbb{R}$ are the states variables, $a, b > 0$ are parameters and u is the control input. By considering $x_1 = \xi$, $\dot{x}_1 = x_2 = \dot{\xi}$, $x = [x_1, x_2]^T$ and $|x| = \sqrt{x_1^2 + x_2^2}$ equation (B.2) can be written in the state-space form as:

$$\begin{aligned} \dot{x}_1 &= x_2 \\ \dot{x}_2 &= -x_1 + au - bx_2\left(|x|^2 - 1\right), \end{aligned} \tag{B.3}$$

where the states of the system (B.3), *i.e.* x, evolve in the manifold $M = \mathbb{R}^2$. By analyzing equation (B.3) it can be seen that the unperturbed system admits two invariant sets: namely, the origin $\mathcal{W}_1 = \{0\}$ and the limit cycle $\mathcal{W}_2 = \Gamma = \{x \in M : |x|^2 = 1\}$. So, the invariant set for the trajectories of (B.3) can be defined as:

$$\mathcal{W} := \mathcal{W}_1 \cup \mathcal{W}_2 = \{0\} \cup \Gamma. \tag{B.4}$$

In order to verify the decomposability of the invariant set $\mathcal{W}$, we need to know the nature of the equilibrium $\mathcal{W}_1$ and the limit cycle $\mathcal{W}_2 = \Gamma$. This information can be obtained by analyzing the Lyapunov stability of the unperturbed system (B.3).

B.2.1 Stability of the autonomous Brockett oscillator

Since, $\mathcal{W}$ is invariant for the trajectories of (B.4), then the following proposition provides the stability of the unforced Brockett oscillator with respect to $\mathcal{W}$.

Proposition B.2. *For the unperturbed Brockett oscillator defined in (B.3) with $u = 0$, the limit cycle Γ is almost globally asymptotically stable and the origin is unstable.*

Proof. The instability of the origin of the unperturbed system (B.3) can be verified for a linearized version of the system. The eigenvalues of the linearized system $\lambda_{1,2} = \frac{1}{2}\left(b \pm \sqrt{b^2-4}\right)$ have always positive real parts for any $b > 0$. Alternatively, this fact can also be checked through LMI formulation which is given in Remark B.3.

To analyze the stability of the limit cycle $\mathcal{W}_2$, let us consider the following Lyapunov function:

$$U(x) = \frac{1}{2}\left(|x|^2 - 1\right)^2,$$

which is zero on the set $\mathcal{W}_2$ and positive otherwise. Evaluating the total derivative of U along the solutions of (B.3), we obtain:

$$\begin{aligned}
\dot{U} &= \left(|x|^2-1\right)\left\{2aux_2 - 2bx_2^2\left(|x|^2-1\right)\right\} \\
&= -2bx_2^2\left(|x|^2-1\right)^2 + 2aux_2\left(|x|^2-1\right) \\
&\leq -2bx_2^2\left(|x|^2-1\right)^2 + bx_2^2\left(|x|^2-1\right)^2 + \frac{a^2}{b}u^2 \\
&\leq -bx_2^2\left(|x|^2-1\right)^2 + \frac{a^2}{b}u^2.
\end{aligned}$$

Then for $u = 0$ we have $\dot{U} \leq 0$ and all trajectories are globally bounded. By LaSalle's invariance principle [99], all trajectories of the system converge to the set where $\dot{U} = 0$. Note that $\{x \in M : \dot{U} = 0\} = \mathcal{W}_2 \cup \{x \in M : x_2 = 0\}$ and on the line x_2 there is the only invariant solution at the origin (in $\mathcal{W}_1$), therefore $\dot{U} = 0$ for all $x \in \mathcal{W}$, which contains all invariant solutions of the system. Since the origin is unstable, it can be concluded that the limit cycle $\mathcal{W}_2$ is almost globally asymptotically stable. □

Remark B.3. To check the instability of the origin in an alternative way, let us consider a small closed ball $B(\rho)$ with the radius ρ around the origin with $B(\rho) = \{x \in \mathbb{R}^2 : |x|^2 \leq \rho\}$. Inside this ball, by imposing the parameter $b = 1$ without loosing generality, the unper-

turbed system of (B.3) can be written as the following uncertain linear system:

$$\dot{x} = Ax, A = \begin{bmatrix} 0 & 1 \\ -1 & -(\tilde{\rho} - 1) \end{bmatrix}, \tilde{\rho} \in [0, \rho], \tag{B.5}$$

where the matrix $A \in \mathbb{R}^{2\times 2}$ belongs to the domain $\mathcal{D}_A$ defined as:

$$\mathcal{D}_A \triangleq \left\{ A : A = \beta_1 A_1 + \beta_2 A_2, \beta_1, \beta_2 > 0, \sum_{i=1}^{2} \beta_i = 1 \right\} \tag{B.6}$$

with $A_1 = \begin{bmatrix} 0 & 1 \\ -1 & 1 \end{bmatrix}$ and $A_2 = \begin{bmatrix} 0 & 1 \\ -1 & -(\rho - 1) \end{bmatrix}$. Then, by applying Chetaev instability theorem [94], it can be concluded that the origin is unstable if there exist $P > 0, Q > 0$ such that for $i = 1, 2$

$$A_i^T P + P A_i \succeq Q. \tag{B.7}$$

The LMI (B.7) can be easily verified by using any standard solvers like Yalmip [104].

In our case, let us select $\rho = 0.2$. With this value of ρ, we obtain the following values for P and Q,

$$P = \begin{bmatrix} 21.4643 & -6.8278 \\ \star & 17.8390 \end{bmatrix}, Q = \begin{bmatrix} 6.1040 & -1.3080 \\ \star & 7.8838 \end{bmatrix}.$$

With these values of P and Q, LMI (B.7) is satisfied. As a result, it can be concluded that the origin is unstable.

B.2.2 Stability of the non-autonomous Brockett oscillator

In the previous section, we have proved the stability of the unperturbed system. In this section, we will analyze the stability of the Brockett oscillator in the presence of input. As it was shown in the previous section, the limit cycle Γ is almost globally asymptotically stable. So, any solution of the unperturbed Brockett oscillator converges to Γ, except for the one initiated at 0, which is unstable. So, it can be concluded that $\mathcal{W}$ contains all $\alpha-$ and $\omega-$limit sets of the unperturbed systems of (B.3) and it admits a decomposition without cycles. Consequently the result of [14, 15] can be applied for our case to show the robust stability of the Brockett oscillator in (B.3) with respect to $\mathcal{W}$:

Proposition B.4. *The system (B.3) is ISS with respect to the set $\mathcal{W}$.*

Proof. To prove the ISS property, let us introduce two new variables y and h as,

$$\begin{aligned} y(x) &= |x|^2 - 1,\ \dot{y} = -2bx_2^2 y + 2ax_2 u; \\ h(x) &= (x_1 + x_2)y,\ \dot{h} = a[y + 2x_2(x_1 + x_2)]u \\ &\quad - (h - 2x_2 y + bx_2 y^2 + 2bx_2^2 h). \end{aligned}$$

Next, let us consider the following Lyapunov function for the unperturbed system of (B.3) for $c, d > 0$:

$$W(x) = \frac{1}{2}\left(h^2(x) + cy^2(x) + \frac{1}{2}dy^4(x)\right). \tag{B.8}$$

Notice that $W(x) = 0$ for all $x \in \mathcal{W}_2$ and positive otherwise. Therefore, there exist α_1,$\alpha_2 \in \mathcal{K}_\infty$ such that the first condition of Definition C.11 (Appendix C) is satisfied for all $x \in M$ for the above function $W(x)$. Evaluating the total derivative of W, along the solutions of (B.3), we obtain

$$\begin{aligned} \dot{W} &= cy\dot{y} + h\dot{h} + dy^3\dot{y} \\ &= 2au[h(x_2^2 + x_1x_2 + 0.5y) + x_2y(c + dy^2)] - h^2 - 2bx_2^2[h^2 + y^2(c + dy^2)] + hx_2y(2 - by). \end{aligned}$$

Next by applying Young's inequality, we can derive the series of relations:

$$\begin{aligned} 2hx_2y &\leq \frac{1}{2}h^2 + 2x_2^2y^2,\ hx_2y^2 \leq \frac{h^2}{4b} + bx_2^2y^4, \\ x_2^2hu &\leq x_2^2\left(\frac{b}{4a}h^2 + \frac{a}{b}u^2\right), \\ hux_1x_2 &\leq \frac{b}{4a}h^2x_2^2 + \frac{a}{b}x_1^2u^2,\ huy \leq \frac{h^2}{16a} + 4ay^2u^2, \\ (c + dy^2)ux_2y &\leq (c + dy^2)\left(\frac{b}{2a}x_2^2y^2 + \frac{a}{2b}u^2\right). \end{aligned}$$

By substituting these inequalities for $c = \frac{3}{b}$, $d = 2b$ and after simplification, we obtain

$$\dot{W} \leq -h^2\left(\frac{1}{8} + bx_2^2\right) - x_2^2y^2(1 + b^2y^2) + \frac{a^2}{b^2}[2b|x|^2 + 10b^2y^2 + 3]u^2.$$

From the properties of the functions h and y we can substantiate that W is a practical ISS Lyapunov function for (B.3). Consequently, using Theorem C.12 (Appendix C) it can be concluded that the system (B.3) is ISS with respect to the set $\mathcal{W}$ from the input

u. □

Remark B.5. It is straightforward to check that there exists a function $\alpha \in \mathcal{K}_\infty$ such that for all $x \in M$ and $u = 0$ we have $\dot{W} \leq -\alpha(|x|_{\mathcal{W}})$. Thus W is a global Lyapunov function establishing multistability of (B.3) with respect to $\mathcal{W}$ for $u = 0$.

B.3 Synchronization of Brockett oscillators

The following family of Brockett oscillators is considered in this section for some $N > 1$:

$$\begin{aligned} \dot{x}_{1i} &= x_{2i}, \\ \dot{x}_{2i} &= a_i u_i - x_{1i} - b_i x_{2i} \left(|x_i|^2 - 1 \right), i = \overline{1, N}, \end{aligned} \tag{B.9}$$

where $a_i, b_i > 0$ are the parameters of an individual oscillator, the state $x_i = [x_{1i}\ x_{2i}]^T \in M_i = \mathbb{R}^2$, the control $u_i \in \mathbb{R}$ ($u_i : \mathbb{R}_+ \to \mathbb{R}$ is locally essentially bounded and measurable signal). Denote the common state vector of (B.9) as $x = [x_1^T, \ldots, x_N^T]^T \in M = \prod_{i=1}^N M_i$, so M is the corresponding Riemannian manifold of dimension $n = 2N$ where the family (B.9) behaves and $u = [u_1, \ldots, u_N]^T \in \mathbb{R}^N$ is the common input. Through propositions B.2 and B.4, it has been shown that each member of family (B.9) is robustly stable with respect to the set $\mathcal{W}_i = \{x_i \in M_i : |x_i|^2 = 1\} \cup \{0\}$. Consequently, the family (B.9) is a robustly stable nonlinear system. As a result, Assumption 5.1 (Chapter 5) is satisfied for the case of the family of Brockett oscillators (B.9).

The synchronization problem is then to find a protocol u that makes the family (B.9) synchronized. There are several works devoted to synchronization and design of consensus protocols for such a family or oscillatory network [102, 127, 151].

B.3.1 Problem statement

Let a $\mathcal{C}^1$ function $\psi : M \to \mathbb{R}^q$, $\psi(0) = 0$ be a synchronization measure for (B.9). We say that the family (B.9) is synchronized (or reached the consensus) if $\psi(x(t)) \equiv 0$ for all $t \geq 0$ on the solutions of the network under properly designed control actions

$$u_i(t) = \varphi_i \left[\psi(x(t)) \right], \tag{B.10}$$

where $\varphi_i : \mathbb{R}^q \to \mathbb{R}$ is a $\mathcal{C}^1$ function, $\varphi_i(0) = 0$. Due to the condition $\varphi_i(0) = 0$, the convergence of ψ (synchronization/consensus) implies that the solutions of the interconnection belong to $\mathcal{W} = \prod_{i=1}^N \mathcal{W}_i$. In this case the set $\mathcal{A} = \{x \in \mathcal{W} \mid \psi(x) = 0\}$ contains

the synchronous solutions of the family in (B.10) and the problem of synchronization of "natural" trajectories is considered since $\mathcal{A} \subset \mathcal{W}$.

In this appendix, we deal with the following synchronization measure:

$$\psi = [\psi_1, \ldots, \psi_N]^T,$$
$$\psi_i = \begin{cases} (x_{2(i+1)} - x_{2i}), & i = \overline{1, N-1} \\ x_{21} - x_{2N}, & i = N \end{cases}.$$

From a graph theory point of view, the oscillators are connected through a N-cycle graph [122] (each oscillator needs only the information of its next neighbor), *i.e.*

$$\psi = M \begin{bmatrix} x_{21} \\ \vdots \\ x_{2N} \end{bmatrix}, \; M = \begin{bmatrix} -1 & 1 & 0 & \cdots & 0 \\ 0 & -1 & 1 & \ddots & \\ & \ddots & \ddots & \ddots & \\ & & & & 1 \\ 1 & & & & -1 \end{bmatrix},$$

and any other connection type can be studied similarly. Moreover, the interconnection matrix M has Metzler form since all off-diagonal elements are positive. Next, let us define the synchronization error among the various states of the oscillators as follows for $i = \overline{1, N-1}$:

$$e_{2i-1} = x_{1i} - x_{1(i+1)}, \; \dot{e}_{2i-1} = x_{2i} - x_{2(i+1)} = e_{2i}$$

and $e_{2N-1} = x_{1N} - x_{11}$, $\dot{e}_{2N-1} = x_{2N} - x_{21} = e_{2N}$. Thus,

$$\psi_i = -e_{2i} \quad i = \overline{1, N},$$
$$\psi_N = \sum_{i=1}^{N-1} e_{2i}$$

and the quantity $e = [e_1, e_2, \ldots, e_{2N}] = 0$ implies that $\psi = 0$ (the synchronization state is reached). For $y_i = |x_i|^2 - 1$ the error dynamics can be written in the form:

$$\begin{aligned} \dot{e}_{2i-1} &= e_{2i}, \; i = \overline{1, N}, \\ \dot{e}_{2i} &= -e_{2i-1} + a_i u_i - a_{i+1} u_{i+1} - b_i x_{2i} y_i + b_{i+1} x_{2(i+1)} y_{i+1}, \; i = \overline{1, N-1}, \\ \dot{e}_{2N} &= -e_{2N-1} + a_N u_N - a_1 u_1 - b_N x_{2N} y_N + b_1 x_{21} y_1. \end{aligned} \tag{B.11}$$

Since $e_{2N-j} = \sum_{i=1}^{N-1} e_{2i-j}$ for $j = 0, 1$, then formally only $N-1$ errors can be considered

in (B.11).

In order to design the controls we will consider in this appendix the following Lyapunov function

$$V(x) = \sum_{i=1}^{N} \frac{\alpha_i}{4} y_i^2 + \frac{1}{2} \sum_{i=1}^{2N} e_i^2, \tag{B.12}$$

where $\alpha_i \geq 0$ are weighting parameters. Notice that $V(x) = 0$ for all $x \in \mathcal{A} \cap \prod_{i=1}^{N} \mathcal{W}_{2i}$ and positive otherwise. Such a choice of Lyapunov function is very natural for our goal since it has two items: the former one characterizes stability of each oscillator, while the latter item evaluates synchronicity of the network.

B.3.2 Preliminary results

In [3] for $N = 2$ and

$$u = k\psi, \; k > 0, \tag{B.13}$$

e.g. $\varphi(\psi) = k\psi$ in (B.10), the following result has been proven using $V(x)$:

Theorem B.6. *[3] The family of Brockett oscillators (B.9) with $N = 2$ is synchronized by (B.13),* i.e. *the system is globally asymptotically stable with respect to the set $\mathcal{A}$.*

It has been observed in numerical experiments that for $N > 2$ and

$$u = k \begin{bmatrix} -1 & 1 & 0 & \cdots & 0 \\ 0 & -1 & 1 & \ddots & \\ & \ddots & \ddots & \ddots & \\ & & & & 1 \\ 1 & & & & -1 \end{bmatrix} \begin{bmatrix} x_{21} \\ x_{22} \\ \vdots \\ x_{2(N-1)} \\ x_{2N} \end{bmatrix} \tag{B.14}$$

the synchronization persists, but the proof cannot be extended to the case $N > 2$ since (B.12) is not a Lyapunov function in such a case.

Remark B.7. To overcome this problem, based on the idea presented in [45], the following modification to the control law (B.14) can be proposed:

$$u_i = k\psi_i + b_i x_{2i} y_i. \tag{B.15}$$

Since the modified control law (B.15) compensates the nonlinear part of (B.9), as a

result the closed loop system becomes linear. In this case, it is trivial to show that the closed loop system (B.9) and (B.15) is globally asymptotically synchronized.

Theorem B.6 guarantees global asymptotic stability of the synchronized behavior, but not the robustness. Note that the controls (B.14) and (B.15) are not bounded, then it is impossible to apply the result of Proposition B.4 to prove robust stability of $\mathcal{W}$. Moreover, in many application areas, the control is bounded due to actuator limitations [86]. With such a motivation, take a bounded version of (B.10), then from Propositions 5.3 (Chapter 5) and B.4 convergence of all trajectories in a vicinity of $\mathcal{W}$ immediately follows. If (B.10) is sufficiently bounded then any accuracy of approaching $\mathcal{W}$ can be guaranteed, and the next result summarizes the conditions of synchronization:

Corollary B.8. *Let the set $\mathcal{A}$ be compact, it contains all $\alpha-$ and $\omega-$limit sets of (B.9), (B.10), and it is decomposable for given bounded $\varphi_i, i = \overline{1,N}$, then the interconnection (B.9), (B.10) is synchronized,* i.e. *the system is globally asymptotically stable with respect to the set $\mathcal{A}$.*

Proof. In the conditions of the corollary Assumption 5.2 (Chapter 5) is satisfied for (B.9), (B.10). The proof follows from the result of Theorem 5.4 (Chapter 5) since Assumption 5.1 (Chapter 5) is satisfied due to Proposition B.4. □

If we assume that (B.10) contains an additional perturbation $d \in \mathbb{R}^N$:

$$u_i(t) = \varphi_i\left[\psi(x(t)) + d_i(t)\right],\ i = \overline{1,N},$$

which models the connection errors and coupling imperfections, then ISS property with respect to the set $\mathcal{A}$ can be proven in the conditions of Corollary B.8 (the result of Theorem 5.4 (Chapter 5)).

B.3.3 Global synchronization control

Consider a variant of synchronization control in the following form:

$$u = k\begin{bmatrix} -2 & 1 & 0 & \cdots & 1 \\ 1 & -2 & 1 & \cdots & 0 \\ 0 & 1 & -2 & \cdots & 0 \\ \vdots & & \vdots & \ddots & 0 \\ 1 & \cdots & 0 & 1 & -2 \end{bmatrix}\begin{bmatrix} x_{21} \\ x_{22} \\ \vdots \\ x_{2(N-1)} \\ x_{2N} \end{bmatrix} = kM\begin{bmatrix} e_2 \\ e_4 \\ \vdots \\ e_{2N-2} \\ e_{2N} \end{bmatrix}, \tag{B.16}$$

where $k > 0$ is the coupling strength and

$$M = \begin{bmatrix} -1 & 0 & 0 & \cdots & 1 \\ 1 & -1 & 0 & \cdots & 0 \\ 0 & 1 & -1 & \cdots & 0 \\ \vdots & & \vdots & \ddots & 0 \\ 0 & \cdots & 0 & 1 & -1 \end{bmatrix}.$$

Obviously, the control (B.16) can be rewritten as (B.10):

$$u = -kM\psi.$$

With such a control each i^{th}oscillator is connected with two of its neighbors, $(i-1)^{\text{th}}$ and $(i+1)^{\text{th}}$ oscillators, and the closed loop network (B.9), (B.16) is organized again in the form of N-cycle graph [122]. Note that for $N = 2$ the control (B.16) takes the form of (B.13).

Let us calculate the derivative of the Lyapunov function $V(x)$ for (B.9), (B.16) (for indexes we will use convention in the calculations below that $N + 1 = 1$):

$$\begin{aligned}
\dot{V} &= \sum_{i=1}^{N}[\alpha_i(-b_i x_{2i}^2 y_i^2 + a_i x_{2i} y_i u_i) + e_{2i}(a_i u_i - a_{i+1}u_{i+1} - b_i x_{2i} y_i + b_{i+1} x_{2(i+1)} y_{i+1})] \\
&= \sum_{i=1}^{N}[a_i(\alpha_i x_{2i} y_i + e_{2i} - e_{2i-2})u_i + b_i(e_{2i-2} - e_{2i})x_{2i} y_i - \alpha_i b_i x_{2i}^2 y_i^2] \\
&= \sum_{i=1}^{N}[a_i(\alpha_i x_{2i} y_i + e_{2i} - e_{2i-2})k(e_{2i-2} - e_{2i}) + b_i(e_{2i-2} - e_{2i})x_{2i} y_i - \alpha_i b_i x_{2i}^2 y_i^2] \\
&= \sum_{i=1}^{N}[\{a_i\alpha_i k + b_i\}(e_{2i-2} - e_{2i})x_{2i} y_i - k a_i (e_{2i-2} - e_{2i})^2 - \alpha_i b_i x_{2i}^2 y_i^2].
\end{aligned}$$

Select $\alpha_i = \frac{b_i}{k a_i}$, then

$$\begin{aligned}
\dot{V} &= \sum_{i=1}^{N} b_i[2(e_{2i-2} - e_{2i})x_{2i} y_i - \alpha_i^{-1}(e_{2i-2} - e_{2i})^2 - \alpha_i x_{2i}^2 y_i^2] \\
&= -\sum_{i=1}^{N} b_i[\alpha_i^{-0.5}(e_{2i-2} - e_{2i}) - \alpha_i^{0.5} x_{2i} y_i]^2 \\
&\leq 0
\end{aligned}$$

Since V is positive definite with respect to the set $x \in \mathcal{A} \cap \prod_{i=1}^{N} \mathcal{W}_{2i}$, which is compact,

then all trajectories in the system are globally bounded. By LaSalle's invariance principle all trajectories of the system converge to the largest invariant set in

$$\begin{aligned}\Omega &= \{x \in M : \dot{V}(x) = 0\} \\ &= \{x \in M : e_{2i-2} - e_{2i} = \alpha_i x_{2i} y_i,\ i = \overline{1,N}\}.\end{aligned}$$

Note that $u_i = k(e_{2i-2} - e_{2i}) = k\alpha_i x_{2i} y_i = \frac{b_i}{a_i} x_{2i} y_i$ in the set Ω, then on that set the control performs compensation of nonlinearity as (B.15) and asymptotically the dynamics of synchronization errors take the form for $i = \overline{1,N}$:

$$\begin{aligned}\dot{e}_{2i-1} &= e_{2i}, \\ \dot{e}_{2i} &= -e_{2i-1} + a_i u_i - a_{i+1} u_{i+1} - b_i x_{2i} y_i + b_{i+1} x_{2(i+1)} y_{i+1} \\ &= -e_{2i-1}\end{aligned}$$

and

$$\begin{aligned}\dot{y}_i &= -2b_i x_{2i}^2 y_i + 2a_i x_{2i} u_i = 0, \\ \dot{x}_{1i} &= x_{2i}, \\ \dot{x}_{2i} &= -x_{1i},\end{aligned}$$

i.e. the norms $|x_i|$ and $|(e_{2i-1}, e_{2i})|$ become constant on Ω. Therefore, the following result has been proven:

Proposition B.9. *For any $k > 0$ in the system (B.9), (B.16) all trajectories are bounded and converge to the largest invariant set in*

$$\begin{aligned}\Omega_\infty = \{&x \in M : |x_i| = const,\ e_{2i-1}^2 + e_{2i}^2 = const, \\ &x_{2(i-1)} + x_{2(i+1)} = (2 + \alpha_i(|x_i|^2 - 1))x_{2i}, \\ &i = \overline{1,N}\}.\end{aligned}$$

As we can conclude, the set Ω_∞ includes the dynamics of interest with synchronization at the unit circle (when $|x_i| = 1$ for all $i = \overline{1,N}$) or on a circle (when $|x_i| \neq 0$ for all $i = \overline{1,N}$). Indeed, the relations

$$\beta_i x_{2i} = x_{2(i-1)} + x_{2(i+1)} \tag{B.17}$$

with constant $\beta_i = (2 + \alpha_i(|x_i|^2 - 1))$, which satisfy in the set Ω_∞ for all $i = \overline{1,N}$, can be interpreted as a kind of synchronization, with another synchronization measure (the

previously introduced $\psi(x(t))$ may be non zero in general case). Note that different, phase or anti-phase, patterns can be obtained in (B.9), (B.16) depending on values of parameters. The case when $|x_i| = 0$ for all $i = \overline{1,N}$ corresponds also to synchronization, but it is not interesting from an application point of view since there is no periodic solution in this case.

Theorem B.10. *For any $k > 0$, if there is an index $1 \leq i \leq N$ such that $2a_ik < b_i$, then in the system (B.9), (B.16) all trajectories are bounded and almost all of them converge to the largest invariant set in*

$$\Omega'_\infty = \{x \in M : |x_i| = const \neq 0,\ e_{2i-1}^2 + e_{2i}^2 = const,\\ x_{2(i-1)} + x_{2(i+1)} = (2 + \alpha_i(|x_i|^2 - 1))x_{2i}, i = \overline{1,N}\}.$$

Proof. Since all conditions of Proposition B.9 are satisfied, then all trajectories converge to the set Ω_∞. By substitution of the control (B.16) in the equations of (B.9) we obtain:

$$\begin{aligned}
\dot{x}_{1i} &= x_{2i},\\
\dot{x}_{2i} &= a_iu_i - x_{1i} - b_ix_{2i}\left(|x_i|^2 - 1\right)\\
&= a_ik(x_{2(i-1)} - 2x_{2i} + x_{2(i+1)}) - x_{1i} - b_ix_{2i}\left(|x_i|^2 - 1\right)\\
&= -x_{1i} - (2a_ik - b_i)x_{2i} + a_ik(x_{2(i-1)} + x_{2(i+1)}) - b_ix_{2i}|x_i|^2
\end{aligned}$$

Linearizing this system around the origin ($|x_i| = 0$ for all $i = \overline{1,N}$) we conclude that this equilibrium is unstable if there exists at least one index $1 \leq i \leq N$ with $2a_ik < b_i$. Thus, for almost all initial conditions trajectories converge to a subset of Ω_∞ where $|x_i| \neq 0$, *i.e.* to the set Ω'_∞. □

On the set Ω'_∞ we have $x_{2i} = r_i \sin(t + \phi_i)$ for all $i = \overline{1,N}$, where $r_i = |x_i|$ and $\phi_i \in [0, 2\pi)$ are some constants depending on the system parameters and initial conditions, then from (B.17)

$$(2 + \alpha_i(r_i^2 - 1))r_i \sin(t + \phi_i) = r_{i-1}\sin(t + \phi_{i-1}) + r_{i+1}\sin(t + \phi_{i+1})$$

and

$$(2 + \alpha_i(r_i^2 - 1))r_i = \sqrt{r_{i-1}^2 + r_{i+1}^2 + 2r_{i-1}r_{i+1}\cos(\phi_{i+1} - \phi_{i-1})},\\ \phi_i = \phi_{i-1} + \arctan\left(\frac{r_{i+1}\sin(\phi_{i+1} - \phi_{i-1})}{r_{i-1} + r_{i+1}\cos(\phi_{i+1} - \phi_{i-1})}\right)$$

providing expressions of possible relations of phases and amplitudes of oscillation for neighboring agents in (B.9), (B.16).

B.4 Simulations and experimental results

B.4.1 Simulation examples

To illustrate the theoretical results, we will consider both identical and non identical Brockett oscillators. First, let us choose 4 non-identical Brockett oscillators (B.9) with parameters $k = 0.5$, $a_i = b_i = i$, $i = \overline{1,3}$, $a_4 = 3$, $b_4 = 4$. For the case of identical oscillators, let us the choose the parameters $k = 0.5$, $a_i = 0.5$, $b_i = 1$, $i = \overline{1,4}$. The chosen parameters respect the condition of Theorem B.10. For both cases, let us consider the control (B.16). Then the system (B.9) synchronizes (in/anti-phase) and converges to the set Ω'_∞ (which includes unit circle) according to Theorem B.10.

The simulation result for non-identical oscillators can be seen in Fig. B.1, while Fig. B.2 shows the simulation result for the case of identical oscillators. From the simulation result, in-phase synchronization is present for non-identical oscillators while anti-phase synchronization is present for identical oscillators. In the case of in-phase synchronization, oscillators converge to the unit circle. However, for anti-phase synchronization, the oscillators converge to a circle which is in Ω'_∞. In this case, the radius of the circle depends on the system parameters and initial conditions.

Moreover, adding a small perturbation in the case of identical oscillators leads to in-phase synchronization (difference in parameters for non-identical oscillators can be considered as a perturbation also). Thus, in this example synchronization is a phenomenon, which follows the agents imperfections rather than similarity.

B.4.2 Experimental results

To validate the theoretical results, we will consider the experimental synchronization of three non-identical Brockett oscillators. For the oscillators, the parameters are chosen such a way that the condition of Theorem B.10 is satisfied. The circuit diagram of a Brockett oscillator can be seen in Fig. B.3[1]. The response of the autonomous Brockett oscillator is given in Fig. B.4. Next, two cases will be considered.

In the first case, low control gain was selected. The response of oscillators in this case can be seen in Fig. B.5. From the thoeretical results, oscillators are supposed to be synchronized with zero error. However, experimental results show that although the oscillators are synchronized but the error is not zero. The non-zero synchronization error is due to the imperfection, nonlinearities and noidealities of the analog implementation. To overcome these problems, one way is to use high control gain. So, next the experiment

[1] Values of the components are avoided here for the purpose of brevity

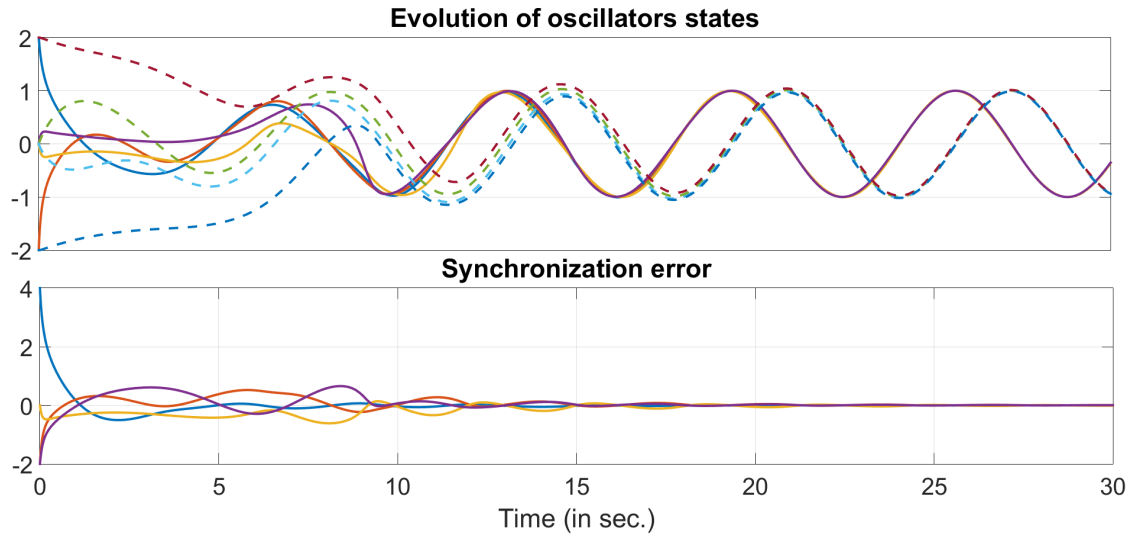

Figure B.1: Synchronization result with control (B.16) for the case of non-identical oscillators. In the top figure, Solid line - x_2, dashed line - x_1

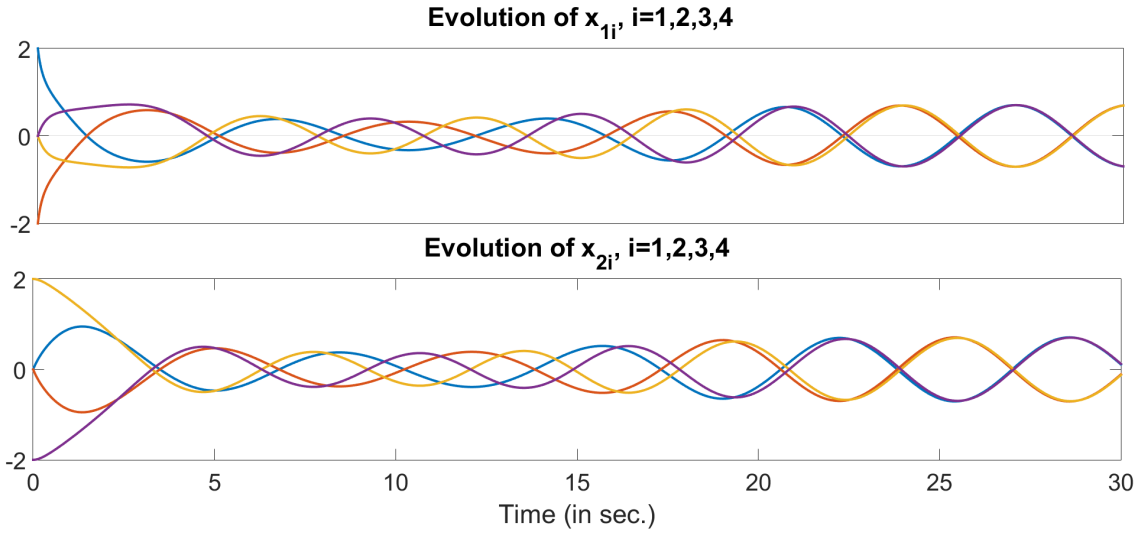

Figure B.2: Synchronization result with control (B.16) for the case of identical oscillators

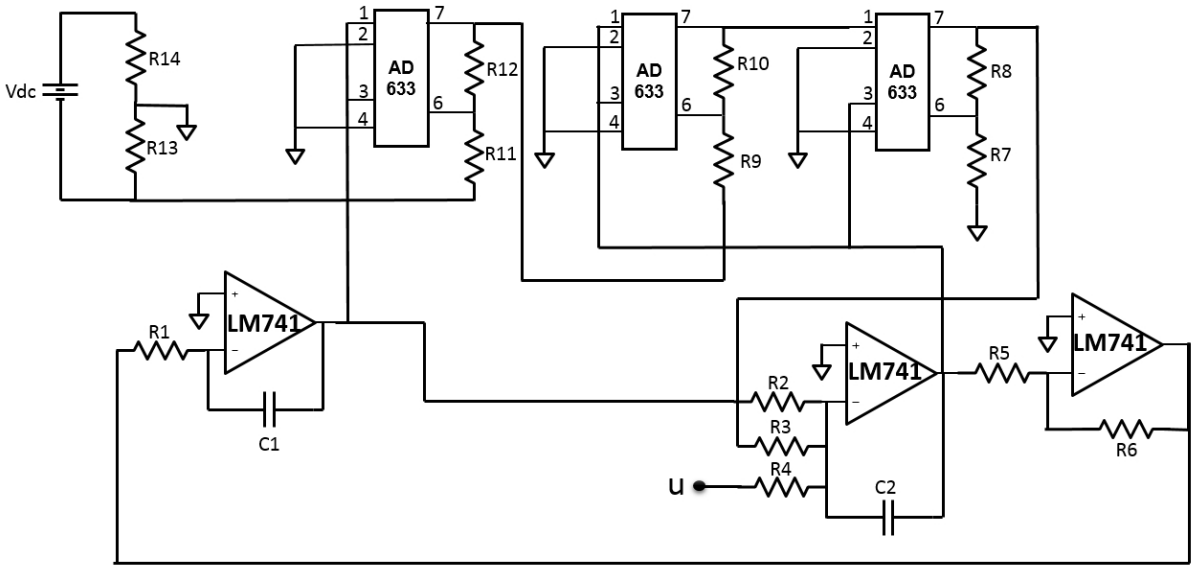

Figure B.3: Analog circuit diagram of a Brockett oscillator

was done using high control gain. The response of oscillators in this case can be seen in Fig. B.6. The results in this case coincide with theoretical findings.

B.5 Conclusions

This appendix studied the problem of robust synchronization of non-identical Brockett oscillators. Sufficient conditions were derived for that purpose based on an extension of the ISS framework to systems evolving on a (non-compact) manifold and with multiple invariant sets. Global asymptotic stability and ISS stability analysis were done for individual oscillator followed by global stability analysis of the closed loop systems with respect to a decomposable invariant set $\mathcal{W}$. Numerical simulations and experimental results demonstrated the effectiveness of our method to network of nonidentical Brockett oscillators.

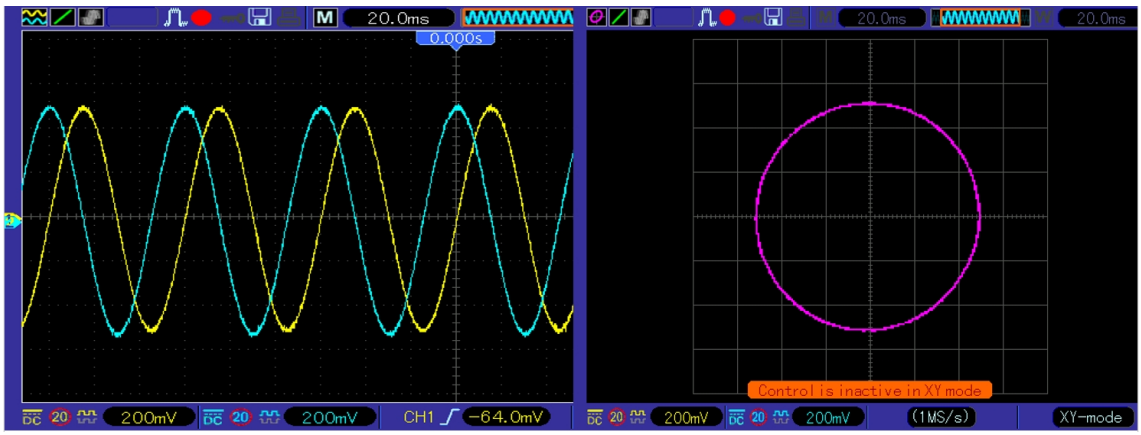

Figure B.4: Response of autonomous Brockett oscillator. Left- state variables evolution, right- unit circle in the in the (x_1, x_2)-space

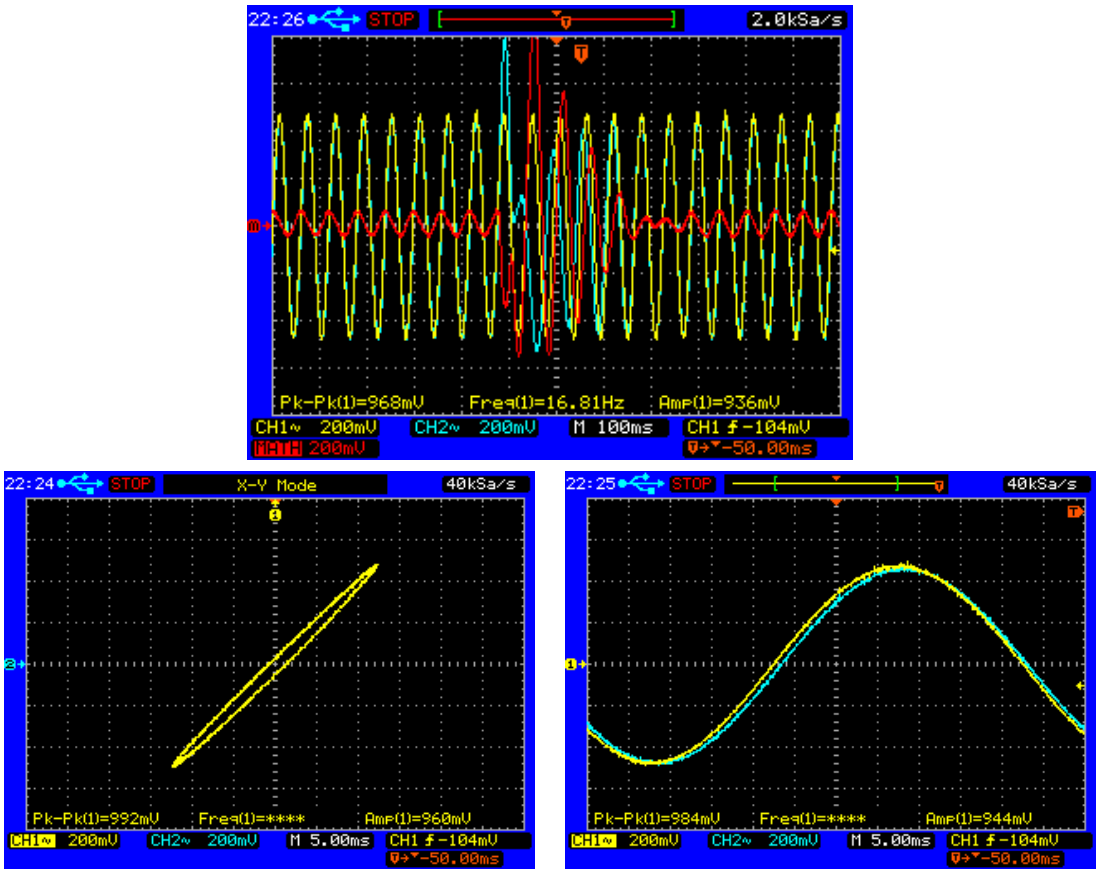

Figure B.5: Results of synchronization with low control gain. Top - x_{21}(cyan), x_{22}(yellow) and $e_1 = x_{21} - x_{22}$(red). Bottom left - x_{21} vs. x_{22}, bottom right - x_{21} and x_{22}

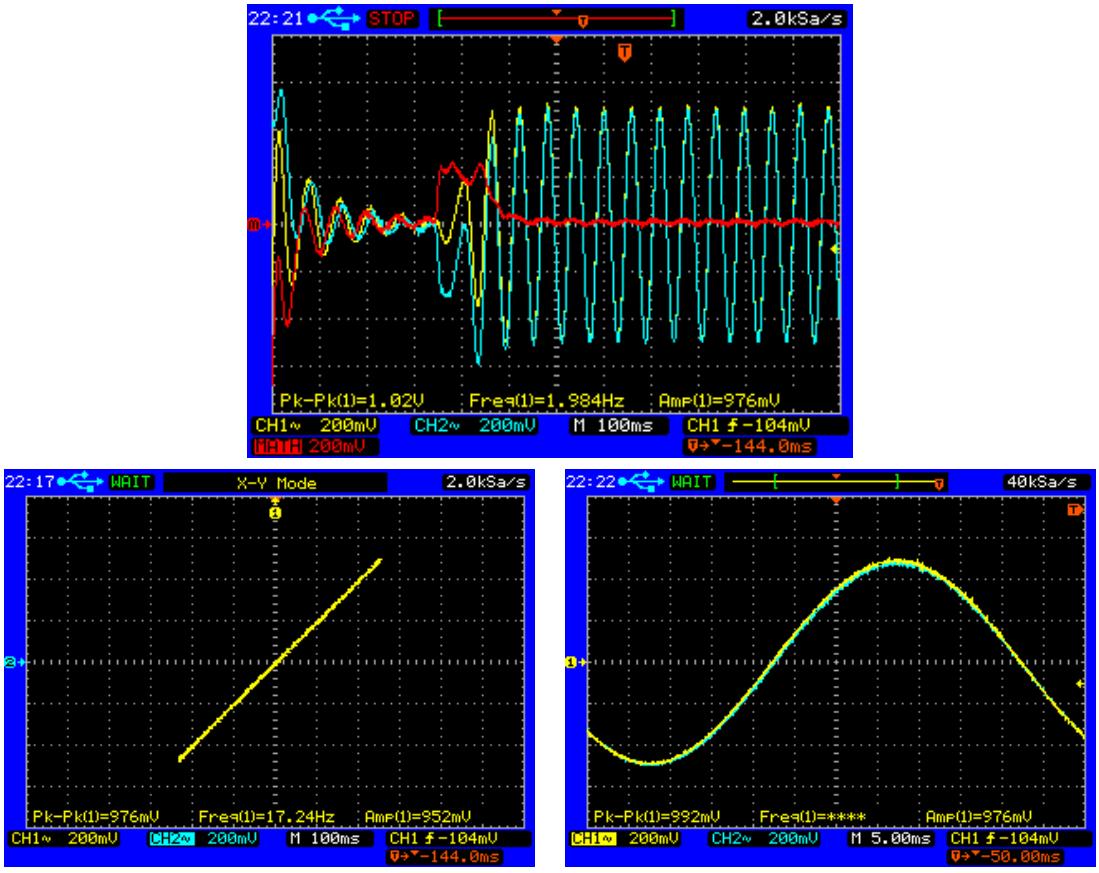

Figure B.6: Results of synchronization with high control gain. Top - x_{21}(cyan), x_{22}(yellow) and $e_1 = x_{21} - x_{22}$(red). Bottom left - x_{21} vs. x_{22}, bottom right - x_{21} and x_{22}

Appendix C

Input-to-State Stability with respect to decomposable invariant sets

For an n-dimensional $\mathcal{C}^2$ connected and orientable Riemannian manifold M without boundary ($0 \in M$), let the map $f : M \times \mathbb{R}^m \to T_xM$ be of class $\mathcal{C}^1$ (T_xM is the tangent space), and consider a nonlinear system of the following form:

$$\dot{x}(t) = f(x(t), d(t)) \tag{C.1}$$

where the state $x \in M$ and $d(t) \in \mathbb{R}^m$ (the input $d(\cdot)$ is a locally essentially bounded and measurable signal) for $t \geq 0$. We denote by $X(t, x; d(\cdot))$ the uniquely defined solution of (C.1) at time t fulfilling $X(0, x; d(\cdot)) = x$. Together with (C.1) we will analyze its unperturbed version:

$$\dot{x}(t) = f(x(t), 0). \tag{C.2}$$

A set $S \subset M$ is invariant for the unperturbed system (C.2) if $X(t, x; 0) \in S$ for all $t \in \mathbb{R}$ and for all $x \in S$. For a set $S \subset M$ define the distance to the set $|x|_S = \min_{a \in S} \delta(x, a)$ from a point $x \in M$, where the symbol $\delta(x_1, x_2)$ denotes the Riemannian distance between x_1 and x_2 in M, $|x| = |x|_{\{0\}}$ for $x \in M$ or a usual euclidean norm of a vector $x \in \mathbb{R}^n$. For a signal $d : \mathbb{R} \to \mathbb{R}^m$ the essential supremum norm is defined as $\|d\|_\infty = \operatorname{ess\,sup}_{t \geq 0} |d(t)|$.

Definition C.1. The point $\bar{x}$ is called an *omega limit point* of the solution of (C.2) $x(t, x_0)$ if there exists a sequence of time instants $t_1, \ldots, t_l, \ldots$ such that $t_k \to \infty$ as $k \to \infty$, for which the following holds:

$$x(t_k, x_0) \to \bar{x}, \qquad k \to 0 \tag{C.3}$$

The set of all such point of $x(t_k, x_0)$ is called ω-limit set of $x(t_k, x_0)$ (or orbit $\gamma(x_0)$) and denoted $\omega(x_0)$.

Definition C.2. The point $\underline{x}$ is called an *alpha limit point* of the solution of (C.2) $x(t, x_0)$ if there exists a sequence of time instants $t_1, \ldots, t_l, \ldots$ such that $t_k \to -\infty$ as $k \to \infty$, for which the following holds:

$$x(t_k, x_0) \to \underline{x}, \qquad k \to 0 \tag{C.4}$$

The set of all such point of $x(t_k, x_0)$ is called α-limit set of $x(t_k, x_0)$ and denoted $\alpha(x_0)$.

Definition C.3. A *heteroclinic orbit* γ_1 between two equilibria ζ_1 and ζ_2 of a continuous dynamical system as (C.2), is a trajectory $x(t, x_0)$ that is backward asymptotic to ζ_1 and forward asymptotic to ζ_1.

Definition C.4. A *heteroclinic cycle* is an invariant topological circle X consisting of the union of a set of equilibria $\{\zeta_1, \ldots, \zeta_k\}$ and orbits $\{\gamma_1, \ldots, \gamma_k\}$, where γ_i is a heteroclinic orbit between ζ_1 and ζ_{i+1}; and $\zeta_{k+1} = \zeta_1$. If $k = 1$ then the single equilibrium and connecting orbit form a *homoclinic cycle*.

C.1 Decomposable sets

Let $\Lambda \subset M$ be a compact invariant set for (C.2).

Definition C.5. [116] A decomposition of Λ is a finite and disjoint family of compact invariant sets $\Lambda_1, \ldots, \Lambda_k$ such that

$$\Lambda = \bigcup_{i=1}^{k} \Lambda_i.$$

For an invariant set Λ, its attracting and repulsing subsets are defined as follows:

$$W^s(\Lambda) = \{x \in M : |X(t, x, 0)|_\Lambda \to 0 \text{ as } t \to +\infty\},$$
$$W^u(\Lambda) = \{x \in M : |X(t, x, 0)|_\Lambda \to 0 \text{ as } t \to -\infty\}.$$

Define a relation on $\mathcal{W} \subset M$ and $\mathcal{D} \subset M$ by $\mathcal{W} \prec \mathcal{D}$ if $W^s(\mathcal{W}) \cap W^u(\mathcal{D}) \neq \oslash$.

Definition C.6. [116] Let $\Lambda_1, \ldots, \Lambda_k$ be a decomposition of Λ, then

1. An r-cycle ($r \geq 2$) is an ordered r-tuple of distinct indices $i_1, \ldots, i_r$ such that $\Lambda_{i_1} \prec \ldots \prec \Lambda_{i_r} \prec \Lambda_{i_1}$.
2. A 1-cycle is an index i such that $[W^u(\Lambda_i) \cap W^s(\Lambda_i)] - \Lambda_i \neq \oslash$.
3. A filtration ordering is a numbering of the Λ_i so that $\Lambda_i \prec \Lambda_j \Rightarrow i \leq j$.

As we can conclude from Definition C.6, existence of an r-cycle with $r \geq 2$ is equivalent to existence of a heteroclinic cycle for (C.2) [80]. And existence of a 1-cycle implies existence of a homoclinic cycle for (C.2) [80].

Definition C.7. The set $\mathcal{W}$ is called decomposable if it admits a finite decomposition without cycles, $\mathcal{W} = \bigcup_{i=1}^{k} \mathcal{W}_i$, for some non-empty disjoint compact sets $\mathcal{W}_i$, which form a filtration ordering of $\mathcal{W}$, as detailed in definitions C.5 and C.6.

Let a compact set $\mathcal{W} \subset M$ be containing all α- and ω-limit sets of (C.2) [26].

C.2 Robustness notions

The following robustness notions for systems in (C.1) have been introduced in [14].

Definition C.8. We say that the system (C.1) has the practical asymptotic gain (pAG) property if there exist $\eta \in \mathcal{K}_\infty$ [1]and a non-negative real q such that for all $x \in M$ and all measurable essentially bounded inputs $d(\cdot)$ the solutions are defined for all $t \geq 0$ and the following holds:

$$\limsup_{t \to +\infty} |X(t, x; d)|_{\mathcal{W}} \leq \eta(\|d\|_\infty) + q. \tag{C.5}$$

If $q = 0$, then we say that the asymptotic gain (AG) property holds.

Definition C.9. We say that the system (C.1) has the limit property (LIM) with respect to $\mathcal{W}$ if there exists $\mu \in \mathcal{K}_\infty$ such that for all $x \in M$ and all measurable essentially bounded inputs $d(\cdot)$ the solutions are defined for all $t \geq 0$ and the following holds:

$$\inf_{t \geq 0} |X(t, x; d)|_{\mathcal{W}} \leq \mu(\|d\|_\infty).$$

[1] A continuous function $h : [0, a) \to [0, \infty)$ belongs to class $\mathcal{K}$ if it is strictly increasing and $h(0) = 0$; it is said to belong to class $\mathcal{K}_\infty$ if $a = \infty$ and $h(r) \to \infty$ as $r \to \infty$ [94].

Definition C.10. We say that the system (C.1) has the practical global stability (pGS) property with respect to $\mathcal{W}$ if there exist $\beta \in \mathcal{K}_\infty$ and $q \geq 0$ such that for all $x \in M$ and all measurable essentially bounded inputs $d(\cdot)$ the following holds for all $t \geq 0$:

$$|X(t, x; d)|_{\mathcal{W}} \leq q + \beta(\max\{|x|_{\mathcal{W}}, \|d\|_\infty\}).$$

It has been shown in [14] that to characterize (C.5) in terms of Lyapunov functions the following notion is appropriate:

Definition C.11. A $\mathcal{C}^1$ function $V : M \to \mathbb{R}$ is a practical ISS-Lyapunov function for (C.1) if there exists $\mathcal{K}_\infty$ functions $\alpha_1, \alpha_2, \alpha$ and γ, and scalar $q \geq 0$ and $c \geq 0$ such that

$$\alpha_1(|x|_{\mathcal{W}}) \leq V(x) \leq \alpha_2(|x|_{\mathcal{W}} + c),$$

the function V is constant on each $\mathcal{W}_i$ and the following dissipative property holds:

$$DV(x)f(x, d) \leq -\alpha(|x|_{\mathcal{W}}) + \gamma(|d|) + q.$$

If the latter inequality holds for $q = 0$, then V is said to be an ISS-Lyapunov function.

Notice that the existence of α_2 and c follows (without any additional assumptions) by standard continuity arguments.

The main result of [14] connecting these robust stability properties is stated below:

Theorem C.12. *Consider a nonlinear system as in (C.1) and let a compact invariant set containing all $\alpha-$ and $\omega-$ limit sets of (C.2) $\mathcal{W}$ be decomposable (in the sense of Definition C.7). Then the following facts are equivalent.*

1. The system admits an ISS Lyapunov function;
2. The system enjoys the AG property;
3. The system admits a practical ISS Lyapunov function;
4. The system enjoys the pAG property;
5. The system enjoys the LIM property and the pGS.

A system in (C.1), for which this list of equivalent properties is satisfied, is called ISS with respect to the set $\mathcal{W}$ [14].